ÉCOLE DE TECHNOLOGIE SUPÉRIEURE
UNIVERSITÉ DU QUÉBEC

MANUSCRIPT-BASED THESIS PRESENTED TO
ÉCOLE DE TECHNOLOGIE SUPÉRIEURE

IN PARTIAL FULFILLMENT OF THE REQUIREMENTS
FOR THE DEGREE OF
DOCTOR OF PHILOSOPHY
Ph. D.

PAR
Albert NUBIOLA BATLLE

CONTRIBUTION TO IMPROVING THE ACCURACY OF SERIAL ROBOTS

MONTRÉAL, DECEMBER 17TH, 2014

BOARD OF EXAMINERS

THIS THESIS HAS BEEN EVALUATED

BY THE FOLLOWING BOARD OF EXAMINERS

M. Ilian A. Bonev, directeur de thèse
Département de génie de la production automatisée, École de technologie supérieure

M. Antoine Tahan, président du jury
Département de génie mécanique, École de technologie supérieure

M. Pascal Bigras, membre du jury
Département de génie de la production automatisée, École de technologie supérieure

M. René Mayer, examinateur externe
Département de génie mécanique, École Polytechnique de Montréal

THIS THESIS WAS PRESENTED AND DEFENDED IN

THE PRESENCE OF A BOARD OF EXAMINERS AND PUBLIC

DECEMBER 17TH 2014

AT ÉCOLE DE TECHNOLOGIE SUPÉRIEURE

ACKNOWLEDGEMENTS

I would like to thank my supervisor Prof. Ilian Bonev for being such a great advisor. I could always count on his support and brilliant ideas his dedication greatly inspired me. There has always been the chance to work on new projects with new companies and state of the art equipment in the CoRo laboratory.

I thank the automation team at Pratt & Whitney Canada for giving me the opportunity to have an industrial experience in the manufacturing of airplane engines at the Longueuil plant. Thanks to Canam Hoang, David Lafortune, Pierre-Phillippe Poirier, Mélanie Tremblay, Yuwen Li and François Dupras, from whom I did not just learn about industrial manufacturing but also about the Quebecoise culture.

I would also like to thank AV&R Global, especially Tommy Gagnon, for trusting our robot calibration methods to calibrate their Fanuc robots.

I am grateful to my colleagues at the CoRo, especially Yanick Noiseux, Mohamed Slamani, Yousef Babazadeh, Andy Yen and Ahmed Joubair, who assisted me in many different ways.

I thank La Caixa d’Estalvis i Pensions de Barcelona, “la Caixa” for funding my studies. I also thank le Fonds québecois de la recherché sur la nature et les technologies (FQRNT) and the Natural sciences and engineering research council of Canada (NSERC) for their funding.

Last but not least, I thank my family for their support. Their constant love, support and encouragement were essential to complete this work. My parents and my three brothers have always been nearby despite the geographical distance.

CONTRIBUTION À L’AMÉLIORATION DE LA PRÉCISION DES ROBOTS SÉRIELS

Albert NUBIOLA BATLLE

RÉSUMÉ

Le but de la présente étude est de contribuer à l’amélioration de la précision absolue des robots manipulateurs sériels à six degrés de liberté. Ces méthodes consistent à identifier les valeurs des paramètres du robot, en vue d’améliorer la correspondance entre le robot réel et le modèle mathématique utilisé par son contrôleur. Le modèle du robot étalonné ajoute des paramètres d’erreur au modèle nominal; ces paramètres correspondent aux erreurs géométriques et au comportement élastique du robot.

Les méthodes développées se concentrent sur les systèmes de mesure à faible coût. Le premier travail fait une comparaison entre un étalonnage robot fait avec un laser de poursuite (« laser tracker ») et une caméra stéréo (MMT optique). L’amélioration de la précision est validée en utilisant une barre à billes pour chacune des deux méthodes d’étalonnage. Le résultat de l’étalonnage est le même pour les deux méthodes tandis que le prix d’un laser de poursuite est plus que deux fois le prix d’une caméra stéréo. La méthode est validée avec un robot ABB IRB 120, un laser de poursuite Faro ION, et une caméra stéréo C-Track de Creaform. Une barre à billes Renishaw QC20-W permet de valider la précision obtenue de manière indépendante.

Un système de mesure innovateur qui permet de mesurer un ensemble de poses est décrit à la deuxième partie de la thèse. Ce dispositif est basé sur une approche d’hexapode connu (la plateforme Stewart-Gough). Une plaque doit s’attacher à la base du robot et une autre à l’outil; chaque plaque contient trois supports magnétiques. Ce système permet de mesurer 144 poses de l’outil par rapport au support de la base en prenant six mesures de la barre à billes pour chaque pose. La précision tridimensionnelle de ce dispositif est 3.2 fois la précision de la barre à billes QC20-W, soit ± 0.003 mm. Dans la troisième partie de cette thèse, on utilise ce nouvel système de mesure 6D pour faire un étalonnage absolue d’un robot. Le robot est étalonné dans 61 configurations et la précision de positionnement absolue est validée avec un laser de poursuite Faro dans environ 10,000 configurations de robot. L’erreur de distance moyenne est améliorée de 1.062 mm à 0.400 mm dans 50 millions de pairs de mesures dans tout l’espace de travail du robot. A titre comparatif, le robot est aussi étalonné avec un laser de poursuite et la précision est validée dans les mêmes 10,000 configurations.

Mots clés: étalonnage de robots, robots sériels, précision absolue.

CONTRIBUTION TO IMPROVING THE ACCURACY OF SERIAL ROBOTS

Albert NUBIOLA BATLLE

ABSTRACT

The goal of the present study is to improve the accuracy of six-revolute industrial robots using calibration methods. These methods identify the values of the calibrated robot model to improve the correspondence between the real robot and the mathematical model used in its controller. The calibrated robot model adds error parameters to the nominal model, which correspond to the geometric errors of the robot as well as the stiffness behavior of the robot.

The developed methods focus on using low cost measurement equipment. For instance, the first work makes a comparison between a robot calibration performed using a laser tracker and a stereo camera (MMT optique) separately. The accuracy performance is validated using a telescoping ballbar for each of the two methods. While the calibration result is the same for both methods, the price of a laser tracker is more than twice the price of a stereo camera. The method is tested using an ABB IRB120 robot, a Faro ION laser tracker, and a Creaform C-Track stereo camera to calibrate the robot. A Renishaw QC20-W ballbar is used to validate the accuracy.

A novel measurement system to measure a set of poses is described in the second work. The device is an extension of a known approach using an hexapod (a Stewart-Gough platform). One fixture is attached to the robot base and the other to the robot end-effector, each having three magnetic cups. By taking six ballbar measurements at a time, it is possible to measure 144 poses of the triangular fixture attached to the robot end-effector with respect to the base fixture. The position accuracy of the device is 3.2 times the accuracy of the QC20-W ballbar: ± 0.003 mm. An absolute robot calibration using this novel 6D measurement system is performed in the third work of this thesis. The robot is calibrated in 61 configurations and the absolute position accuracy of the robot after calibration is validated with a Faro laser tracker in about 10,000 robot configurations. The mean distance error is improved from 1.062 mm to 0.400 mm in 50 million pairs of measurements throughout the complete robot workspace. To allow a comparison, the robot is also calibrated using the laser tracker and the robot accuracy validated in the same 10,000 robot configurations.

Keywords: robot calibration, serial robots, absolute accuracy

TABLE OF CONTENTS

Page

LIST OF TABLES

Page

LIST OF FIGURES

LIST OF ABBREVIATIONS AND ACRONYMS

CAD	Computer assisted design
CMM	Coordinate measuring machine
CNC	Computer numerical control
CoRo	Control and robotics laboratory
CPC	Complete and parametrically continuous
CRIAQ	Consortium for research and innovation in aerospace in Québec
D-H	Denavit-Hartenberg
D-H M	Denavit-Hartenberg modified, as defined in (Craig, 1986)
DBB	Double-ball bar
DOF	Degree of freedom
EE	End-effector
ETS	École de Technologie Supérieure
HMI	Human-machine interface
IDP	Inverse displacement problem
ISO	International organization for standardization
MMT	Machine à mesurer tridimensionnelle
NSERC	Natural sciences and engineering research council of Canada
OLP	Off-line programming
TCP	Tool center point
SMR	Spherically-mounted reflector
Std	Standard deviation

s(θ)	sin(θ)
c(θ)	cos(θ)
s_i	sin(q_i)
c_i	cos(q_i)
Trans(x,y,z)	Geometrical translation $\{x,y,z\}$
Rot($\mathbf{v}$,θ)	Geometrical rotation of θ around unit vector $\mathbf{v}$
RMS	Root mean square
LAN	Local area network

LIST OF SYMBOLS AND UNITS OF MEASUREMENT

kg	Kilogram
g	Gram
N	Newton
Hz	Herz (measures/second)
s	Second
ms	Millisecond
º	Degree (“deg” is used in some figures)
rad	Radian
m	Meter
mm	Millimeter
µm	Micrometer
Nm	Newton-meter (torque)
mm/s	Millimeter per second

INTRODUCTION

Industrial robots are mainly conceived and used in repetitive applications, therefore, they successfully perform tasks programmed in teach mode. Some examples of typical robot applications are pick and place operations, welding, painting, machine tending, palletizing and assembly. These types of applications do not require high robot accuracy levels as long as the robot path is manually taught; in this case, the accuracy is the same as the repeatability. However, there is an increasing demand of applications where the robot should be programmed through off-line programming (OLP). Robot paths can be more sophisticated by programming a robot using simulator software; therefore, the robot can be used in a more extended number of applications, such as inspection, machining, drilling or composite fiber placement. Furthermore, the production of the robot does not need to be interrupted. Even though robots are highly repeatable, their accuracy is far below their repeatability. Therefore, the accuracy of a robot can be improved through robot calibration.

The demand of industrial robots having better accuracy and reduced cost has been constantly growing in the past decade, especially in the aerospace sector (Summers, 2005). Today, most industrial robot manufacturers and a few service providers offer robot calibration services. Furthermore, many industrial robot manufacturers now adopt the ISO 9283 norm, which was not the case a decade ago (Greenway, 2000; Schröer, 1999). Nevertheless, the only information regarding the positioning performance of an industrial robot continues to be a single measure specified as “positioning performance according to ISO 9283”, which actually refers to the average unidirectional position repeatability and accuracy at five poses obtained from thirty cycles. A few additional performance measures might be obtained from certain robot manufacturers (*e.g.*, found in the product manual of the robot), such as *linear path repeatability* and *linear path accuracy*, but even this information is highly insufficient and impossible to use if we want to compare two robots manufactured by different companies.

The absolute accuracy of a robot is not usually specified by its manufacturer. The accuracy of a robot is not important as long as the robot path is manually taught. In this case we only want the robot to be repeatable. However, in off-line programming the accuracy becomes an important issue since positions are defined in a virtual space from an absolute or relative coordinate system. There are also some industrial applications where a robot is used as a measurement system, for example, when the robot holds a touch probe to locate the part to be processed; in this case, the accuracy of the robot becomes the accuracy of the measurement system.

It is required to study the forward kinematic model to improve robot accuracy. Starting with the nominal kinematic model of a robot and adding error parameters we can find a mathematical model that represents the robot better than the nominal kinematic model. This improved model must make the robot more accurate, improving position and orientation errors.

This work focuses on finding new robot calibration methods for six-revolute industrial serial robots. The calibration methods must give good accuracy results while maintaining the cost of the measurement equipment as low as possible. The calibrated robot model used only physically meaningful parameters into account, which allows for extrapolation if the robot environment is modified, such as the robot payload or the inclination angle of the robot.

This thesis is organized in four chapters. Chapter 1 presents a literature review on robot calibration. Chapter 2 compares two different measurement systems to be used in robot calibration: a laser tracker and a stereo camera. A novel six-dimensional (6D) measurement system is introduced in Chapter 3. This measurement system can measure the pose of 144 configurations by using only one telescoping ballbar, very accurate 6D measurements can be obtained with low-cost one-dimensional equipment. Finally, Chapter 4 performs a robot calibration using the novel 6D measurement system. Chapters 2, 3 and 4 have been published as articles in scientific journals (A Nubiola et al., 2013; A. Nubiola and Bonev, 2014; Albert Nubiola et al., 2013).

CHAPTER 1

LITTERATURE REVIEW

This chapter describes the calibration methods established in the literature, more precisely the robot calibration process, the three levels of robot calibration, the kinematic representation used for calibrated robots and the optimization methods used for parameter identification. The most relevant commercial solutions for robot calibration are also mentioned in this chapter, as well as some recent robot calibration results reported in literature.

Industrial robots propose an interesting alternative to dedicated machines. A robot should be calibrated to get the best production performance. Robots require high accuracy levels to perform advanced operations; for example, an accurate robot is much more suitable to perform tasks that have been programmed off-line. Furthermore, if we have a stiffness model of the robot, we could compensate any forces applied to the robot end-effector (EE), such as in a machining operation (Dumas et al., 2011).

Although robot calibration has been studied for more than two decades, the theory remains the same as in the early 1980s (Barker, 1983). What is different nowadays is that robots are better built (i.e., their repeatability is greater) and the sources of errors, with respect to their nominal models, are slightly different. Measurement equipment is also better, i.e., more accurate, though certainly not much more affordable. The mathematical models that used to work for robots a decade or two ago are no longer optimal for today's robots. Furthermore, the accuracy required today in some potential robot applications is much higher than a couple decades ago.

Nowadays, two measures are commonly used for describing the positioning performance of industrial robots: *repeatability* and *accuracy*.

Loosely speaking, *pose repeatability* is the ability of a robot to repeatedly return to the same pose. In robotics, the ISO 9283 defines the repeatability term and it is used by most industrial robot manufacturers. The ISO norm actually refers to *unidirectional repeatability* only, which is the ability to return to the same pose coming from the same direction, thus minimizing the effect of backlash. Multidirectional repeatability can be twice the unidirectional repeatability or even worse.

Repeatability can be improved by either high-precision gear trains (as in most Staübli robots), by placing high-resolution encoders at the output of the gear trains or using direct-drive motors (as in some SCARA robots). However, all of these solutions raise the manufacturing cost of an industrial robot.

Loosely speaking, *volumetric accuracy* (also called *absolute accuracy*) is the ability of a robot to attain a pose with respect to a reference frame. Since identifying such a reference frame is not always simple with a robot (for example, it might require using a touch probe), accuracy is most typically tested in relative measurements, *e.g.*, *distance accuracy* is the ability of the robot to displace its tool center point (TCP) a prescribed distance.

Robot accuracy is affected by the same factors as multidirectional repeatability; it is obviously lower bounded by the multidirectional repeatability of the robot. Accuracy is influenced mostly by geometric inaccuracies and elasticity, present in both the links and the transmissions. Fortunately, these two types of errors can be modeled to some extent in the robot calibration process (Abderrahim et al., 2007).

There are five factors that cause robot errors (Andrew Liou et al., 1993; Karan and Vukobratovic, 1994): environmental (such as temperature or the warm-up process), parametric (for example, kinematic parameter variation due to manufacturing and assembly errors, influence of dynamic parameters, friction and other nonlinearities, including hysteresis and backlash), measurement (resolution and discretisation of joint position sensors), computational (computer round-off and steady-state control errors) and application (such as installation errors).

Robot calibration can be divided into several categories and subcategories. The following two sections compare an absolute calibration with a relative calibration and an open-loop with a closed-loop calibration respectively.

1.1 Absolute vs. relative calibration

An absolute calibration allows attaining accurate positions with respect to a physically measurable frame. A relative calibration disregards the actual location of the robot base whereas an absolute calibration takes into account where the robot base is placed. In other words, if we want more than one robot to share the same coordinate system they need to be "absolute" calibrated to agree with the same "absolute" reference frame (also called world frame). An absolute calibration is not needed if we are positioning the robot relatively to a local frame (also called object or user frame), so we need a tool, such as a touch probe, which allows us to locate objects in the robot working space. An absolute calibration needs six more parameters than a relative calibration because we need to represent the relative frame with respect to an absolute frame.

1.2 Open-loop vs. closed-loop calibration

In short, a closed-loop calibration uses the robot encoders as a measurement system and an object of precisely known geometry is used as a reference to perform calibration. Whenever we use a measurement system to directly measure the pose of the robot tool, such as a laser tracker, we apply an open-loop calibration. On the other hand, a closed-loop method is used if the robot tool is constrained to lie on a reference object of precisely known geometry. This method only needs a switch such as a touch probe to detect the contact with an obstacle, when the robot is placed at the contact position the joint values given by the encoders are registered.

We can find several methods used for measuring robot position as the measurement system technology has improved a lot in the past two decades. Some examples of open-loop methods are acoustic sensors (Stone and Sanderson, 1987), visual systems such as cameras (Meng and Zhuang, 2001; Puskorius and Feldkamp, 1987), coordinate measuring machines (CMM) (M R Driels et al., 1993; Lightcap et al., 2008; B. W. Mooring and Padavala, 1989) and, of course, laser tracking systems (Shirinzadeh, 1998). There has also been some research work that allows a laser tracking system to identify the 6 parameters of the tool pose (Vincze et al., 1994).

One example of closed-loop calibration is the MasterCal commercial product from American Robot, where the constraints are the diameter of two spheres and the distance between their centers. Other examples are the use of planar constraints (Ikits and Hollerbach, 1997), or point constraints (Meggiolaro et al., 2000) or (Houde, 2006).

1.3 Robot calibration process

A robot calibration process is divided in four sequential steps (Roth et al., 1987): modeling, measurement, identification and correction. The modeling step consists of finding a model that represents the real robot through its kinematics equations. It is the robot model that takes into account the various error parameters to calculate the pose with respect to the robot joints. Data from the real robot allows generating the equations that the identification algorithm will use to find an improved robot model, better than the nominal kinematic model.

It is important to differentiate tool calibration from robot calibration. We may usually calibrate the tool at the same time as the robot is being calibrated. However, a separate tool calibration must be taken into account when the tool which we want to be precisely positioned is not the one that we used during calibration.

Through robot calibration we obtain a new model that can represent the real robot better than the nominal model. The nominal model is the one used in the robot controller, and for decoupled robots, with the so-called inline wrists (the axes 4, 5 and 6 intersect at one point), the inverse kinematics of the nominal model is simple and can be solved analytically. A robot calibration implies error parameters inserted to design parameters (nominal model) that represent the real source of errors. These parameters are called error parameters which must be found by the calibration method.

Although optimization algorithms are not primordial when calibrating a robot, they can be very helpful in improving precision if they are used appropriately. Some optimization algorithms are described in Section 1.6.

A robot calibration can be divided in three levels (B. Mooring et al., 1991). The calibration level will be defined depending on which real error parameters the model represents.

1.3.1 Level-1 calibration

The goal in a level-1 calibration is to properly define the relationship between the desired joint position (θ_d) and the real joint position (θ_r). In the nominal model we consider that they are both the same, however, in real life we have a more complex relationship where the real joint positions are a function of the desired joints $\theta_r = \mathrm{f}(\theta_d)$. This relationship may be difficult to obtain properly but we can reach good approximations with linear functions in a reduced workspace. The most basic linear relationship would be:

$$\theta_r = k_1 \theta_d + k_0. \tag{1.1}$$

Where k_0 is the offset constant and is close to zero whereas k_1 is the proportionality constant. A level-1 calibration is also known as a "joint level" calibration.

1.3.2 Level-2 calibration

A level-2 model is defined as a robot *kinematic calibration*. That means that some, or all, of the geometric parameters are modelled. Distance and angle offsets are added as error parameters to the robot's nominal design. At the same time, a level-2 model can include a level-1 model to model the behavior of the joints.

When an entire kinematic calibration is needed we can identify the robot's joint axes and extract the kinematic parameters placing frames that relate each joint axis with the next one. The calibration needs the virtual joint axes in the same absolute reference frame and the geometry of the end-effector referred to the robot's tool frame. To extract the virtual axes we must set the robot at the home position, and moved each joint one by one taking measures by intervals (B. Mooring et al., 1991). A circle that minimizes the sum of error squares can fit these points. From these circles we can extract the axes.

This idea was developed independently by several researchers. Once we have the virtual robot axes there are basically two methods to extract the kinematic parameters: Stone's method and Sklar's method (B. Mooring et al., 1991). Stone's method (Stone and Sanderson, 1987) finds the kinematic model known as "S-model" (6 parameters per joint) and Sklar's method finds the D-H representation of the robot placing the frames at the appropriate place. Both methods are explained and compared in (B. Mooring et al., 1991).

1.3.3 Level-3 calibration

A level-3 model takes into account any non-geometrical error sources. Non-geometrical sources of errors can be stiffness, friction, backlash, dynamical parameters, etc. A level-3 model usually contains level-2 and level-1 error parameters. Most common robot calibrations include a full kinematic calibration (level-2) and sometimes a few parameters describing the stiffness of the robot's arm (level-3) (Aoyagi et al., 2010; Dumas et al., 2011; Lightcap et al., 2008; Marie et al., 2013; Saund and DeVlieg, 2013).

1.4 Kinematic modeling

The best-known four-parameter representation model in robotics is the one given by Denavit-Hartenberg (Denavit and Hartenberg, 1955). This so-called D-H notation is widely used in robotics. There is also a very similar and well-known representation commonly referred to as Denavit-Hartenberg Modified (D-H M) notation, which is the notation defined by (Craig, 1986). Both representations model the kinematic parameters of the robot, the main difference remains on the order of the geometrical transformations. Both make a translation and rotation over the *X* and *Z* axis (one translation and one rotation each). The D-H notation starts with a rotation about the *X* axis while the D-H M notation starts with a rotation about the *Z* axis (translation and rotation around the same axis can be alternated with no final effect). For a detailed review of the direct kinematic modeling, see (Craig, 1986; Paul, 1981; Slotine and Asada, 1992).

The D-H notation has been used by several researchers for robot calibration, such as (Veitschegger and Wu, 1987; Wei and De Ma, 1993). However, this representation introduces singularity problems when two consecutive axes are parallel or almost parallel (Hayati and Mirmirani, 1985). The complete and parametrically continuous (CPC) model eliminates this problem (Hanqi Zhuang et al., 1992) by representing the relationship between each link with three translations and one rotation instead of two translations and two rotations. Similarly, the product of exponentials (POE) representation makes the error parameters vary smoothly with changes in joint axes so that no special descriptions are required when consecutive joint axes are close to parallel (Brockett, 1984; I.-M. Chen et al., 1997; Okamura and Park, 1996; Park, 1994).

Finally, other types of representations have also been used. There is a five-parameter representation for prismatic joints (Hayati and Mirmirani, 1985) or even six parameter representation (Stone and Sanderson, 1987), but if we insert more than four parameters the calibration problem becomes redundant.

1.5 Inverse kinematics computation

Solving the inverse kinematics of a decoupled 6R serial robot is straightforward, and it can be achieved using analytical methods (Craig, 1986). For a calibrated robot it is also necessary to find a way to calculate the inverse solution for a given model and pose, also known as the inverse displacement problem (IDP). Modifying the robot model's parameters within the robot controller is usually difficult or impossible depending on the complexity of the model chosen. Therefore, the best solution is to use fake targets which modify the real coordinates by a slightly modified target which takes into account the nominal model calculations of the robot controller.

Once the robot model is defined, we should describe how we are going to solve the inverse solution of the calibrated robot. There are many solutions available in the literature but not all of them are suitable to all robot models. Depending on what level of calibration we use we will need one or another inverse solution. Inverse kinematics calculation can be divided in two main types: analytical and numerical.

1.5.1 Analytical

We should use an analytical solution to the IDP for the calibrated robot model whenever possible. However, as we add error parameters to our basic kinematic model, the simplifications that we can usually do on a nominal model can no longer be done due to the complexity of the equations. A semi-algebraic method to solve the IDP was found to simplify a level-2 model (geometric model) into a 16th degree polynomial (Angeles, 2007), at this point numerical computations are needed to obtain the solution. To the best of our knowledge, there has not been any work that obtains an analytical solution for a level-3 calibration.

1.5.2 Numeric

Iterative solutions offer an easy way to solve complex problems at a cost of computation time. Obviously, when an algebraic solution cannot be found, an iterative method must be applied. This numerical method approaches the solution at each iteration. In some cases, the robot model can be seen as a black box that can only compute the forward calculation obtaining the pose given the joint angles. Industrial robots have path motion planners that cut a path (trajectory) into a large number of targets and the inverse solution must be applied to each point of the path.

Any generic optimization method could be applied to solve the IDP, such as the optimization algorithms used to obtain the modelled error parameters; however, better optimization methods exist as the problem is more specific. In the worst case we have to find as many parameters as the number of joints that the robot has.

Numerical methods can be divided in three types (N. Chen and Parker, 1994): (1) Newton-Raphson methods, (2) predictor-corrector type algorithms, and (3) optimization techniques using the formulation of a scalar cost function. Examples of the first method can be found in (Angeles, 1985), where a modified Newton-Gauss method is used. Such methods involve the computation of the Jacobian matrix. A comparison between Newton-Raphson methods and predictor-corrector-type algorithms is provided in (Gupta and Kazerounian, 1985), where the authors conclude that the latter are faster.

An example of a predictor-corrector algorithm is given in (Tsai and Orin, 1987). This type of method often requires a large number of iterations, and does not always converge. Some of these algorithms also require computation of the Jacobian matrix, like the algorithm proposed in (Goldenberg et al., 1987), which combines a predictor-corrector type of algorithm with a least-squares optimization technique, or the closed-loop method (Siciliano, 2009) where the inverse kinematic problem is solved as a control problem for a simple dynamic system. However, optimization techniques are usually complex, and several iterations are needed to achieve a solution.

Two approaches for level-2 calibrations are proposed in (Vuskovic, 1989) using the nominal inverse kinematics. However, the solution becomes complex when the number of error parameters increases. The resolution of a nonlinear programming problem is divided into two phases in (L. C. T. Wang and Chen, 1991) for greater efficiency.

The amount of computing time to solve the IDP is greatly improved in (N. Chen and Parker, 1994) by calculating a so-called pose shift by iteratively adding and subtracting computed poses based on a truncated-series expansion of the desired pose. However, we realized that their method could be further improved by using pose multiplications based on a geometric principle, instead of adding and subtracting the poses of the truncated-series expansion of the desired pose.

Finally, we introduced a new geometrical approach to solving the IDP (Albert Nubiola and Bonev, 2014). Similar to (N. Chen and Parker, 1994), our method does not need the computation of the Jacobian matrix or derivatives of any kind. Up to eight solutions can be obtained from the sixteen possible solutions of the IDP.

1.6 Optimization algorithms

Once we have defined a robot model we must obtain the error parameters by taking measurements from the real robot. The most suitable optimization algorithms for most types of robot models are nonlinear and unconstrained. Plenty of algorithms, more precisely the genetic algorithm (K. Wang, 2009), represent small variations of kinematic parameters and the end-effector error is represented by a fitness function. At every generation, a population of parameters is created and brings a better solution to replace the existing solution. This technique does not need computationally expensive calculations such as the inverse of the Jacobian matrix.

Other alternatives for robot calibration have been reported in the literature, such as the Taguchi method (Judd and Knasinski, 2002; Karan and Vukobratovic, 1994) or (Judd and Knasinski, 2002). The work (H Zhuang and Roth, 2002), for example, uses different methods to identify the unknown error parameters (similar to the CPC model).

Optimization methods can be mainly classified in two types: line-search methods and trust-region methods. We can also describe an optimization method that differs from the first two types: the Nelder-Mead method.

1.6.1 Line-search methods

There are different types of line-search optimization methods. They differ by the way they compute the line search direction. We can find the following line-search methods: Newton's method, gradient descent method and Quasi-Newton method (Bonnans and Lemaréchal, 2006).

Newton's method is also known as Newton-Raphson method. Newton algorithms are implemented in Matlab's optimization toolbox in the functions fsolve, fminunc and lsqcurvefit.

1.6.2 Trust-region method

The trust-region method is also known as restricted step method. It handles the case when the Jacobian matrix is singular and it is useful when the initial guess is far from a local minimum. This method approximates the objective function with a simpler function in the neighborhood of the solution at each iteration.

Trust region methods are dual to line search methods. The first one chooses a step size before a search direction while the second one chooses a search direction and then a step size.

1.6.3 Nelder-Mead

This optimization algorithm was proposed by John Nelder and Roger Mead (Nelder and Mead, 1965). It is also called simplex method (a non linear method that is different from the known linear simplex method). It evaluates the objective function over a polytope in the parameter space. If we have two parameters, the polytope is a triangle as we are in a 2D plane. If there are n-dimensions, we have an (n+1)-sided polytope.

The algorithm compares these n+1 points and deletes the worst one. The worst point is replaced by its reflection through the remaining points in the polytope. This algorithm is simple and does not need gradient information but it takes time to achieve a solution when we have more than six variables. This method is also implemented in Matlab's optimization toolbox, in the function fminsearch.

1.7 Commercial solutions for robot calibration

Most robot manufacturers offer calibration as an option. For example, in the case of ABB Robotics, most of its robots can be calibrated at the factory with the CalibWare software for about C$2,000 per robot, using a Leica laser tracker, a single SMR (Spherically-mounted reflector) and around 40 error parameters. However, ABB does not offer an on-site calibration service, unlike KUKA. ABB also has a tool to improve resolver offsets due to motor exchange and maintenance: the calibration pendulum.

As an example, L-3 MAS Canada at Mirabel use Motoman industrial robots and have them calibrated on-site by Motoman, who use a third-party calibration software (from Dynalog). Similarly, Messier-Dowty at Mirabel use three KUKA industrial robots and have them calibrated on-site by KUKA.

1.7.1 Dynalog

Dynalog is a Detroit-based privately held company founded in 1990 by Dr. Pierre De Smet, then professor at Wayne State University. Dynalog is the most renowned expert in robot calibration. While the company offers several products improving the accuracy of industrial robots, the two of greatest interest are the CompuGauge hardware and the DynaCal software. The first is a 3D (x, y, z) measurement device based on four string encoders that intersect at one point. Dynalog claims that the volumetric accuracy of the CompuGauge measurement device is 0.150 mm and its repeatability is 0.020 mm inside a cubic working volume of side 1.5 m. The price of this device is at least US$9,000, but while not expensive, the device is quite bulky and difficult to install.

Figure 1.1 Robot calibration using the CompuGauge device[1]

DynaCal is the software for robot calibration that accepts measurement data from the CompuGauge device or from any other precise 3D or 6D measurement device. The software and the adapters for fixing SMRs are sold to industry for more than US$40,000. While all demonstrations of DynaCal show the use of a laser tracker and a single SMR, it seems that DynaCal can also work with three SMRs, thus calibrating the complete pose of the end-effector.

Dynalog also has a specific patented product to calibrate robots that is used for part inspections (De Smet, 2001). Dynalog offers a complete robot library which makes it possible to calibrate many robots from different brands.

1.7.2 Nikon Metrology

Metris International Holding was purchased by Nikon in 2009 to create Nikon Metrology. Metris, a market leader for CMM based laser scanning, was founded in 1995 and is

---

[1] http://www.dynalog-us.com/images/imageLibrary/_ClientAndPartner/CompuGauge.jpg

headquartered in Belgium. In 2005, Metris acquired Belgium-based Krypton, which was specializing in robot calibration since 1989.

Nikon Metrology offers a large number of metrology systems, but the two that are of particular interest to us are the K-Series Optical CMM and the ROCAL software. The first one is basically a three-camera system that measures the spatial coordinates of up to 256 infrared LEDs (thus, it can provide 6D measurements). The volumetric accuracy of the K-Series Optical CMM is better than 0.090 mm which is close to the laser tracker accuracy and certainly sufficient for robot calibration. Its price is about C$80,000.

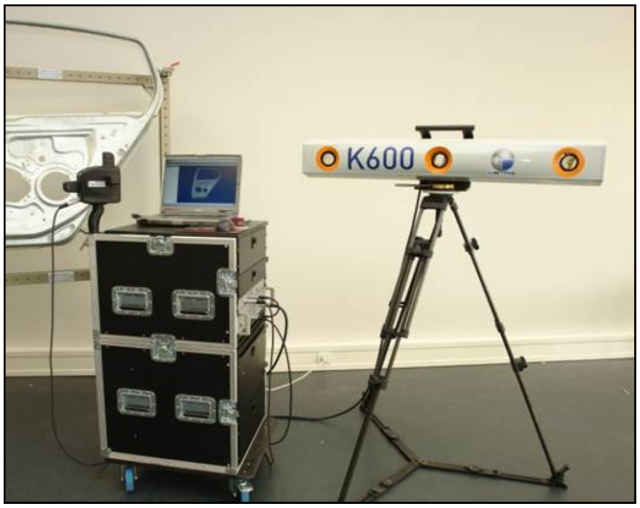

Figure 1.2 Nikon K-Series optical CMM[2]

ROCAL is software for robot calibration, very similar to Dynalog's DynaCal. It seems that some of the differences are a better integration with some robot brands (KUKA, Mitsubishi and COMAU) and the software's incompatibility with measurement devices other than the K-Series Optical CMM. The software also relies on complete pose measurement data.

---

[2] http://www.nikonmetrology.com/var/ezwebin_site/storage/images/products/portable-measuring/optical-cmm/k-series-optical-cmm/179510-2-eng-GB/K-Series-Optical-CMM.jpg

1.7.3 Teconsult

Teconsult is a Germany based university spin-off offering a unique 3D optional measurement device called ROSY and the robot calibration software that goes with it. Teconsult was founded by Prof. Lukas Beyer in 1999. ROSY is a measuring tool based on a videometric principle with two digital CCD cameras. Two cameras are used in order to get a more uniform volumetric accuracy. The tool is attached to the robot flange and is used to measure, with respect to the robot flange frame, the spatial position of the center of a small white ceramic ball that is fixed with respect to the robot's base. The ROSY device itself is calibrated on a CMM before shipment.

The calibration procedure consists of reorienting the tool and measuring the position of the ball for 40 different poses (Beyer and Wulfsberg, 2004), for a single location of the ceramic ball. According to reference (Beyer and Wulfsberg, 2004) the volumetric accuracy of ROSY is ±0.020 mm inside a spherical measurement range of ±2 mm. However, ROSY is offered in several different sizes, and there is no information whether that volumetric accuracy is for a small or for a large ROSY device.

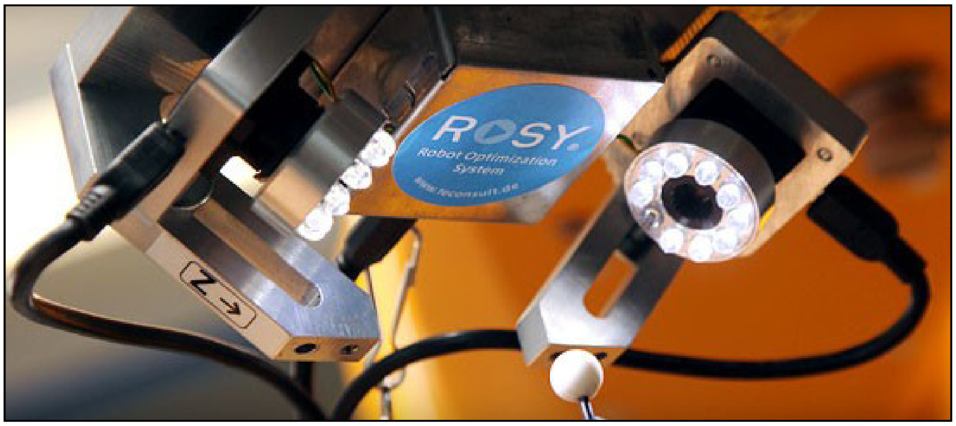

Figure 1.3 Rosy measurement device[3]

---

[3] http://www.teconsult.de/sites/default/files/styles/header_content/public/1304_rosy1_695_240_0.jpg

ROSY is rather bulky and requires removal of the end-effector from the robot. Furthermore, it requires several relatively thick cables to be run along the robot arm. A complete ROSY system for tool, base and robot calibration is about €17,500 (US$21,000). However, it seems that Teconsult does not offer any means to calculate the inverse kinematics.

1.7.4 Wiest AG

Wiest is another Germany based university spin-off offering another unique 3D optical measurement device called LaserLAB and the robot calibration software that goes with it. Wiest AG was founded by Dr. Ulrich Wiest who has been working in the field of robot calibration since 1996 (he obtained his doctoral degree in 2001).

LaserLAB is patent-pending (Wiest, 2003) and consists of five small-range one-dimensional laser distance sensors mounted to a common frame and with their lasers intersecting at a common point. A ball is attached to the end-effector of the robot while the LaserLAB device is stationary. By measuring the five distances to the ball (when the center of the ball is approximately at the lasers intersecting point), the spatial coordinate of the center of the ball with respect to the LaserLAB are determined. The repeatability of the LaserLAB is ±0.020 mm, while its volumetric accuracy is better than ±0.100 mm (typically ±0.035 mm), inside a measurement range of 39.5 mm × 38.5 mm × 36.5 mm.

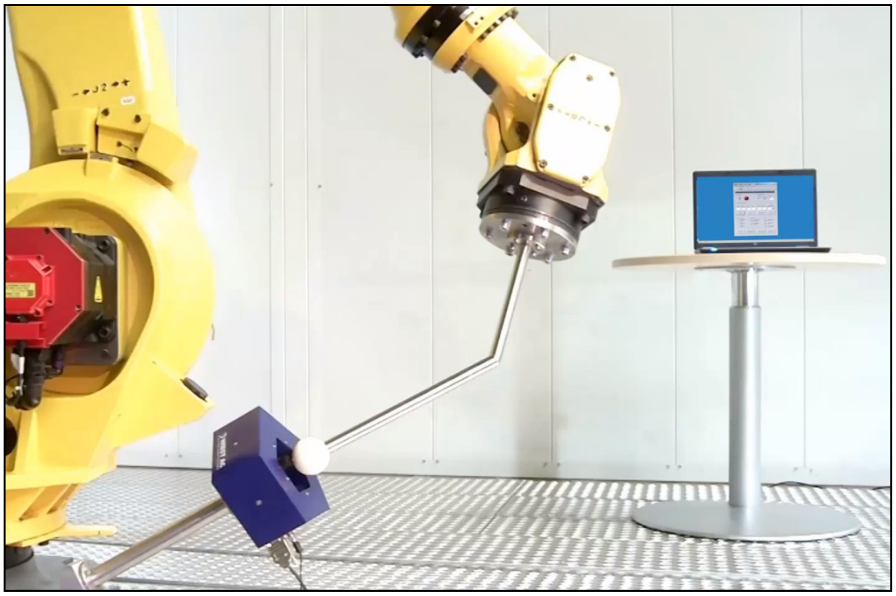

Figure 1.4 Robot calibration using LaserLAB[4]

One disadvantage of the LaserLAB is the high likelihood of the sphere colliding with the measurement device while the robot is re-oriented. Furthermore, the only way to measure with a wide range of robot configurations is to use extension rods of different lengths at the end of which a sphere is mounted, rendering that solution practically inconvenient and therefore realistically inaccurate.

1.7.5 American Robot Corporation

American Robot Corporation (ARC) is a US company based in Pittsburg, Pennsylvania. ARC was established in 1982 and is a manufacturer of industrial robot controllers, industrial robots, and automation systems. It has three major product lines, the Universal Robot Controller, the Merlin articulated six axis robot, and the Gantry 3000 modular gantry robot. ARC also offers a robot calibration software called MasterCal, which makes use of a standard touch probe attached to the flange of a robot and two fixed precision balls separated by a precisely known distance.

---

[4] https://www.youtube.com/watch?v=GywDyZIVwmI

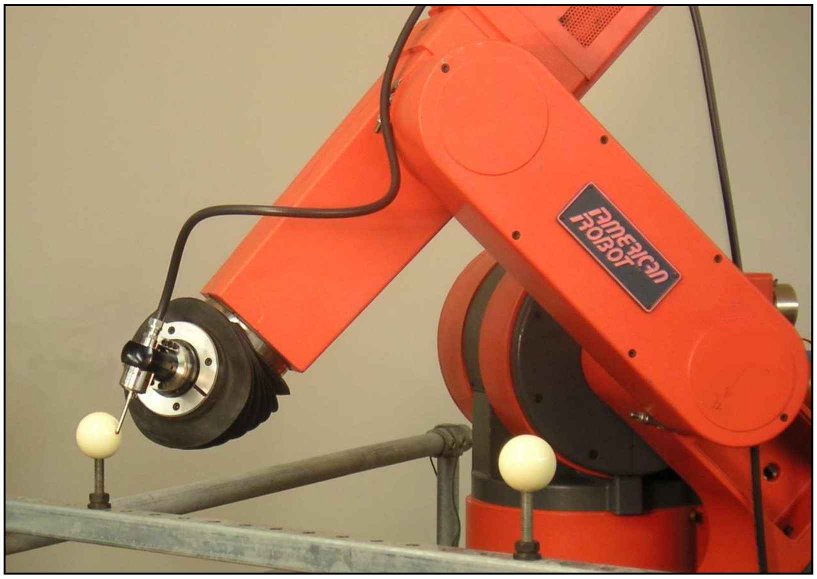

Figure 1.5 MasterCal calibration setup[5]

The MasterCal calibration procedure was invented and patented by Mr. Wally Hoppe (Hoppe, 2011), a Group Leader and Senior Research Engineer at the University of Dayton Research Institute in Ohio, USA. The basic concept for Mr. Hoppe's calibration method is an extension of (Meggiolaro et al., 2000), where a single ball-in-socket mechanism was used. Mr. Hoppe's institution had a huge military contract for robot inspection of aircraft engines and this is how he ended up devising a robot calibration method (he no longer works in robotics). In the course of the patent application, he eventually came across some inventions that are pretty close to this one, although he worked with his lawyer to demonstrate that they do not infringe. The closest method to his invention is by ABB (Snell, 1997). That method uses a single large-diameter precision ball of known diameter and a touch probe. Another very close invention is (Knoll and Kovacs, 2001), which is very general and does not give a lot of detail.

---

[5] http://www.americanrobot.com/images_products/kinecal_image02_t.jpg

1.8 Recent calibration results reported in the literature

Research in robot calibration has always been focused on level-2 and level-3 calibrations. A typical example of a level-3 calibration using a stiffness model is (Lightcap et al., 2008), that applies a torsional spring model to represent the flexibility of the harmonic drives by physically meaningful parameters, this model takes into account the flexibility caused by the end-effector. The model improves the mean / maximum error values from 1.77 mm / 4.0 mm to 0.55 mm / 0.92 mm for a Mitsubishi PA10-6CE when loaded at 44 N (validated with only ten measurements on a CMM). This method is more simple than the one proposed in (Khalil and Besnard, 2002) as it does not need the computation of the generalized Jacobian. Also (Caenen and Angue, 1990) represented the angular deformation caused by gravity force. A similar method exists dealing with joint angle dependent errors (Jang et al., 2001).

An example of a kinematic calibration is given in (Ye et al., 2006), where an absolute calibration was performed to an IRB 2400/L with a Faro *Xi* laser tracker. The mean position error is reduced from 0.963 mm to 0.470 mm for twenty measurements (maximum values are not given, the area of calibration is not given either).

Another example of absolute calibration with a laser tracker is (Newman et al., 2000). Using a Motoman P8 robot, the 27 error parameters from their kinematic model are identified by measuring 367 targets moving each axis separately. The kinematic model that gave best results (for a validation of 21 measurements) corresponds to a "circle-point" algorithm that improves the RMS error from 3.595 mm to 2.524 mm.

We can also mention the work performed by (Bai et al., 2003) that uses a modified CPC model (MCPC) (H Zhuang et al., 1993) to improve the kinematics of a PUMA 560 with 30 error parameters and a laser tracker measurement system. Using 25 measures for parameter identification and 15 measures for verification they reach a mean position error of 0.1 mm, however, when they use a CMM they find that the same position error is 0.4-0.5 mm. The CPC model avoids the singularities associated with parallel axes.

Other examples of stiffness kinematic models that do not use meaningful parameters are (Jang et al., 2001; Meggiolaro et al., 2005). As stated by (Lightcap et al., 2008), it is better to use meaningful parameters to be able to extrapolate to unknown charges.

The most recent robot calibration research has been focused on modelling the joint stiffness to improve robotic machining applications (Dumas et al., 2011; Marie et al., 2013; Saund and DeVlieg, 2013; Sornmo et al., 2012). For example, (Marie et al., 2013) use a level-3 model (which they call elasto-geometrical) to improve the robot accuracy in machining, forming or assembly applications. The level-3 model contains 27 geometrical error parameters plus 10 error parameters to model the stiffness behavior of the robot. To test the accuracy performance, a KUKA-IR663 robot is calibrated in 126 poses with a payload of 90 kg using the Nikon K600-10 optical CMM, the poses are distributed in a vertical plane grid. The robot accuracy is validated in another set of 63 poses for a 90 kg load and 60 kg separately, the maximum error accuracy of the robot is improved up to 0.371 mm. The robot calibration is compared to a fuzzy logic calibration in the vertical plane of interest. Using this fuzzy logic calibration the maximum error is improved to 0.183 mm.

Another example that focuses on improving the robot accuracy for machining applications is (Sornmo et al., 2012). In this case, the accuracy is not improved through robot calibration but by using a piezo-actuated high-dynamic micro manipulator and a Keyence laser sensor LK-G87 as a tracking system. This paper focuses on improving the surface roughness after a machining process. The surface roughness is improved by a factor of 2.7 in the best case scenario (from 67.0 μm to 24.5 μm).

We can even find companies that perform robot calibration driving the robot using a custom-made controller. This is the case of Electroimpact (Saund and DeVlieg, 2013), that calibrate a Kuka KR360-2 robot as well as the linear axis replacing the original controller for a Siemens 840Dsl CNC controller.

Finally, we can find a level-3 calibration using 26 geometrical error parameters plus 4 parameters to model the stiffness of joints 2 to 5 (Albert Nubiola and Bonev, 2013). The ABB IRB 1600-6/1.45 robot is calibrated using a Faro ION laser tracker in 52 configurations using three different targets. The maximum position error of the robot is improved from 2.158 mm to 0.696 mm in 1000 configurations using eight different targets. It is also found that the axis 6 has a peculiar error following a Fourier series, probably due to the gear chain in the robot wrist. In the product documentation of a calibrated ABB IRB 1600-6/1.45, it is stated that the typical mean / maximum positioning accuracy is 0.300 / 0.650 mm. We know from Dr. Torgny Brogardh, scientist at ABB Robotics, that this is validated for one tool target (apparently the same target used for calibration). However, we do not have more information regarding the validation procedure, such as the number of measurement configurations.

CHAPTER 2

COMPARISON OF TWO CALIBRATION METHODS FOR A SMALL INDUSTRIAL ROBOT BASED ON AN OPTICAL CMM AND A LASER TRACKER

Albert Nubiola, Mohamed Slamani, Ahmed Joubair and Ilian A. Bonev,
1100 Notre-Dame Ouest, Montréal, Québec, Canada H3C 1K3

This chapter has been published as an article in
Robotica: vol. 32, n° 3 (2014), pp 447-466

Abstract

The absolute accuracy of a small industrial robot is improved using a 30-parameter calibration model. The error model takes into account a full kinematic calibration and five compliance parameters related to the stiffness in joints 2, 3, 4, 5, and 6. The linearization of the Jacobian is performed to iteratively find the modeled error parameters. Two coordinate measurement systems are used independently: a laser tracker and an optical CMM. An optimized end-effector is developed specifically for each measurement system. The robot is calibrated using fewer than 50 configurations and the calibration efficiency validated in 1000 configurations using either the laser tracker or the optical CMM. A telescopic ballbar is also used for validation. The results show that the optical CMM yields slightly better results, even when used with the simple triangular plate end-effector that was developed mainly for the laser tracker.

2.1 Introduction

It is well known that the accuracy of an industrial robot can be improved through a process known as *robot calibration* (Roth et al., 1987). The first step in this process is to choose a theoretical model that is closer to reality than the nominal model used in the robot controller (e.g. the wrist axes are no longer concurrent and the gearboxes are flexible in the new model). The parameters of this model are then identified by measuring the *complete pose* or *partial pose* of the robot end-effector in a set of *calibration configurations*. In practice, the most critical issue is the choice of measurement system, as the latter determines the efficiency and cost of the robot calibration process.

The identification process can be performed using a wide range of commercially available or custom-designed measurement tools, such as a touch probe and a reference artifact (Besnard et al., 2000; Hayati and Mirmirani, 1985), a telescopic ballbar (M.R. Driels, 1993; Juneja and Goldenberg, 1997), a small-range 3D (position) measurement device, such as a camera-based system (Beyer and Wulfsberg, 2004) and acoustic sensors (Stone and Sanderson, 1987), a large-range 3D measurement device (such as a laser tracker (Dumas et al., 2010; Meng and Zhuang, 2001; Albert Nubiola and Bonev, 2013; Puskorius and Feldkamp, 1987) or CMM (M.R. Driels, 1993; Lightcap et al., 2008; B. W. Mooring and Padavala, 1989)) and a 6D (pose) measurement device, such as a camera-based system (Gatla et al., 2007; Meng and Zhuang, 2001; Puskorius and Feldkamp, 1987) or a laser tracker with a 6D probe (Boochs et al., 2010).

To the best of our knowledge, most industrial robot manufacturers who offer calibration as an option use either a laser tracker (one manufactured by Leica, in the case of ABB and FANUC) or a 6D optical CMM (Nikon Metrology's K-series optical CMM, in the case of KUKA). Furthermore, at least two commercial robot calibration software packages exist, based on 3D or 6D measurement data: DynaCal from Dynalog, and Rocal from Nikon Metrology (both companies based in the US).

In practice, two types of commercially available position/pose measurement tools can be used for calibrating industrial robots: laser trackers (from Leica, FARO, or API) and optical CMMs (from Nikon Metrology, Northern Digital, Metronor, Geodetic Systems, AICON, GOM, or Creaform). Laser trackers are more accurate and have a very large measurement range, but they are highly sensitive to the ambient conditions (e.g. the air currents present in factory hangars) and are extremely expensive (from at least $100,000 US to nearly $200,000 US or more). Laser trackers generally measure the 3D coordinates of a single point at a time, but they can also be used to measure the complete pose of the robot end-effector in static conditions, by measuring three SMRs (spherically mounted reflectors), or, in dynamic conditions, by using a special 6D probe for measuring. However, at each moment, a laser tracker measures the position or pose of a single body relative to its own reference frame. Therefore, vibrations of the factory floor can significantly decrease the accuracy to which the position or pose of the robot end-effector is measured with respect to the robot base frame.

In contrast, optical CMMs can measure the pose of the robot end-effector dynamically (i.e. at frequencies of 30 Hz or more) with respect to its base. Their measurement volume is smaller than that of laser trackers and they are slightly less accurate (though probably not in real factory conditions), but they are much less expensive and easier to use. Furthermore, optical CMMs can also be used to correct the pose of the end-effector iteratively, as is currently done by Nikon Metrology's Adaptive Robot Control software in conjunction with their K-series optical CMMs.

Some optical CMMs (e.g. those from Nikon Metrology and Northern Digital) use *active targets*, which are basically infrared LEDs emitting light at prescribed frequencies. Active targets are relatively expensive and cumbersome, but have the advantage of being easily identifiable (targets are illuminated one at a time) and not sensitive to external light conditions. Other systems, such as Creaform's C-Track, use *passive targets*, which are basically small circular stickers covered with retro-reflective material and costing no more than a few cents each. The main advantage of passive targets is that one can use plenty of them to build a spatial artifact, the pose of which can be measured with the optical CMM in virtually any orientation.

What motivated this work is the question of whether or not an optical CMM that can measure the pose of a robot end-effector in any orientation is as efficient as a laser tracker in calibrating industrial robots, even in perfect laboratory conditions (where laser trackers have the advantage). Of course, a laser tracker can also be used to measure the pose of an object in any orientation, but this would either require too much operator intervention during the measurement process, or an artifact with dozens of SMRs that would cost thousands of dollars to manufacture. Note that there are commercial 6D tracking devices that can be used in conjunction with a laser tracker (e.g. Leica's T-Mac or API's SmartTRACK); however, these are not only very expensive, but also function in a rather limited orientation range (Boochs et al., 2010). In contrast, developing such a spatial artifact out of passive reflectors would add only a small fraction to the cost of an optical CMM.

We believe that our work here is the first to compare the efficiency of a laser tracker in industrial robot calibration and that of a commercially available optical CMM. In particular, we use a FARO laser tracker in conjunction with three SMRs and Creaform's C-Track (launched in 2010), in conjunction with two custom designed artifacts. The robot to be calibrated is an ABB IRB 120. This model is ABB's smallest industrial robot, launched in 2009, and is one of the few robots for which ABB does not offer factory calibration. We used a standard calibration model that takes into account all 25 kinematic parameters, as well as 5 compliance parameters, for the harmonic gearboxes of axes 2, 3, 4, 5, and 6. These 30 parameters are identified by linearization of the model in fewer than 50 calibration poses obtained through an observability study. Finally, the efficiency of the robot calibration process in each of three different setups is validated with a Renishaw telescopic ballbar.

The three experimental setups used are described in the next section. Section 2.3 describes the robot kinematic model, while Section 2.4 shows the sources of non geometric errors and summarizes the non kinematic model. The calibration procedure is described in Section 2.5, and the results are given in Section 2.6. Our conclusions are presented in Section 2.7.

2.2 Experimental setups

Figure 2.1 shows the installation used for calibrating the ABB IRB 120 robot with a FARO laser tracker ION. Our laser tracker has only the ADM option, which means that it is slightly less accurate (compared to when using the interferometry option) but allows full automation of measurements, as the laser beam can be redirected from one SMR to the other without the need for manual initialization. The robot was fixed to a heavy steel table which was immobilized with about 200 kg of additional load on its lower shelf. An SMR fixed on the table was measured using the laser tracker in various robot configurations, and it was shown that the table top does not deflect by more than ±0.010 mm at the SMR's location for the speeds and accelerations used. A special triangular artifact with three 0.5″ SMRs (and nine retro-reflective self-adhesive targets on each planar face) was used, and will be described in section 2.1.

According to the specifications of our laser tracker, its typical accuracy when measuring the length of a 2.3 m horizontal scale bar at a distance of 2 m is 0.022 mm. According to our own tests, the largest error when measuring the length of a 1 m scale bar mounted on the end-effector of our robot and located at various places within the robot workspace is about 0.060 mm (the mean error being only 0.035 mm). The laser tracker was not moved from the position depicted in Figure 2.1 at any time during measurement.

Figure 2.2a shows the installation used for calibrating the robot with Creaform's C-Track and the same triangular artifact. Figure 2.2b shows the fifteen retro-reflective self-adhesive targets that were attached to the base of the robot. All measurements with the C-Track (with both artifacts) were taken relative to the robot's base (unlike the case with the laser tracker). The device was not moved from the position depicted in Figure 2.2a at any time during measurement (with both the triangular and the spatial artifacts).

The C-Track comes with a special hand-held planar artifact, called the HandyPROBE, which has a rigid probe. The HandyPROBE is used for measuring 3D coordinates, and its volumetric accuracy is 0.075 mm, as per ASME standard B89.4.22. Our own tests showed that the largest error when measuring the length of a 0.5 m scale bar using the HandyPROBE was about 0.065 mm.

The C-Track model used for the tests is the 780, with a measurement volume of 7.8 m^3. However, we calibrated it in a volume of 3.4 m^3, which was enough for our tests. The accuracy recorded by the C-Track's software after completion of the calibration procedure with a special 1 m scale bar was 0.040 mm.

Figure 2.3 shows a close-up of the installation used for calibrating the robot with the C-Track and the spatial artifact described in section 2.2.

All measurements were performed in a relatively small laboratory at temperatures varying between 22.5°C and 23.5°C. The C-Track, the laser tracker, and the robot were controlled by MATLAB, via Ethernet LAN. Thus, the procedure for taking measures is fully automated and requires no manual intervention (e.g. for reorienting the SMRs or moving the tool-changer's two air hoses). The position commands sent to the robot are the joint values (i.e. we send *jointtargets* and use the RAPID instruction *MoveAbsJ*).

In each of the three setups, the range of measurable end-effector orientations is obviously different. To take full advantage of each setup, any pose can be a candidate for the identification or the validation phase, as long as it is measurable (with the laser tracker in the first setup, and the C-Track in the second and third setups). In the first setup, the SMRs are orientated outward (see Figure 2.1), and the only end-effector orientations used are those in which the ±30° visibility cone of at least one of the SMRs covers the laser tracker. In the second setup, the angle between the normal to the planar surface of the triangular artifact and the line of sight of the C-Track is limited to 15° (both sides of the artifact are used). In the third setup, there are no limits to the orientation of the robot end-effector. However, because the robot arm partially hides the artifacts in some robot configurations, a condition is imposed such that at least nine retro-reflective targets from the triangular artifact are seen by the C-Track and twenty from the spatial artifact.

Note that, initially, we also considered a fourth case in which the position of one of three SMRs mounted on the spatial artifact was measured with the laser tracker. However, this fourth case was promptly discarded, since there is obviously no advantage of using the spatial artifact with a laser tracker.

A video showing the experiments described in this paper can be seen at http://youtu.be/i0ztjX0jlSU.

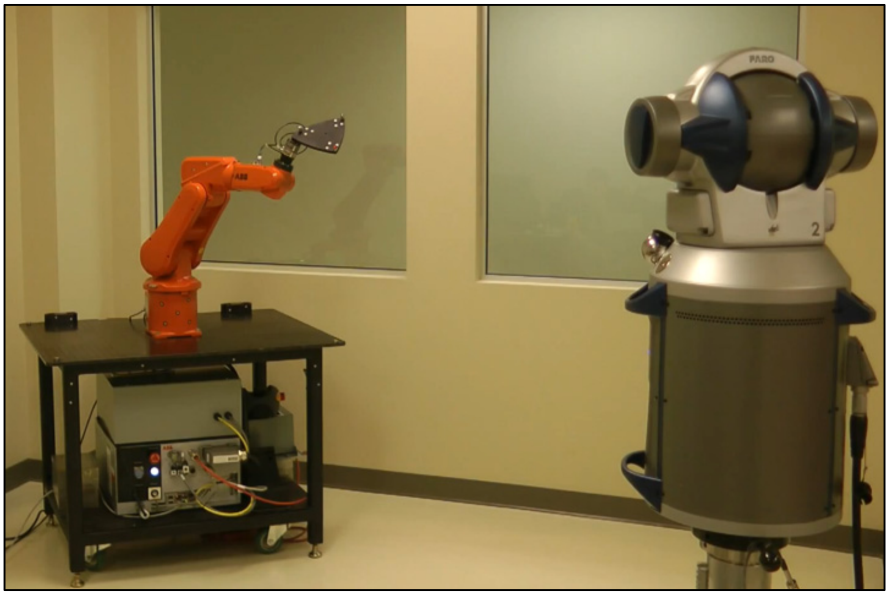

Figure 2.1 Experimental setup for calibrating the robot with FARO's ION laser tracker

(a)

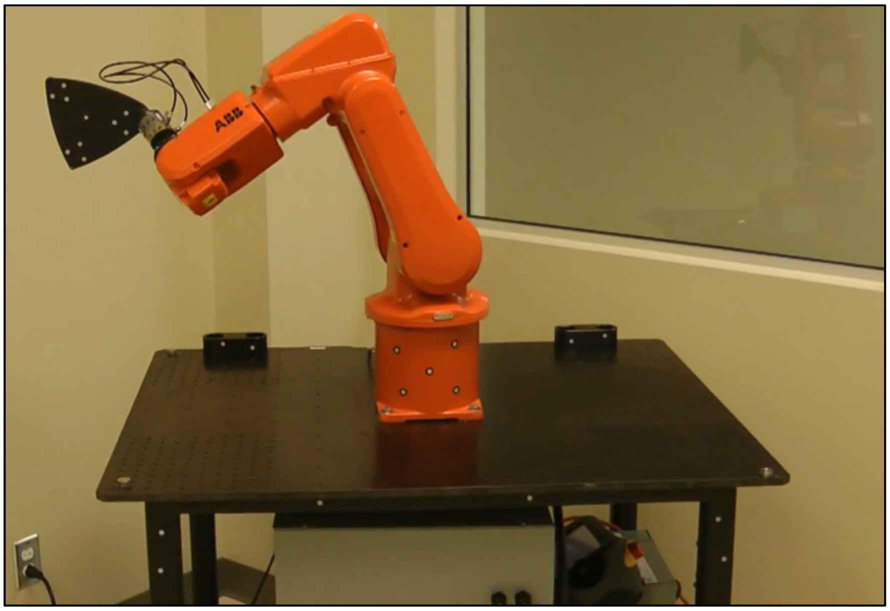

(b)

Figure 2.2 Experimental setup for calibrating the robot with Creaform’s C-Track and the triangular artifact: (a) overall setup; (b) close-up showing the back side of the triangular artifact and the fifteen retro-reflective targets on the robot’s base

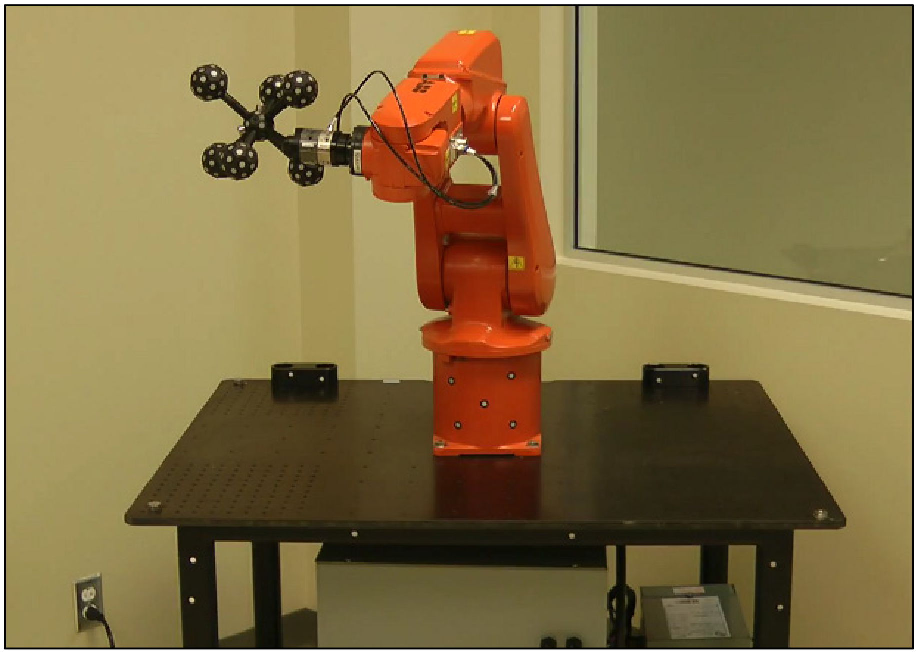

Figure 2.3 Experimental setup for calibrating the robot with Creaform's C-Track and the spatial artifact

2.2.1 Triangular artifact

The triangular artifact (Figure 2.1) is made of steel and holds three magnetic nests for 0.5″ spheres (SMRs or one end of Renishaw's telescopic ballbar). The distance between the centers of these nests is 150 mm. One of the centers (nest 1) lies on axis 6 of the robot, about 125 mm away from the robot tool flange *xy* plane, another (nest 3) lies in the plane passing through the first center and normal to axis 6, approximately 150 mm away from this axis, and the last one (nest 2) is about 115 mm away from axis 6 and about 215 mm away from the tool flange *xy* plane. Nine retro-reflective self-adhesive targets are attached to each side of the tool, as shown in Figures 2.2b and 2.4.

Creaform's MaxSHOT 3D photogrammetry system was used to acquire the position of all eighteen retro-reflective targets with respect to a common reference frame, located in the centroid of all targets. The positions of the centers of the three magnetic nests with respect to this reference frame are measured using the HandyPROBE.

The triangular artifact is mounted on an ATI QC-5 tool changer, and, along with the three magnetic nests, weighs approximately 2.4 kg. The master side of the tool changer weighs an additional 0.3 kg, so the complete end-effector weighs about 2.7 kg, the robot rated payload being 3 kg. The coordinates of the center of gravity of the complete end-effector are approximately {50 mm, 25 mm, 100 mm} with respect to the robot flange reference frame, according to the CAD model of the end-effector.

2.2.2 Spatial artifact

The design of the spatial artifact was based on the imposed condition that there be as many retro-reflective targets visible as possible, at any orientation, and the objective that these visible targets be as far as possible from one another. This artifact is to be used with the C-Track and with the ballbar (using one of the three 0.5” nests), although it can also be used with the laser tracker (Figure 2.4). Indeed, there is no advantage of using such a complex artifact with a laser tracker.

The artifact consists of a steel sphere 45 mm in diameter and with 26 facets. Seven of these facets are used for attaching steel poles 45 mm long, three are used for attaching magnetic nests for 0.5″ spheres (for use with Renishaw’s telescopic ballbar), twelve are used for fixing retro-reflective self-adhesive targets, and three have threaded holes for future needs (Figure 2.4). Six of the steel poles are orthogonal and of slightly different lengths. At the end of each of these six poles, there is a truncated icosahedron (the shape used for soccer balls) with twelve regular pentagonal faces and twenty regular hexagonal faces. Each truncated icosahedron is made by rapid prototyping from black thermoplastic (ABS-700) and has a diameter of about 54 mm. A retro-reflective self-adhesive target is fixed on 31 of its 32 facets, randomly offset from the center of each facet. There are a total of 198 retro-reflective targets, the retro-reflective circle of which is 8 mm in diameter. Finally, the centers of the three magnetic nests are approximately 150 mm away from the robot flange *xy* plane, and 45 mm offset from robot axis 6.

Creaform's MaxSHOT 3D photogrammetry system was used to acquire the position of every target with respect to a common reference frame, located at the centroid of all targets (Figure 2.4). The positions of the centers of the three magnetic nests with respect to this reference frame are measured using the HandyPROBE.

This spatial artifact, too, is mounted on an ATI QC-5 tool changer and, along with the three magnetic nests, weighs approximately 2.3 kg. The weight of the complete end-effector is about 2.6 kg. The coordinates of the center of gravity of the complete end-effector are approximately {−23 mm, 0 mm, 100 mm} with respect to the tool flange reference frame, according to the CAD model of the end-effector. Therefore, both end-effectors exert approximately the same reaction forces and moments on the robot flange.

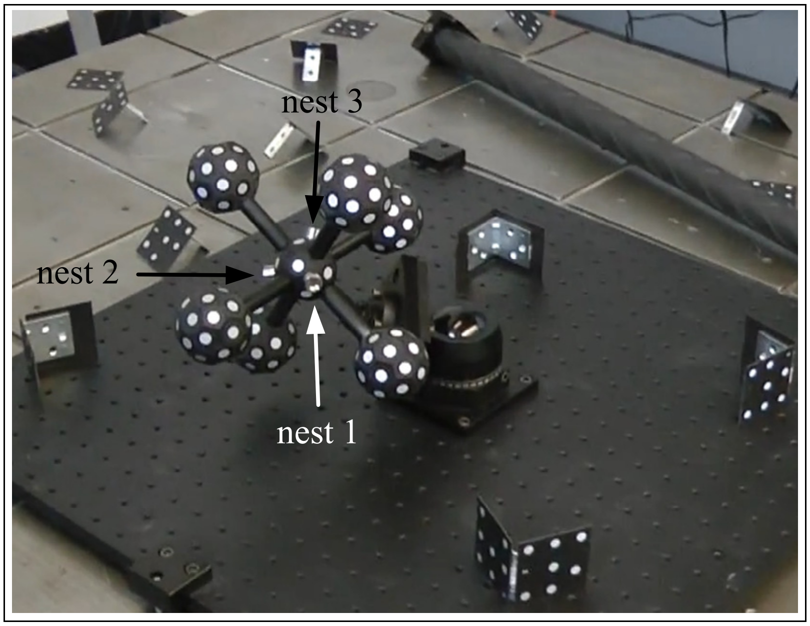

Figure 2.4 The spatial artifact during photogrammetry

To the best of our knowledge, very few such spatial artifacts exist. One is the cover of Creaform's MetraSCAN 3D, but this artifact is an integral part of a hand-held 3D scanner and cannot be mounted on the tool flange of a robot. Another is Northern Digital's Multi-Sided Probe (MSP). The MSP is made of four orthogonal 50 mm struts, with five orthogonally placed active targets at the end of each strut, and weighs only 0.125 kg. The problem with this artifact is that there exist orientations at which no target has a visibility angle of less than 45°. Finally, Boochs et al. (2010) presented another spatial artifact made up of 54 active targets equally distributed on a sphere and tracked by a custom optical CMM consisting of four 4-Mpx cameras. The problem with this artifact is that the visible targets are very close to each other.

2.3 Robot kinematic model

The level-3 robot model that we use corresponds to a complete kinematic calibration of the robot, including the base frame, and the five parameters related to the stiffness (Albert Nubiola and Bonev, 2013) of joints 2, 3, 4, 5, and 6. Tables 2.1 and 2.2 show a summary of all 31 parameters.

Table 2.1 Pose of the base frame with respect to the world frame with six error parameters

Parameter	x	y	z	α	β	γ
Value	$x_w + \delta x_w$	$y_w + \delta y_w$	$z_w + \delta z_w$	$\alpha_w + \alpha x_w$	$\beta_w + \delta\beta_w$	$\gamma_w + \delta\gamma_w$

* The parameters α, β, and γ are the Euler angles, according to the XYZ convention.

Table 2.2 Complete D-H M (Craig, 1986) robot model with 25 error parameters

i	α_i [º]	a_i [mm]	θ_i [º]	d_i [mm]
1	0	0	θ_1	290
2	$-90 + \delta\alpha_2$	δa_2	$\theta_2 - 90 + \delta\theta_2 + c_2\tau_2$	δd_2
3	$\delta\alpha_3$	$270 + \delta a_3$	$\theta_3 + \delta\theta_3 + c_3\tau_3$	δd_3
4	$-90 + \delta\alpha_4$	$70 + \delta a_4$	$\theta_4 + \delta\theta_4 + c_4\tau_4$	$302 + \delta d_4$
5	$90 + \delta\alpha_5$	δa_5	$\theta_5 + \delta\theta_5 + c_5\tau_5$	δd_5
6	$-90 + \delta\alpha_6$	δa_6	$\theta_6 + 180 + \delta\theta_6 + c_6\tau_6$	$72 + \delta d_6$

The location of the nominal robot base frame with respect to the world frame is first measured by rotating joints 1 and 2 (Albert Nubiola and Bonev, 2013). The nominal position of the tool frame is also initially measured by rotating joints 5 and 6 (Albert Nubiola and Bonev, 2013). However, we will keep the parameters $\delta\theta_6$ and δd_6, which position the tool frame with respect to the robot end-effector frame.

Although neither the laser tracker nor the C-Track are displaced during measurement, the world frame is defined using three 0.5″ magnetic nests fixed in three of the four corners of the robot table (Figures 2.2b and 2.3). All measurements performed with the laser tracker and the C-Track will therefore be taken with respect to a world frame defined by the centers of these three nests. In the first setup, the base is measured only once, using the three 0.5″ SMRs. In the second and third setups, fifteen retro-reflective self-adhesive targets are attached to the robot base and table.

We define the nominal base frame with respect to frame $\mathbf{\Phi}_1$ (which depends on axes 1 and 2) using the corresponding nominal geometric parameters that relate these axes as follows: the base frame $\mathbf{\Phi}_0$ is obtained by translating $\mathbf{\Phi}_1$, when at the nominal $\theta_1 = 0°$, along the negative direction of its z_1 axis by the nominal offset $d_1 = 290$ mm.

The robot flange frame can be directly measured, by probing the robot flange. However, for various reasons, we chose to identify this frame without having to remove our special-purpose end-effector. In fact, this is often what happens in industry, in the case where a robot is already fully installed and its operators need to calibrate the whole system (i.e. improve the accuracy of the positioning of the tool frame with respect to the world frame) without having to remove the end-effector.

For the nominal $\theta_6 = 0°$, we define $\mathbf{\Phi}_6$ such that its z_6 axis is along axis 6, its x_6 axis is parallel to the normal between axes 5 and 6 and is obtained by normalizing $\mathbf{z}_6 \times \mathbf{z}_5$, and, finally, the distance from the normal to x_6 is the nominal distance $d_6 = 72$ mm. The tool frame $\mathbf{\Phi}_{\text{tool}}$ is fixed with respect to $\mathbf{\Phi}_6$, and is therefore measured directly. In the case of the C-Track (setups 2 and 3), the tool frame is the one in which the positions of the retro-reflective targets are obtained during photogrammetry. Because the C-Track measures the pose of this frame directly, we chose an end-effector pose that would be visible to the C-Track and reoriented the three SMRs so that all of them would be visible by the laser tracker. In the case of setups 2 and 3, $\mathbf{\Phi}_{\text{tool}}$ is found with respect to $\mathbf{\Phi}_6$. Then, the position of the center of each nest is measured using the HandyPROBE with respect to Φ_{tool}. In the case of setup 1, we measured the positions of the nests with respect to Φ_6 directly, as we considered that Φ_{tool} is coincident with Φ_6. Note that in all three setups, the positioning accuracy of the robot is evaluated at the centers of the magnetic nests, and so the location of Φ_{tool} has no effect on the final results.

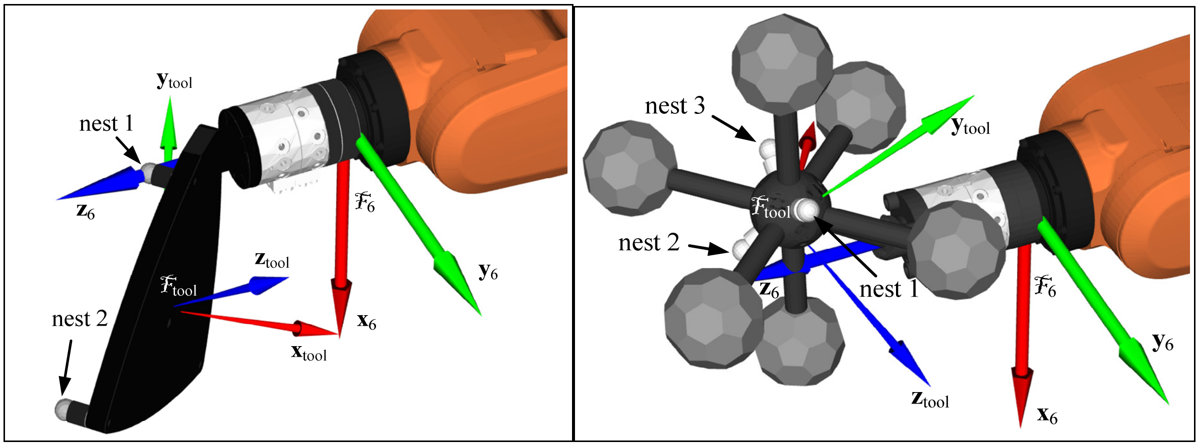

(a) (b)

Figure 2.5 The positions of the three magnetic nests with respect to Φ_6 are measured directly

2.4 Analysis of non kinematic robot behavior

It is often said that the non geometric errors in an industrial robot (such as joint compliance) affect the robot accuracy very little, but this is not true for robots such as the ABB IRB 120, which use harmonic drive gearboxes. To gain an insight into the elastic behavior of the robot, a series of simple tests was performed.

2.4.1 Axis analysis with the laser tracker

A third end-effector was used for these tests. The weight of this end-effector is 2.75 kg and its center of gravity is located at {−31 mm, −13 mm, 85 mm} with respect to Φ_6. One 1.5″ SMR is attached at position {−114.4 mm, −46.2 mm, 124.5 mm} with respect to Φ_6. The position of this SMR is measured with the laser tracker when each joint is displaced in equal increments within an interval (Table 2.3), first in the positive and then in the negative direction, while the other five joints are kept at 0°. (The configuration with all joints at 0° is shown in Figure 2.6). For each joint, errors are calculated with respect to the circle centered at the joint axis (obtained by least squares using all the measurements of each axis) and passing through the position of the target when the joint is at 0°. Radial and axial displacements are in the order of 0.050 mm, mostly corresponding to measurement noise. Therefore, we only analyze the tangential error, caused mainly by the elasticity of the gearboxes (Figure 2.6).

Table 2.3 Ranges of motion for each joint for the test, the results of which are shown in Figure 2.6

Joint	Interval	Increment	Tangential error range	Angular error range	Backlash
1	−60°, 60°	5°	0.114 mm	0.013°	0.004°
2	−40°, 40°	1°	1.363 mm	0.116°	0.002°
3	−40°, 40°	1°	0.912 mm	0.098°	0.004°
4	−155°, 155°	5°	0.445 mm	0.207°	0.037°
5	−90°, 90°	5°	0.606 mm	0.153°	0.017°
6	−400°, 400°	1°	0.156 mm	0.072°	0.037°

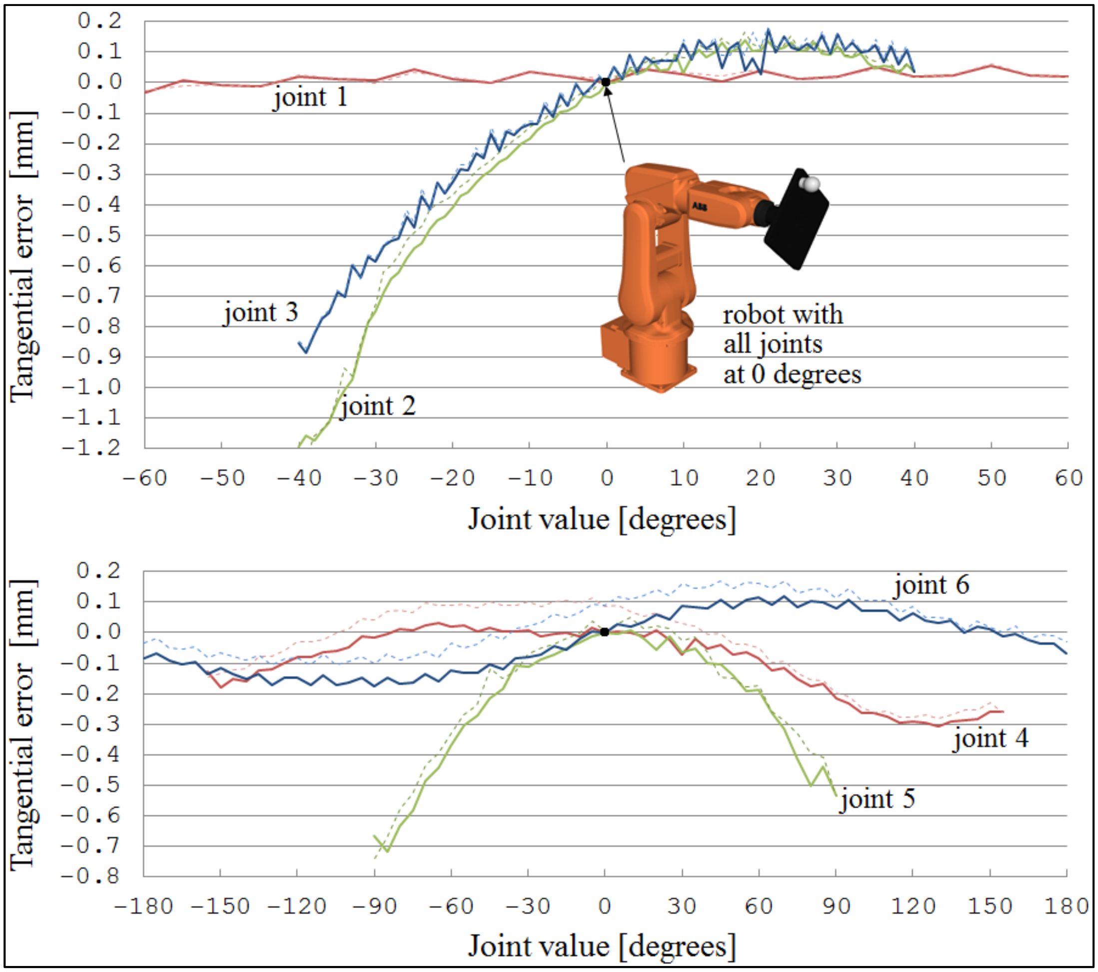

Figure 2.6 Tangential errors measured when rotating a single joint

Note that the backlash between positive and negative rotation is very small for joints 1, 2, and 3 (less than 0.005°), which is because of the harmonic drives. However, it is relatively large for joints 4, 5, and 6, which also use harmonic drives.

The tangential errors shown in Figure 2.6 are clearly due to the elasticity of the gear boxes. The displacement of joint 1 and joint 6 contributes to the smallest errors. In fact, there is virtually no change in the deflection of the robot as measured at the end-effector, since axis 1 is parallel to the direction of gravity. Note that only the range [−200°, 200°] is displayed for axis 6, since the errors are no larger for the full range. This is because the motor and the harmonic drive gearbox of joint 6 are directly installed in link 6.

Due to the varying gravity effect of the robot arm as a function of θ_2 and the long lever effect, the tangential errors caused by rotating joints 2, 3, and 5 are significant, and should be taken into account in the stiffness model. The tangential error associated with joints 4 and 6 is smaller, but will also be taken into account. In fact, note that the peaks for these two joints are separated by 180°. This deflection is due mainly to the weight of the SMR and to an extra load mounted beneath SMR. In other words, if the center of gravity of the end-effector were farther from axis 6, the errors would have been much larger.

2.4.2 Stiffness model

As previously mentioned, a five-parameter model is used to represent the elastic behavior of the robot (Albert Nubiola and Bonev, 2013). This model takes into account the elasticity of the gearboxes of joints 2, 3, 4, 5, and 6 (one parameter per joint). The elasticity in each gearbox is modeled as a linear torsional spring, so this parameter represents the effective constant compliance c_i of each joint i. Traction and compression effects are neglected. Torsional effects are also neglected.

We took into account the gravity forces due to the masses of links 2, 3, 4, and the tool. We neglected the masses of links 5 and 6, as they are relatively small, as well as the mass of link 0 (the base). The mass of link 1 is not needed, because we did not consider a compliance parameter to model the flexibility of joint 1, since the axis of that joint is parallel to the gravity vector. We simplified the specifications provided by ABB into the parameters shown in Table2.4.

Table 2.4 Masses and centers of gravity of each robot link in our model

i	m_i [kg]	$c_{x,i}^{i}$ [mm]	$c_{y,i}^{i}$ [mm]	$c_{z,i}^{i}$ [mm]
1	0	0	0	0
2	4.2	140	0	0
3	0	0	0	0
4	5	0	0	−193.6
5	0	0	0	0
6 (triangular artifact)	2.6	−23	0	100
6 (spatial artifact)	2.7	50	25	100

Note that links 3 and 4 are considered as one, and the effect of link 3 is transferred to link 4. The center of gravity of these two links lies on axis 4, and therefore the compliance parameter for that axis is not affected by the weight of links 3 and 4.

2.5 Calibration

The complete model consists of 31 error parameters: 6 parameters to locate the robot base frame, 20 geometric parameters (4 D-H M parameters for links 2 to 6), and 5 compliance parameters (for joints 2 to 6). However, since axes 2 and 3 are parallel, and because we find the parameters by linearization of the system, one of the 20 geometric parameters becomes redundant and so we exclude it from the model.

In order to minimize the backlash effect, the robot is first moved, in absolute joint mode (*MoveAbsJ*), to the configuration $\{\theta_1 - 5°, \theta_2 - 5°, \theta_3 - 5°, \theta_4 - 5°, \theta_5 - 5°, \theta_6 - 5°\}$ and then to the final configuration $\{\theta_1, \theta_2, \theta_3, \theta_4, \theta_5, \theta_6\}$ for each calibration or validation robot configuration. Furthermore, $\theta_2 \geq 0°$ and $\theta_3 \geq -80°$, in order to keep the torques in joints 2 and 3 negative and be able to use a linear model for the stiffness of the gearboxes, which are, in fact, much less stiff when they are not loaded. In addition, the workspace of the robot is further limited by imposing $-90° \geq \theta_1 \geq 90°$, in order to maximize the visibility of both artifacts, and $-150° \geq \theta_4 \geq 150°$, $-90° \geq \theta_5 \geq 90°$, and $-180° \geq \theta_6 \geq 180°$ because of the tool changer pneumatic hoses. Finally, we recall that in each of the three setups, the range of end-effector orientations is quite different, being virtually unlimited in the third setup.

2.5.1 System linearization

All the kinematic error parameters are considered very small. Those of the base are $[\delta x_b, \delta y_b, \delta z_b, \delta\alpha_b, \delta\beta_b, \delta\gamma_b]$ according to Table 2.1, those of link 2 are $[\delta\alpha_2, \delta a_2, \delta\theta_2, \delta d_2]$ according to the third row of Table 2.2, etc. The robot model can be expressed as

$$\mathbf{f} = \mathbf{f}(\mathbf{p}, \mathbf{q}) \tag{2.1}$$

where $\mathbf{f} = [x, y, z]^{\mathrm{T}}$ is the position of the end-effector (note that only the position data are taken into account), $\mathbf{p}$ is the vector containing all 31 error parameters, and $\mathbf{q} = [\theta_1, \theta_2, \ldots, \theta_6]^{\mathrm{T}}$ is the vector of the joint variables. The expression of equation (2.1) is quite complex, because it is a function of 37 parameters and other constant parameters, like masses and centers of gravity. If we derive the Jacobian matrix of this robot model, the expression becomes even more complex. Fortunately, this expression can be obtained easily using the MATLAB Symbolic Toolbox, so the linearized equations can be expressed at iteration i as

$$\Delta\mathbf{f}^i = \mathbf{J}^i \Delta\mathbf{p}^i \tag{2.2}$$

where $\Delta\mathbf{f}^i$ is the difference between the measured position and the position predicted by the model for a given robot configuration, $\mathbf{J}^i$ is the Jacobian matrix, and $\Delta\mathbf{p}^i$ are the values to add to the error parameters. Using enough end-effector position measurements for different robot configurations, we can obtain the least squares solution of the error parameters using the pseudo inverse of the Jacobian:

$$\Delta\mathbf{p} = \left(\mathbf{J}^{\mathrm{T}}\mathbf{J}\right)^{-1} \mathbf{J}^{\mathrm{T}} \Delta\mathbf{f} \, . \tag{2.3}$$

The Jacobian is slightly different at each iteration, because it depends on the error parameters found in each step, where we verify that all the columns of **J** are linearly independent. If they are not, we must discard the useless error parameters. When we verified the linear dependency, in our case, the error parameters δd_2 and δd_3 were found to be linearly dependent (because of the parallel axes). So we did not consider δd_3 in the model. We also realized that the solution was stable after four iterations.

2.5.2 Observability

To measure the goodness of a set of robot configurations, we used an observability index and an iterative algorithm (Albert Nubiola and Bonev, 2013; Sun and Hollerbach, 2008). This index emphasizes the volume of a hyper-ellipsoid (Borm and Meng, 1991), the directions of which are represented by the singular values (Stone and Sanderson, 1987):

$$O = \frac{\sqrt[m]{\sigma_1 \sigma_2 \dots \sigma_m}}{\sqrt{n}} \tag{2.4}$$

where n is the number of configurations, m is the number of error parameters, and σ_i are the singular values of the singular value decomposition:

$$\mathbf{J} = \mathbf{U\Sigma V}' \tag{2.5}$$

where

$$\mathbf{\Sigma} = \begin{bmatrix} \sigma_1 & 0 & \cdots & 0 \\ \vdots & \vdots & \vdots & \vdots \\ 0 & 0 & \cdots & \sigma_m \\ 0 & 0 & \cdots & 0 \\ \vdots & \vdots & \vdots & \vdots \\ 0 & 0 & \cdots & 0 \end{bmatrix} \tag{2.6}$$

We applied a numerical algorithm to find a good set of calibration measurements for each of the three setups (Albert Nubiola and Bonev, 2013). With a random set of 5000 robot configurations and a random start subset of 11 of them, we use an iterative algorithm to change this subset to obtain a better observability index. At each iteration, we remove from the subset the configuration that leaves the highest observability index (if the index increases by removing a configuration) and we add the configuration that results in the highest observability index (again, if adding a configuration increases the observability index). Finding the optimal subset of calibration configurations is performed offline, through simulations.

2.5.3 Laser tracker and triangular artifact (setup 1)

The base reference frame is measured only once, using the three nests placed on the table depicted in Figures 2.2b and 2.3. For each robot configuration, we measure the position of only one of the three SMRs (shown in Figure 2.2b). Figure 2.7a shows the positions of the SMR that is measured, with those corresponding to calibration configurations depicted in red. There are only 38 calibration configurations, which are found using the observability study previously explained. The remaining black dots correspond to the position of one of the three SMRs in the 1000 random robot configurations used for validating the efficiency of the robot calibration.

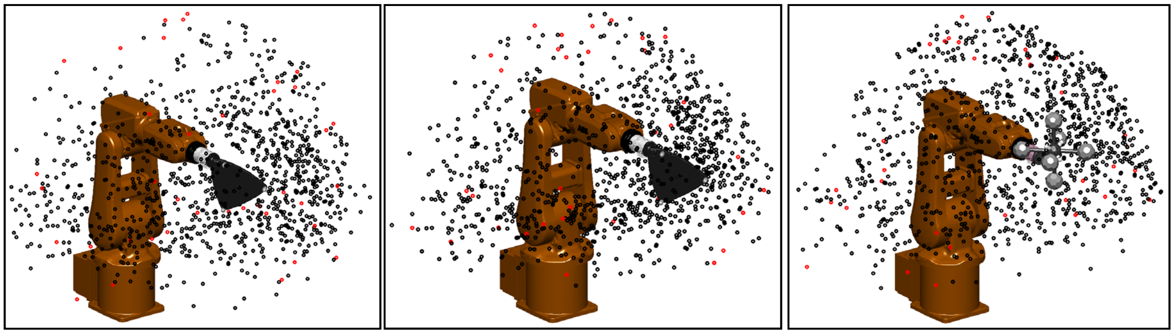
(a) (b) (c)

Figure 2.7 Calibration and validation positions using (a) the laser tracker and the triangular artifact (setup 1); (b) the C-Track and the triangular artifact (setup 2); (c) the C-Track and the spatial artifact (setup 3)

2.5.4 C-Track and triangular artifact (setup 2)

As already mentioned, both the front face and the back face of the triangular artifact are measured in the second setup. However, the back side is visible in only one of every five robot configurations. For each configuration, we measure the pose of the triangular artifact Φ_{tool} with respect to the base Φ_{world}. The positions of the origin of Φ_{tool} (Figure 2.5a) corresponding to each robot configuration measurement are shown in Figure 2.7b. We found 36 calibration configurations, depicted in red, using the observability study explained above. The black dots correspond to the 1000 random robot configurations used to validate the calibrated model. In this study, we did not consider a measurement to be valid unless there were a minimum of 12 and 9 visible targets from the base and end-effector respectively.

Note that, although the C-Track measures the pose of the robot end-effector, we only consider the position of all three magnetic nests (on the robot end-effector). Consequently, for each robot configuration measured, we have the position of all three magnetic nests.

2.5.5 C-Track and spatial artifact (setup 3)

As in setup 2, we measure the pose of the spatial artifact Φ_{tool} with respect to the base frame Φ_{world} in each robot configuration. The positions of the origin of Φ_{tool} (Figure 2.5b) corresponding to each robot configuration measurement are shown in Figure 2.7c. There are 35 calibration configurations, in red, which are found using the observability study explained. The black dots correspond to the 1000 random robot configurations used to validate the calibrated model. In this study, we did not consider a measurement to be valid unless there were a minimum of 12 and 20 visible targets from the base and end-effector respectively.

2.6 Results

The calibration method was first tested with simulations using the robot model described in Section 2.3. Forcing a set of error parameters that provoke a nominal position measurement of 5 mm (maximum value), the maximum position measurement error after calibration is 0.004 mm, if we do not consider noise measurement and if the masses and their centers of gravity are perfectly known (note that these parameters are not identified by the model). If we apply a measurement noise of 0.070 mm and consider a 10% error for the masses and centers of gravity, the mean/maximum position measurement errors are in the order of 0.050 mm to 0.100 mm for the 1000 random robot configurations for each of the three setups. We also tried several other observability indices (Morris R. Driels and Pathre, 1990;

Nahvi et al., 1994; Nahvi and Hollerbach, 1996) (with simulation and experimental results), but the results we obtained were worse.

Note, too, that the 0.004 mm error after calibration and without noise measurement is due to the parametric redundancy caused by the consecutive and parallel axes 2 and 3. This error is so small that we discarded a specific link model between these two joints to properly represent the physical link (such as the CPC model (Caenen and Angue, 1990; Hayati and Mirmirani, 1985; H Zhuang and Roth, 1992; Hanqi Zhuang and Roth, 1993)).

Finally, to perform the experimental tests, the robot was warmed up for one hour and then programmed to go to the planned configurations with the end-effector speed limited to 500 mm/s and 20 degrees/s. Furthermore, for each robot configuration, the robot was programmed to pause for 4 seconds while either the laser tracker or the C-Track performed the measurement. As already mentioned, the measurement acquisition process is fully automated.

2.6.1 Analysis of the measurement devices

To evaluate the volumetric accuracy of each of the two measurement systems, both artifacts were measured on a Mitutoyo Bright-STRATO 7106 CMM with a total measurement uncertainty of 0.0027 mm at a 95% confidence level. The setup is shown in Figure 2.8. Four 0.5″ precision balls were mounted on magnetic nests which were fixed with respect to the granite base of the CMM. Three of these balls were used to define the common reference frame, and, for each artifact, the coordinates of the centers of the three magnetic nests were measured with respect to that frame. In each setup, all seven centers were first measured by the CMM (by probing 0.5″ precision balls), then by the laser tracker (using 0.5″ SMRs), and finally by the C-Track (measurements obtained indirectly from the pose of the artifact).

In the case of the C-Track, the pose of the end-effector was measured with respect to a set of eight retro-reflective targets fixed with respect to the CMM's granite table. The centers of the four magnetic nests mounted on the base were measured using the HandyPROBE (equipped with a 0.5″ precision ball tip) with respect to the eight targets. In a previous step, the positions of the centers of the magnetic nests on each artifact with respect to the photogrammetry frame were measured using the HandyPROBE.

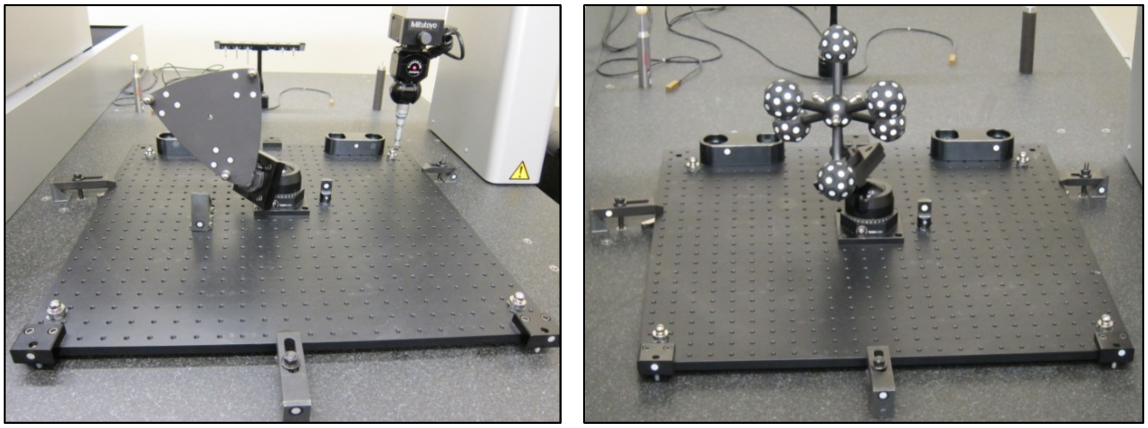

(a) (b)

Figure 2.8 Accuracy validation of the C-Track and laser tracker on the CMM

Table 2.5 shows the distance errors between the centers of four of the seven magnetic nests measured using the C-Track and the laser tracker with respect to the centers measured by the CMM. All the measurements were taken by the CMM, the C-Track, and the laser tracker with respect to the common reference frame defined by three of the four magnetic nests mounted on the base of the CMM. The first three nests in Table 2.5 are the ones mounted on the artifact, while the fourth is the one mounted on the base and not used to define the common reference frame (the one being probed in Figure 2.8a).

Table 2.5 Distance errors for the C-Track and the laser tracker with respect to the CMM

		Nest 1 (on the artifact)	Nest 2 (on the artifact)	Nest 3 (on the artifact)	Nest 4 (on the base)
Triangular artifact	Laser tracker	0.034 mm	0.029 mm	0.035 mm	0.034 mm
	C-Track	0.124 mm	0.061 mm	0.082 mm	0.124 mm
Spatial artifact	Laser tracker	0.015 mm	0.015 mm	0.010 mm	0.038 mm
	C-Track	0.129 mm	0.118 mm	0.138 mm	0.177 mm

We performed the same test for two other orientations for each artifact, and the results were very similar to the ones presented in Table 2.5. Nevertheless, these tests are inconclusive, and do not necessarily give an estimate of the volumetric accuracy of either the laser tracker or the C-Track. However, they demonstrate that, in perfect laboratory conditions, the accuracy of the C-Track is worse than that of the laser tracker, especially in the case of the spatial artifact.

2.6.2 Validation using the laser tracker and the C-Track

The validation tests compare the position errors at the three magnetic nests on each of the end-effectors with respect to the world reference frame defined on the robot table, between the uncalibrated robot and the calibrated one, in 1000 random robot configurations (which are different for the three setups). For each setup, the results are shown in the form of a histogram of the position errors, and a list of the parameters identified is included.

It is very surprising that the nominal position accuracy of the ABB IRB 120 robot is worse than 5 mm. Note that the nominal model used is the one that corresponds to the nominal geometric parameters of the robot, but includes the base and tool frame identifications previously described. In other words, if these frames had been measured by probing the robot base and robot tool flange instead, the accuracy of the nominal model would most probably have been worse.

2.6.2.1 Laser tracker with triangular artifact (setup 1)

Figure 2.9 shows the accuracy results after calibration for the 1000 position measurements illustrated in Figure 2.7a. For clarity, the results before calibration are not shown. Suffice to say that the mean position error improved from 3.168 mm to 0.146 mm. The robot model obtained after calibration is shown in Tables 2.6 and 2.7. As we can see, the errors are very small, but their combined effect is large.

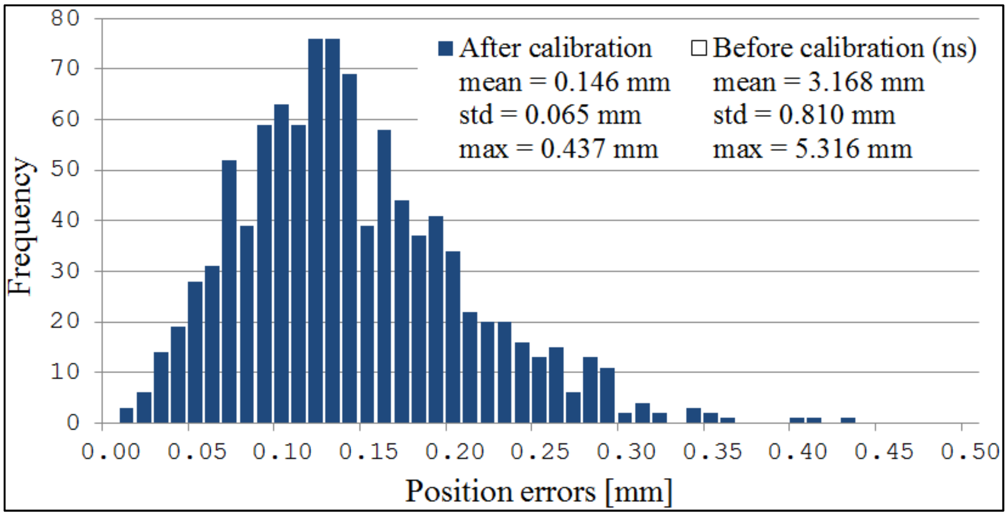

Figure 2.9 Histogram of position errors using the laser tracker and the triangular artifact

Table 2.6 Robot base errors obtained with the laser tracker and the triangular artifact

Parameter	δx_w [mm]	δy_w [mm]	δz_w [mm]	$\delta \alpha_w$ [°]	$\delta \beta_w$ [°]	$\delta \gamma_w$ [°]
Value	−0.075	−0.096	0.103	0.003	0.008	−0.033

Table 2.7 Robot model obtained with the laser tracker and the triangular artifact

i	α_i [°]	a_i [mm]	θ_i [°]	d_i [mm]
1	0.000	0.000	θ_1	290.000
2	−90.006	0.134	$\theta_2 - 89.909 + 0.032\times10^{-6}\,\tau_2$	0.000
3	−0.011	270.236	$\theta_3 + 0.054 + 0.130\times10^{-6}\,\tau_3$	0.006
4	−90.009	70.138	$\theta_4 - 0.027 + 0.605\times10^{-6}\,\tau_4$	302.246
5	89.984	−0.061	$\theta_5 + 0.067 + 0.419\times10^{-6}\,\tau_5$	−0.067
6	−89.969	0.022	$\theta_6 + 179.913 + 0.647\times10^{-6}\,\tau_6$	72.050

2.6.2.2 C-Track with triangular artifact (setup 2)

Figure 2.10 shows the position errors after calibration for 3000 measurements of the centers of the three magnetic nests, obtained using the pose measurement of the 1000 configurations illustrated in Figure 2.7b. The errors before calibration are not shown, since they are too large. The mean position error improved from 4.639 mm to 0.176 mm. The robot model obtained after calibration is shown in Tables 2.8 and 2.9. Clearly, the robot accuracy after calibration is very similar to that obtained when calibrating with a laser tracker.

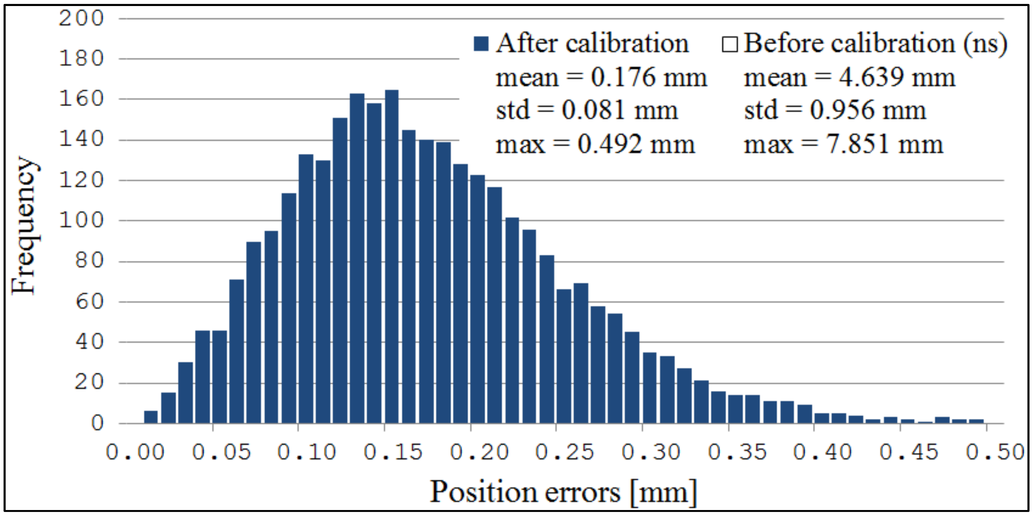

Figure 2.10 Histogram of position errors using the C-Track and the triangular artifact.

Note that the nominal accuracy for this test is much worse than for the previous test. This may be because we had to modify the position of the end-effector orientation when moving axes 1 and 2 to identify the base frame, so that the front side of the tool was facing the C-Track within a ±30° range. We can clearly see that, after calibration, the errors made when measuring the base frame were quite significant ($\delta y_w = 2.403$ mm and $\delta y_w = -0.994$ mm). These errors in the base only affect the nominal model, however, and are probably due to the flexibility behavior of the robot, which seems to be quite different when the wrist angles are changed (while moving axes 1 and 2, we kept $\theta_3 = \theta_4 = 0°$, $\theta_5 = -40°$, and $\theta_6 = 80°$). The results for the robot parameters are very similar (Table 2.9 vs. Table 2.7).

Table 2.8 Robot base errors obtained with the C-Track and the triangular artifact

Parameter	δx_w [mm]	δy_w [mm]	δz_w [mm]	$\delta\alpha_w$ [°]	$\delta\beta_w$ [°]	$\delta\gamma_w$ [°]
Value	0.047	2.403	−0.994	0.118	0.028	−0.070

Table 2.9 Robot model obtained with the C-Track and the triangular artifact

i	α_i [°]	a_i [mm]	θ_i [°]	d_i [mm]
1	0.000	0.000	θ_1	290.00
2	−90.008	0.052	$\theta_2 - 89.891 + 0.028\times10^{-6}\,\tau_2$	0.048
3	−0.023	270.223	$\theta_3 + 0.071 + 0.122\times10^{-6}\,\tau_3$	0.000
4	−90.015	70.164	$\theta_4 - 0.027 + 0.646\times10^{-6}\,\tau_4$	302.187
5	89.988	−0.086	$\theta_5 + 0.062 + 0.476\times10^{-6}\,\tau_5$	0.009
6	−89.982	−0.007	$\theta_6 + 180.000 + 0.243\times10^{-6}\,\tau_6$	72.373

2.6.2.3 C-Track with spatial artifact (setup 3)

Figure 2.11 shows the accuracy results after calibration for the 3000 position measurements of the centers of the three magnetic nests, obtained using the pose measurement of the 1000 configurations illustrated in Figure 2.7c. The mean position error improved from 2.913 mm to 0.149 mm. The robot accuracy after calibration in this setup is very similar to the accuracy obtained in the first two setups.

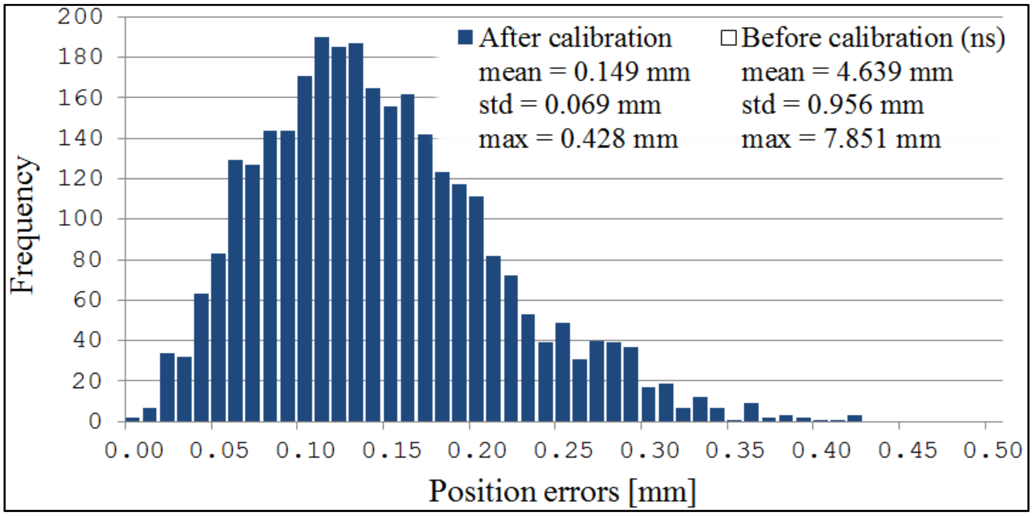

Figure 2.11 Histogram of position errors using the C-Track and the spatial artifact

Table 2.10 Robot base errors obtained with the C-Track and spatial artifact

Parameter	δx_w [mm]	δy_w [mm]	δz_w [mm]	$\delta \alpha_w$ [°]	$\delta \beta_w$ [°]	$\delta \gamma_w$ [°]
Value	−0.099	0.024	0.184	0.003	−0.012	−0.023

Table 2.11 Robot model obtained with the C-Track and the spatial artifact

i	α_i [º]	a_i [mm]	θ_i [º]	d_i [mm]
1	0.000	0.000	θ_1	290.000
2	−90.013	0.095	$\theta_2 - 89.914 + 0.037\times10^{-6}\,\tau_2$	−0.024
3	−0.018	270.156	$\theta_3 + 0.073 + 0.112\times10^{-6}\,\tau_3$	0.000
4	−90.018	70.153	$\theta_4 - 0.026 + 0.462\times10^{-6}\,\tau_4$	302.232
5	89.995	−0.055	$\theta_5 + 0.064 + 0.301\times10^{-6}\,\tau_5$	0.062
6	−90.004	0.004	$\theta_6 + 179.946 + 2.000\times10^{-6}\,\tau_6$	71.991

2.6.3 Validation using a telescopic ballbar

The results shown in Figures 2.9–2.11 suggest that the C-Track is as effective as the laser tracker in calibrating the ABB IRB 120 robot. However, these validation results are not directly comparable, since the robot configurations (although random and excessive in number) are not the same and are not measured with the same tool. Therefore, in order to perform a fair comparison, the efficiency of the three robot calibrations was tested using a QC20-W telescopic ballbar by Renishaw in the same (for calibration models 1 and 2) and almost the same (for calibration model 3) set of robot configurations and in the same manner (Figure 2.12). The ballbar sensor accuracy (at 20 °C) is ±0.5 µm, and its measuring range is only ±1.0 mm, which is why we have no measurements for the nominal model.

The three calibration models were used to perform the spherical ballbar tests, around the same center point at a radius of 300 mm, and at a speed limited to 500 mm/s and 20 degrees/s. The robot pauses for 2 seconds before each measurement (we repeated the tests twice, and found that the results were very repeatable). The ballbar is magnetically attached to two nests of the end-effector (using a different path for each nest). The center of the sphere was taught to the robot manually, using nest 1 for both artifacts. Finally, note that we do not perform the backlash suppression procedure that we use when measuring with the laser tracker or the C-Track.

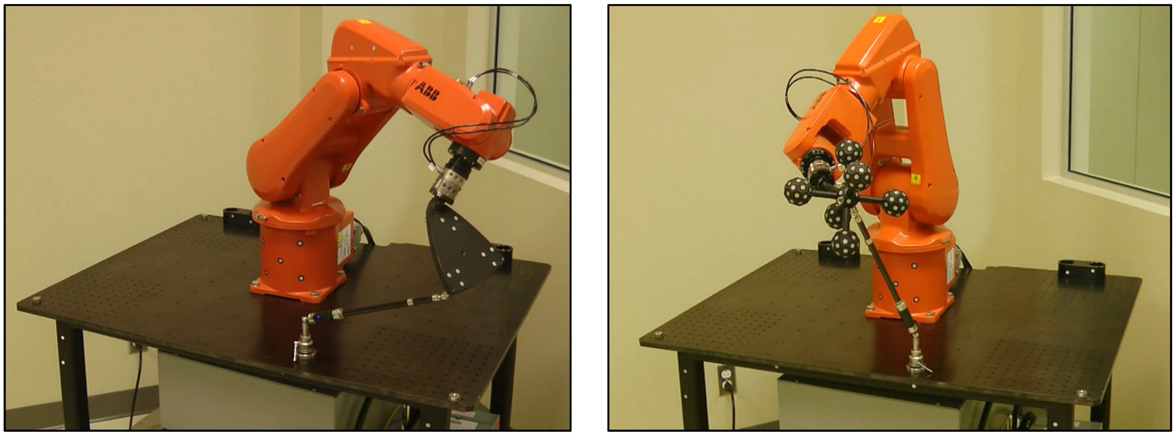

(a) (b)

Figure 2.12 Measuring distance accuracy with a Renishaw telescopic ballbar

2.6.3.1 Results using the triangular artifact

Figures 2.13 and 2.14 show the results of the two paths performed with the triangular artifact, with the ballbar attached to nests 1 and 2 respectively. The laser tracker model (calibration model 1) and the C-Track model (calibration model 2) are therefore directly compared. The first path consists of 123 ballbar measurements using nest 1 (Figure 2.13), and the second path consists of 95 ballbar measurements using nest 2 (Figure 2.14).

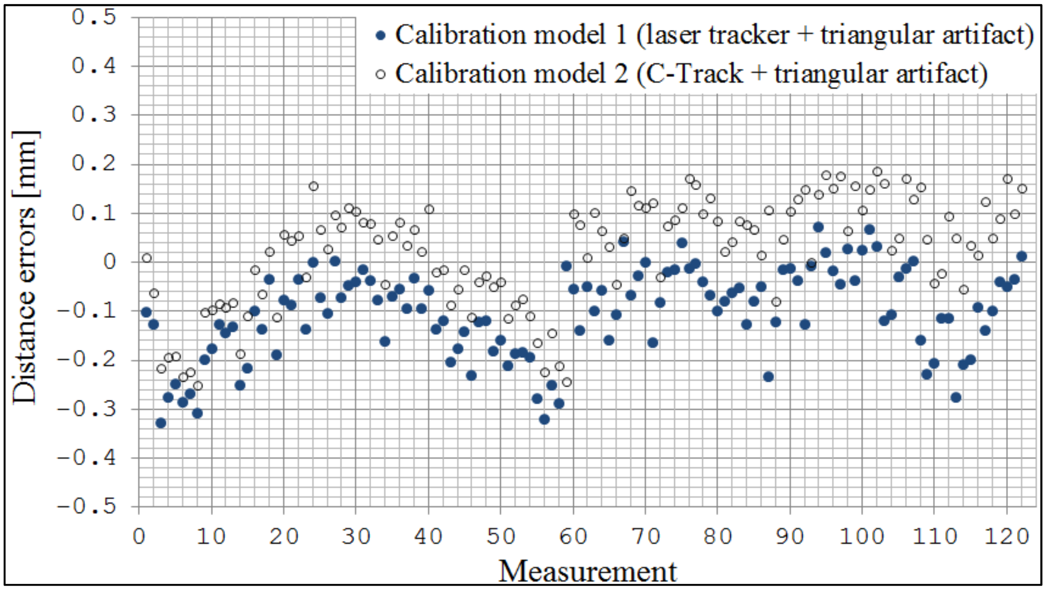

Figure 2.13 Results for the path with the ballbar attached to nest 1 of the triangular artifact

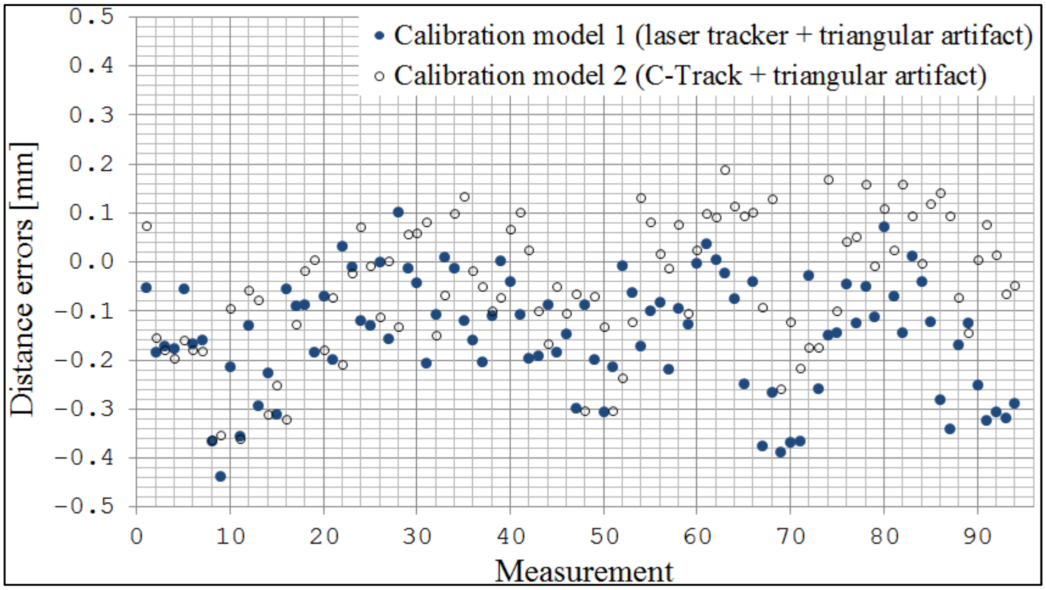

Figure 2.14 Results for the path with the ballbar attached to nest 2 of the triangular artifact

Table 2.12 Summary of ballbar results obtained using the triangular artifact

Ballbar attached to	Robot model	Mean error	Standard deviation	Maximum error
nest 1	laser tracker	−0.105 mm	0.091 mm	0.327 mm
	C-Track	0.022 mm	0.110 mm	0.250 mm
nest 2	laser tracker	−0.148 mm	0.118 mm	0.437 mm
	C-Track	−0.048 mm	0.135 mm	0.363 mm

From Figures 2.13 and 2.14, we can see that the two calibrations result in similar improvements for each robot configuration. From Table 2.11, however, we can see that the overall efficiency of the robot calibration with the C-Track is better.

2.6.3.2 Results using the spatial artifact

Figures 2.15 and 2.16 show the results of the two paths performed with the spatial artifact, with the ballbar attached to nests 1 and 3 respectively. Only calibration model 3 (C-Track and spatial artifact) is shown. The first path consists of 108 ballbar measurements using nest

1, and the second path consists of 90 ballbar measurement using nest 3. The center of the sphere is the same as the one used for the paths of the triangular artifact (Figure 2.12).

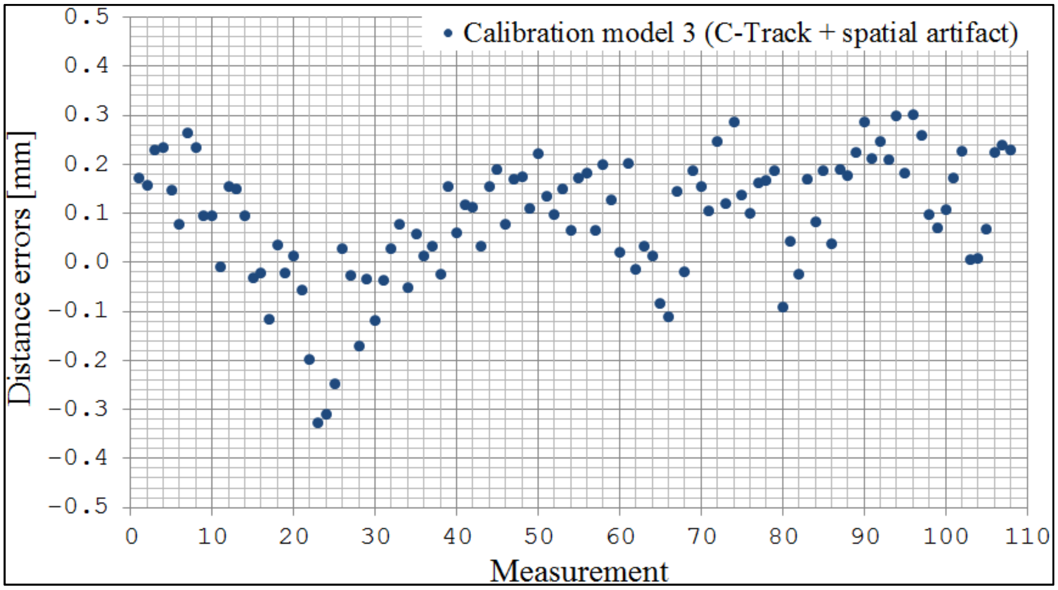

Figure 2.15 Results for the path with the ballbar attached to nest 1 of the spatial artifact

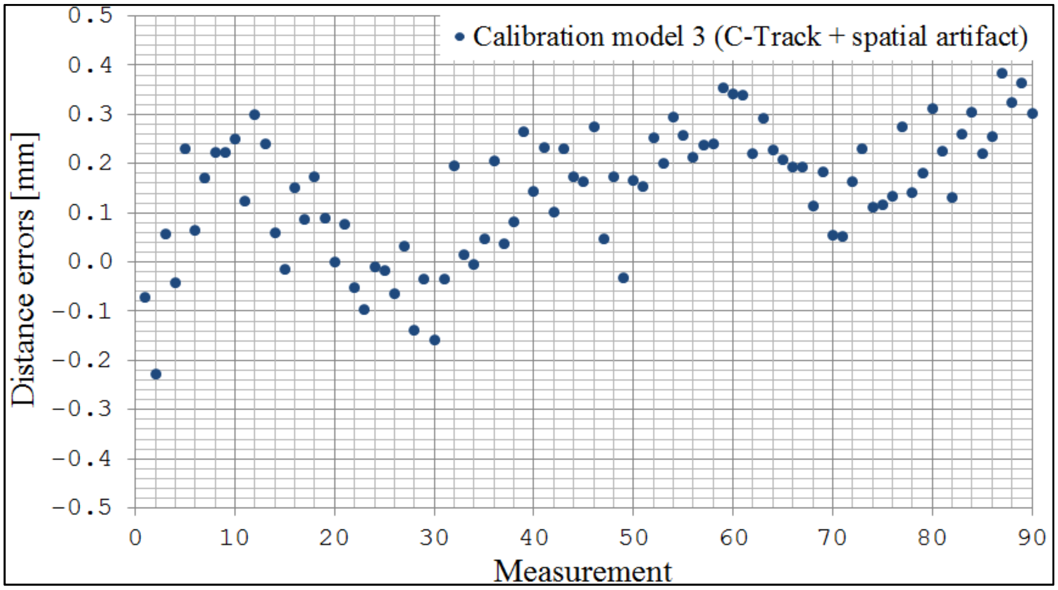

Figure 2.16 Results for the path with the ballbar attached to nest 3 of the spatial artifact

Table 2.13 Summary of ballbar results obtained using the spatial artifact

Ballbar attached to	Robot model	Mean error	Standard deviation	Maximum error
Nest 1	C-Track	0.091 mm	0.126 mm	0.328 mm
Nest 3	C-Track	0.146 mm	0.130 mm	0.385 mm

These results are similar to the results obtained using the triangular artifact. Note, however, that the robot configurations are not exactly the same, and neither are the measurements points.

2.7 Conclusions

We demonstrated clearly that the efficiency of the C-Track in calibrating the ABB IRB 120 industrial robot is equivalent to that of the FARO laser tracker, and costs half as much. We also demonstrated, to our surprise, that there is no benefit to using the C-Track with a complex spatial artifact that allows the pose of the robot end-effector to be measured in any orientation. It is very difficult to manufacture such an artifact, to inspect it through photogrammetry, or even to handle it, so this observation comes as a relief.

The C-Track has another advantage over the laser tracker. To acquire the laser tracker measurements, we need to make an initial guess as to the location of the target. Otherwise, the laser tracker will spend too much time searching for the SMR. Of course, we could track dynamically and always measure the same SMR, but measuring three SMRs (as we do) gives much better results that measuring only one.

Furthermore, we showed that a relatively simple calibration model with only five non geometric error parameters can improve the volumetric accuracy of the ABB IRB 120 industrial robot significantly. In fact, the mean and maximum position errors were reduced from more than 3 mm and 5 mm respectively to about 0.150 mm and 0.500 mm. Note that if we do not use the five compliance parameters in our robot model, the mean and maximum position errors are reduced to only 0.4 mm and 1.0 mm approximately.

Our calibration procedure, especially in the case of the C-Track, is very quick. In order to calibrate the robot using the C-Track and the triangular artifact, we need only measure the pose of the robot end-effector in 36 robot configurations. In contrast, ABB uses 100 position measurements taken with a Leica laser tracker.

In conclusion, we demonstrated for the first time that using Creaform's C-Track and a simple planar end-effector to calibrate a small industrial robot is as efficient as when using a laser tracker, yet much cheaper, quicker and easier.

2.8 Acknowledgments

We thank the Canada Research Chair program and the Natural Sciences and Engineering Research Council of Canada for financing this work. We also express our gratitude to Dr. Torgny Brogardh, Corporate Executive Engineer at ABB Robotics, for his help in preparing the work. Finally, we thank Creaform for lending us a C-Track, performing the photogrammetry of our artifacts, and assisting us with some of the tests.

CHAPTER 3

A NEW METHOD FOR MEASURING A LARGE SET OF POSES WITH A SINGLE TELESCOPING BALLBAR

Albert Nubiola, Mohamed Slamani and Ilian A. Bonev,
1100 Notre-Dame Ouest, Montréal, Québec, Canada H3C 1K3

This chapter has been published as an article in
Precision Engineering: vol. 37, n° 2 (2013), pp 451-460

Abstract

This paper presents a novel method of measuring a set of more than fifty poses under static conditions, using a single telescoping ballbar and two fixtures, each bearing three equally spaced magnetic cups. The position accuracy of the device is in the ± 0.003 mm range, making it suitable for measuring the pose accuracy and repeatability of industrial robots and even calibrating them. The proposed method is an extension of a known approach using a hexapod (a Stewart-Gough platform) comprising telescoping ballbar legs and provides an original solution to the constraint imposed by the limited measurement range of current telescoping ballbars, namely an innovative hexapod geometry capable of assembly in 144 different configurations. An additional advantage of the method is that the pose of one fixture with respect to the other can be obtained for each of these configurations by solving a cascade of three quadratic equations using the six hexapod leg lengths as input. The application of the device and method to measuring numerous poses of an ABB IRB 120 industrial robot is presented.

3.1 Introduction

Precise and accurate measurement is required in order to evaluate the end-effector pose (position and orientation) repeatability and accuracy of six-degree-of-freedom (6-DOF) machines such as six-axis industrial robots, as it is for their calibration. Under static conditions, any 3D coordinate measurement system can be used to measure the pose of a rigid body by measuring the position of three non-collinear points on that body. Conventional coordinate measurement machines (CMMs) provide some of the most accurate measurements for this purpose, but are bulky and very expensive. Laser trackers are an excellent alternative for applications involving industrial robots (robots being much less precise than machine tools), but they too are expensive (over $100,000) and have the additional drawback of high sensitivity to ambient disturbances. Measurement arms are probably the least expensive 3D measurement systems, and the smaller units may provide volumetric measurement accuracies of 0.020 mm.

There are also 6D measurement systems such as so-called optical trackers (*e.g.* the C-Track from Creaform or the OPTOTRAK from NDI) or laser trackers combined with a 6D probe (*e.g.* Leica's T-Mac or API's Smart-TRACK). The cost of these systems is often prohibitive and the accuracy provided is not comparable to that of a CMM (A Nubiola et al., 2013).

A much less expensive yet very accurate commercially available system for measuring 6D poses (under static conditions) is single-camera photogrammetry (*e.g.* the MaxSHOT 3D from Creaform or the DPA from AICON). The volumetric accuracy of these systems is comparable to that of measurement arms. Unfortunately, they are relatively difficult to operate. A single pose measurement requires a multitude of photos taken from relatively long distances and various viewpoints.

Measurement arms and almost all conventional CMMs are based on so-called serial mechanisms (all links are connected in series through revolute or prismatic joints instrumented with encoders). However, parallel mechanisms can potentially improve accuracy and lower cost. For example, Lapic (Russian Federation) has been manufacturing CMMs for at least two decades, based on 6-DOF parallel mechanisms called *hexapods* (Figure 3.1). A hexapod (also called a *Stewart-Gough platform*) most often consists of an end-effector connected to a base through six telescoping legs.

Although the origin of hexapods with telescoping legs dates back at least to the late 1940s (Bonev, 2003), the idea of using them as passive 6D pose measurement devices seems more recent. Schiele *et al.* (Schiele et al., 1986) patented in 1986 a method for measuring the position or pose of a robot end-effector using respectively three (Figure 3.2a) or six telescoping ballbars. Seven years later, Goswarni *et al.* (Goswami et al., 1993)

reported the development of a very similar hexapod pose measurement device (Figure 3.2b, courtesy of Prof. Michael Peshkin) consisting of two fixtures with magnetic cups, the distances between each cup center of one fixture to at least two cup centers of the other fixture being measured using a single telescoping ballbar from API. An industrial robot was thus guided through the same path nine times, with dynamic measurement of one of the possible nine distances each time, and the resulting data were used to calibrate the robot. Renishaw co-founder David R. McMurtry was later granted a US patent for a very similar device (Figure 3.3c) and Paul C. Sheldon was granted a US patent (Sheldon, 1999) in 1999 for a hexapod CMM such as the one shown in Figure 3.1. More recently, Gilles Diolez (Diolez, 2006) developed three 6D pose measurement devices, two of these being hexapods each using six custom-designed telescoping ballbars simultaneously and one being an octopod using eight custom-designed telescoping ballbars simultaneously.

Since the telescoping ballbar is a relatively low-cost off-the-shelf high-accuracy device, the previously proposed pose measurement methods (Goswami et al., 1993; McMurtry, 2007; Schiele et al., 1986) illustrated in Figure 3.2 seem suitable for robotic applications. Unfortunately, these methods no longer work with today’s commercially available telescoping ballbars.

Figure 3.1 A CMM of hexapod design
(courtesy of Lapic, Russian Federation)

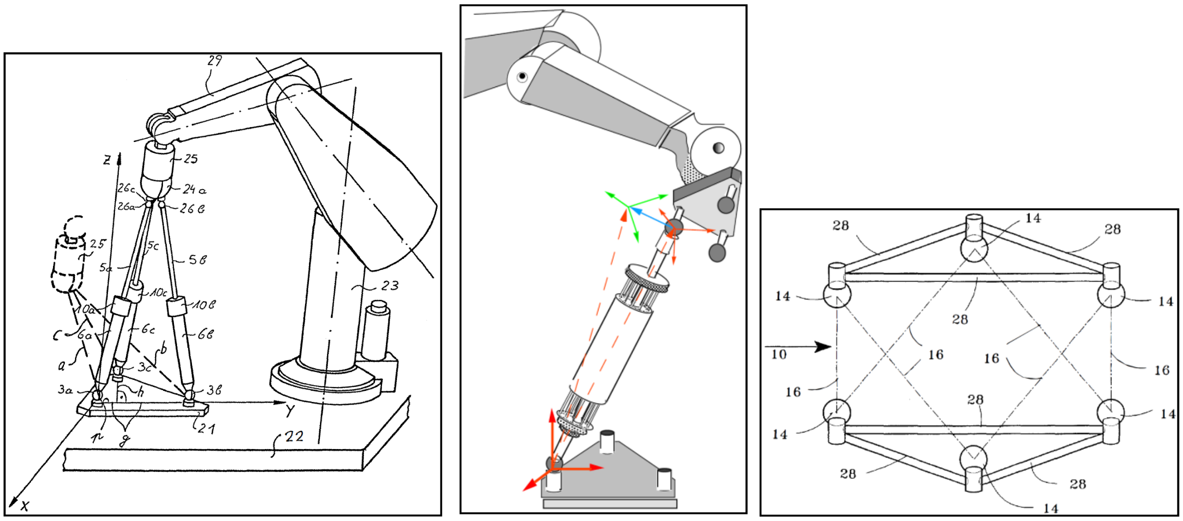

(a) (b) (c)

Figure 3.2 Early designs using telescoping ballbars in a hexapod arrangement for pose measurements

The telescoping ballbar was invented in the USA in the early 1980s by James B. Bryan at the Lawrence Livermore National Laboratory (J B Bryan, 1982; James B Bryan, 1984) and licensed in 1986 to Renishaw, who introduced their first commercial version in 1992. In 1987, Drs Naren Vira and Kam Lau, then of the US National Bureau of Standards and unsatisfied with the limited measurement range of Bryan's ballbar (making it unsuitable for testing robot poses), developed a telescoping ballbar with a measurement range of 50 mm (Vira and Lau, 1987). Dr. Lau founded API that same year and commercialized the improved device (as well as the first laser tracker that he had invented).

The problem with the previous designs (Goswami et al., 1993; McMurtry, 2007; Schiele et al., 1986) is that all of them rely implicitly on telescoping ballbars that have a broad measurement range. Their use essentially involves placing the tool in any pose within a 6D volume (which is very small even in the best case (Goswami et al., 1993)) and then measuring at least six base-fixture-to-tool-fixture distances between magnetic cups. However, even API eventually stopped offering telescoping ballbars with broad measurement ranges. Since the main application of the telescoping ballbar has always been evaluating the accuracy of numerically controlled machine tools as per standards such as ISO 230-4:2005 ("Test code for machine tools - Part 4: Circular tests for numerically controlled machine tools," 2005), the measurement range of today's telescoping ballbars is at most a mere few millimetres.

The only telescoping ballbars currently available for commercial sale are those produced by Renishaw and Cullam Technologies (in Taiwan). API and Heidenhain ceased their manufacture a few years ago. The Renishaw device has a measurement range of only 2 mm, whereas the Cullam version has a 12 mm measurement range.

In this paper, we expand ideas proposed previously (Goswami et al., 1993; McMurtry, 2007; Schiele et al., 1986) and apply them using today's commercially available telescoping ballbars. Namely, we examine the idea that a hexapod with fixed leg lengths can be assembled in many different configurations to allow the measurement of many different poses.

Section 3.2 of this paper describes Renishaw's telescoping ballbar and presents the optimal hexapod design for our 6D measurement device. Section 3.3 presents the algorithm for computing the pose of the tool, given the six leg measurements. Section 3.4 presents our analysis of the accuracy the measurement device. Section 3.5 presents the experimental validation of our device using an ABB IRB 120 industrial robot. Our conclusions are presented in Section 3.6.

3.2 Choosing the Optimal Hexapod Design for our 6D Measurement Device

For the purposes of the present study, we chose Renishaw's latest telescoping ballbar, the QC20-W, since it is compact and wireless. Renishaw's ballbars are also by far the most popular, many thousands of units having been sold. Figure 3.3 shows the main components of the QC20-W standard kit, which costs slightly less than $10,000. The nominal length of the QC20-W is 100 mm. The extension bars and calibrator allow highly accurate measurement of lengths near 100 mm, 150 mm and 300 mm. Other lengths can be measured using a custom-designed third-party calibrator.

Figure 3.4a shows a general 6-6 hexapod design representing a possible candidate for our purpose. In this section, design refers to the relative locations of the base attachment points, the relative locations of the tool attachment points, and the way the legs are connected. The two digits indicate the number of leg attachment points to the base and tool fixtures.

More than a century ago, Bricard (R Bricard, 1906; Raoul Bricard, 1897) studied the 6-DOF mechanism shown in Figure 3.4b, which he called an *articulated octahedron*. More specifically, he studied what we now call the *direct kinematic problem* (*DKP*). The objective of solving the DKP is to determine all possible poses of the tool, using the lengths of the six legs as input. Each of these solutions belongs to a different *assembly mode*, a term that is well suited to our application since we actually assemble our device in numerous configurations.

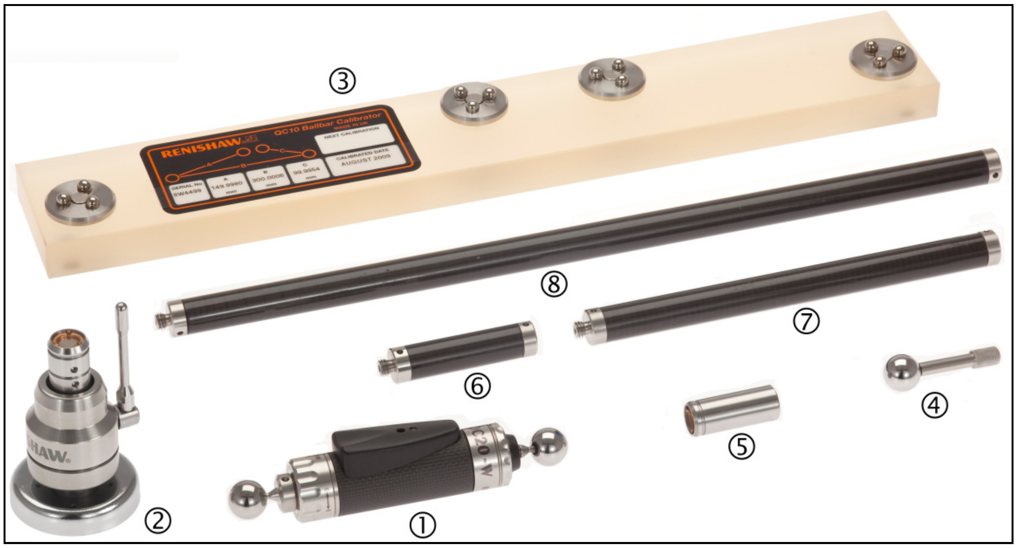

Figure 3.3 The main components of the standard QC20-W kit from Renishaw: (1) QC20-W ballbar; (2) center pivot assembly; (3) Zerodur calibrator; (4) setting ball; (5) magnetic cup; (6-8) 50 mm, 150 mm and 300 mm extension bars

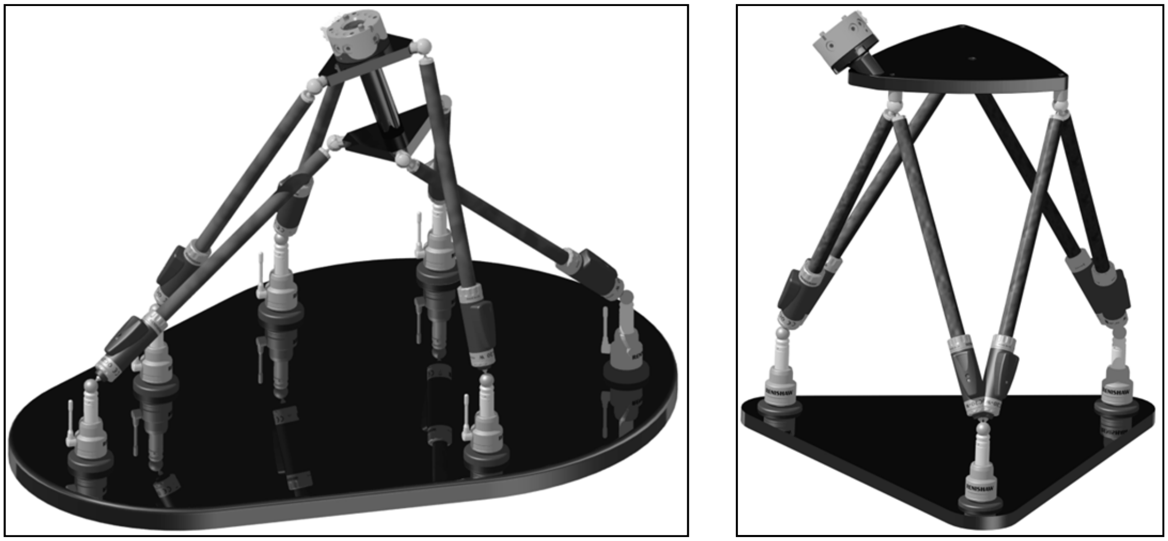

(a) (b)

Figure 3.4 (a) A general 6-6 hexapod and (b) the most common example of a 3-3 hexapod

It is now well known that the DKP of a general 6-6 hexapod design can have up to 40 real solutions (Dietmaier, 1998) and that these can be found by solving a univariate polynomial of degree 40 (Husty, 1996). However, the process is very complex and prone to numerical errors that can exceed the effects of leg length measurement errors. In addition, having six distinct base attachment points and six distinct tool attachment points increases the cost of the 6D measurement device and the risks of mechanical interference, complicates the calculation of measurement uncertainty, and most importantly requires the use of a high-accuracy 3D device in order to measure the relative positions of the base attachment and tool fixture attachment points.

The fewer the attachment points (the minimum being three on the base and three on the tool fixture), the simpler the DKP of the hexapod design. In practice however, very few positioning hexapods have fewer than twelve attachment points, for the simple reason that double or triple spherical joints are difficult to manufacture. However, this is not an issue in our application, since we do not need to use six telescoping ballbars simultaneously the way Diolez did (Diolez, 2006). We therefore focused our attention on the so-called 3-3 hexapod design, meaning that there are only three attachment points to the base fixture and three to the tool fixture. This means that we need purchase from Renishaw only an additional two center pivot assemblies (part number A-8014-1281) and three magnetic cups (part number A-8014-0522), for a cost of about $1500.

For our application, the main advantage of the 3-3 hexapod design is that no 3D measurement device is necessary in order to measure the relative positions of the base and tool attachment points. The telescoping ballbar itself can be used to measure the distances between the attachment points, with increased accuracy. The nominal lengths provided with the standard QC20-W kit (100 mm, 150 mm, and 300 mm) were chosen, 300 mm (the longest) for the distance between base attachment points and 150 mm for the distance between tool fixture attachment points (for reasons explained in Section 3.3). Finally, since the lengths of six hexapod legs must be measured for each pose of the tool, it would be too time consuming to use more than one nominal length. Legs of equal nominal length were therefore chosen, and since the longer the legs the larger the measurement range of the device, this length was 300 mm.

In the most common 3-3 hexapod design, denoted $1^{23}2^{13}3^{21}$ (i^{jk}), base attachment point i is connected to tool attachment points j and k ($i, j, k = 1, 2, 3; j \neq k$). Each attachment point is thus connected to two legs (Figure 3.4b). This design has sixteen DKP solutions, which can be obtained by solving a univariate polynomial of degree eight (Innocenti and Parenti-Castelli, 1990). Of these solutions, only eight are above the base plane and hence propose usable assembly modes for our purpose. However, this design was rejected, since the DKP of a $1^{23}2^{13}3^{21}$ hexapod with six legs of nearly equal length yields multiple solutions and is numerically unstable. We nevertheless note with interest that the approaches presented previously (Goswami et al., 1993; McMurtry, 2007; Schiele et al., 1986) used this exact design.

There are three other 3-3 designs, denoted $1^{12}2^{123}3^{1}$, $1^{12}2^{12}3^{23}$ and $1^{12}2^{123}3^{3}$, and each of these has a trivial DKP with eight solutions found by solving three quadratic equations in cascade (Faugère and Lazard, 1995). Unfortunately, the assembly of the latter two cannot be completed when the legs are of equal length and both the base attachment and tool attachment points form equilateral triangles. (The DKP has no solutions in this case.) These two designs were therefore also rejected for our application.

The remaining hexapod design, namely $1^{12}2^{123}3^{1}$, was first proposed in 1991 (Zhang and Song, 1992). The four assembly modes are illustrated in Figure 3.5. The other four DKP solutions place the tool below the base, making them unusable in practice. In fact, the solutions shown in Figures 3.5b and 3.5c are not usable either, due to interference between the telescoping ballbar and the tool fixture, although it would be possible to design the tool fixture so that all four of these DKP solutions are mechanically feasible.

The ability to measure only two distinct poses (represented in Figures 3.5a and 3.5d) is obviously insufficient. Fortunately, for both of these poses, we can measure two additional poses simply by rotating the tool ±120° about the axis normal to and passing through the center of the tool fixture triangle. Furthermore, in the configurations shown in Figures 3.5b and 3.5c, we can flip the tool 180° and obtain three measurable poses by rotating the tool ±120° about this axis. Finally, we can use all six permutations, namely 123, 132, 213, 231, 312, and 321 for the base connection points. The device can thus actually measure a total of 72 poses (2×3×2×6) with 36 hexapod designs denoted as $1^{12}2^{123}3^{1}$, $1^{23}2^{231}3^{2}$, $1^{31}2^{312}3^{3}$, $1^{32}2^{321}3^{3}$ and so on. Since this is difficult to visualize, we show all 72 configurations in Figure 3.6.

A QC-5 tool changer from ATI for attaching the tool fixture to an industrial robot is visible in Figure 3.5, which also shows the robot flange reference frame, called the *tool reference frame*. The location of the tool changer with respect to the tool fixture was chosen for the purposes of a project in which the robot was being calibrated using a laser tracker and an optical tracker (A Nubiola et al., 2013) and is not likely optimal for the present study. In that project, we needed to have an end-effector with three measurement points that are located as differently as possible with respect to the robot's flange. We only had a vague idea of the method proposed in this paper in mind. Figure 3.7 shows a plot of the angle of rotation between two poses (called *orientation distance*) according to the axis-angle representation versus the 3D distance (called *position distance*) between the two poses using the tool reference frame origin as the point of measurement for each pairing (72×71/2) of the 72 poses shown in Figure 3.6. It should be noted that due to the symmetry of our device, each point in this plot corresponds to anywhere from 3 to 24 pairs of poses.

Figure 3.7 shows that the pairs of poses very close to each other (less than 30° and 50 mm apart) are clustered in only three groups (represented as red points). This means that for the chosen tool reference frame, there are a few redundant measurement configurations that can be eliminated. The point closest to the origin thus corresponds to six pairs, namely {10, 37}, {46, 49}, {2, 70}, {34, 61}, {22, 25} and {13, 58} (numbers corresponding to the pose order presented in Figure 3.6, from left to right and top to bottom). The second closest point corresponds to pairs {14, 59}, {35, 62}, {11, 38}, {47, 50}, {23, 26} and {3, 71}. Finally, the third closest point corresponds to pairs {1, 72}, {12, 39}, {15, 60}, {48, 51}, {24, 27} and {36, 63}. We can therefore eliminate poses 1, 2, 3, 10, 11, 12, 13, 14, 15, 22, 23, 24, 34, 35, 36, 46, 47 and 48 (marked with a white cross in Figure 3.6) and retain the remaining 54 poses. Thus, the device described here can be used to measure 54 different poses of the flange of an industrial robot, the positions of which are situated within a large portion of a sphere of approximately 240 mm in radius. Finally, it should be noted that a different choice of tool reference frame will produce different position distances, but the orientation distances will remain the same.

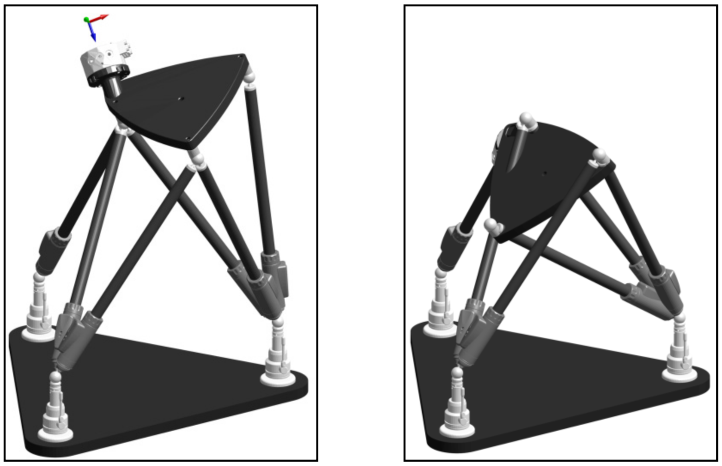

(a) DKP solulution (b) DKP solution 2

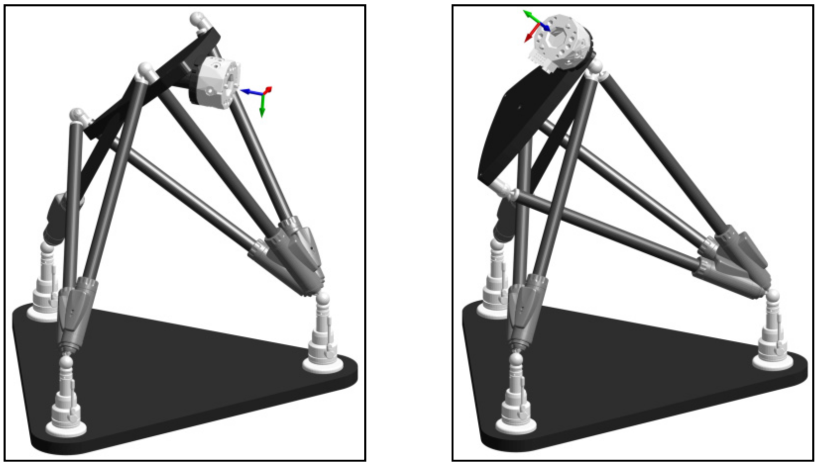

(c) DKP solution 3 (d) DKP solution 4

Figure 3.5 Four of the eight possible DKP solutions for the $1^{12}2^{123}3^{1}$ hexapod

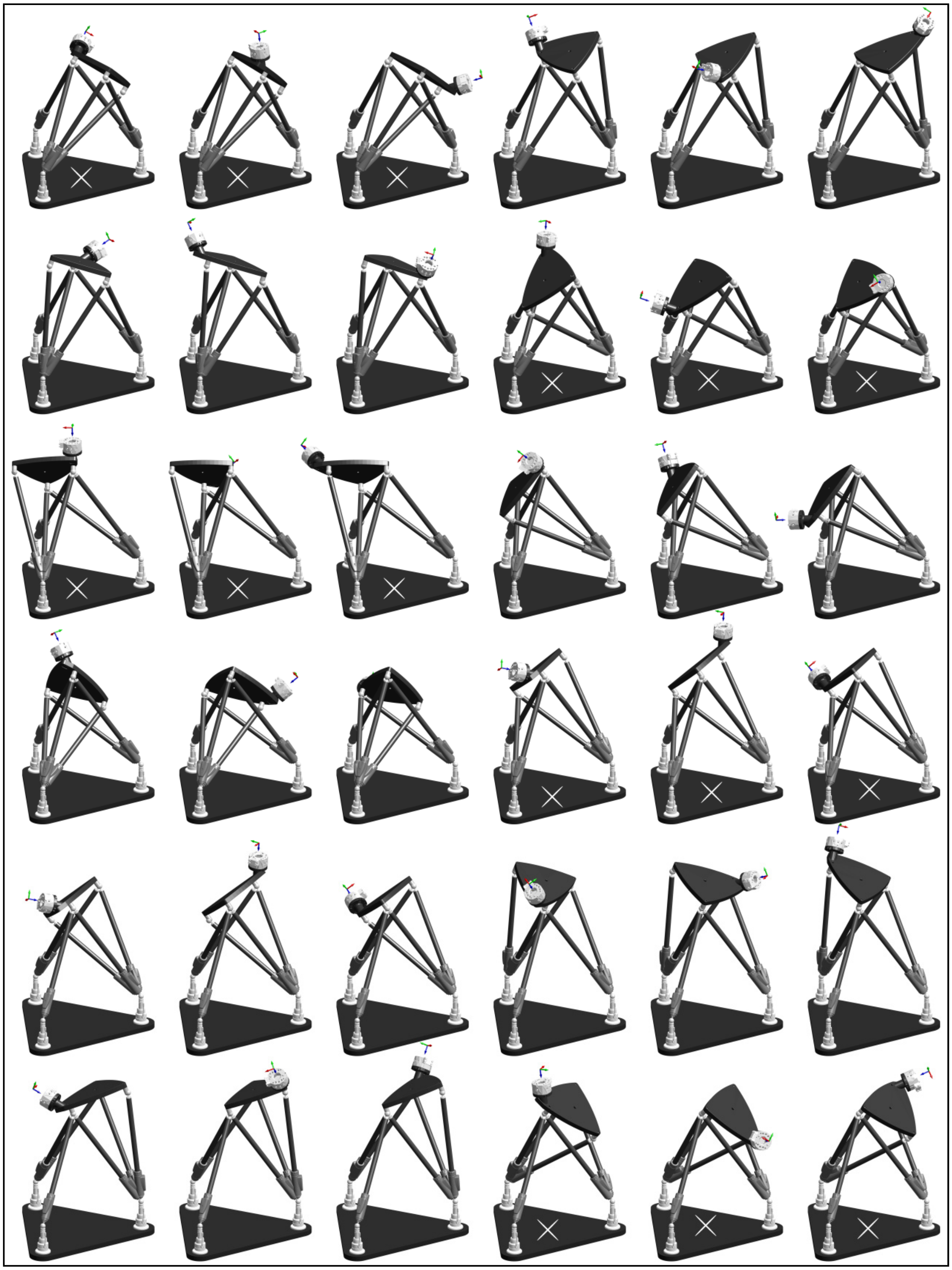

Figure 3.6 The 72 different tool poses that can be measured using our device (18 of these, marked with a white cross, are superfluous)

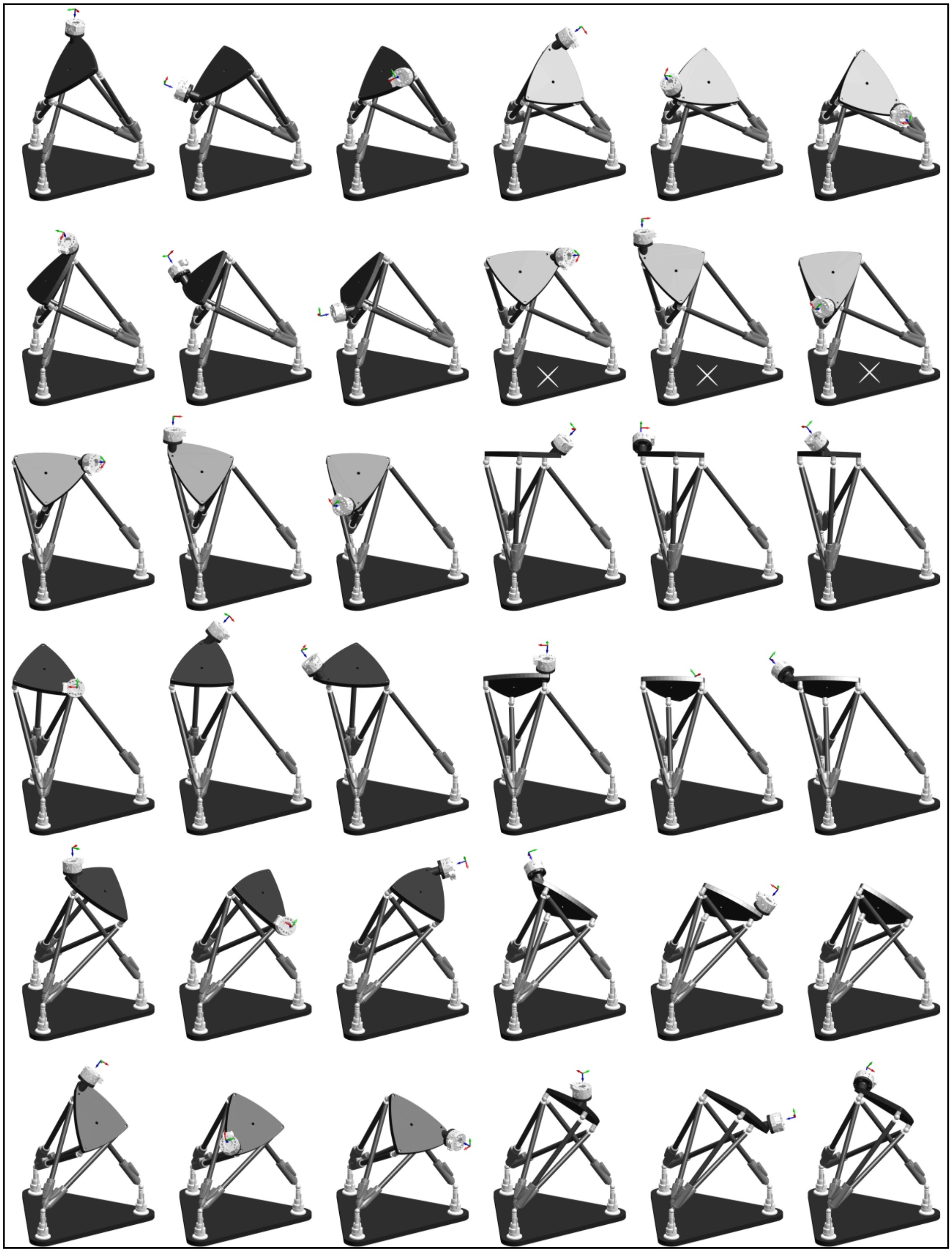

Figure 3.6 (continued) The 72 different tool poses that can be measured using our device (18 of these, marked with a white cross, are superfluous)

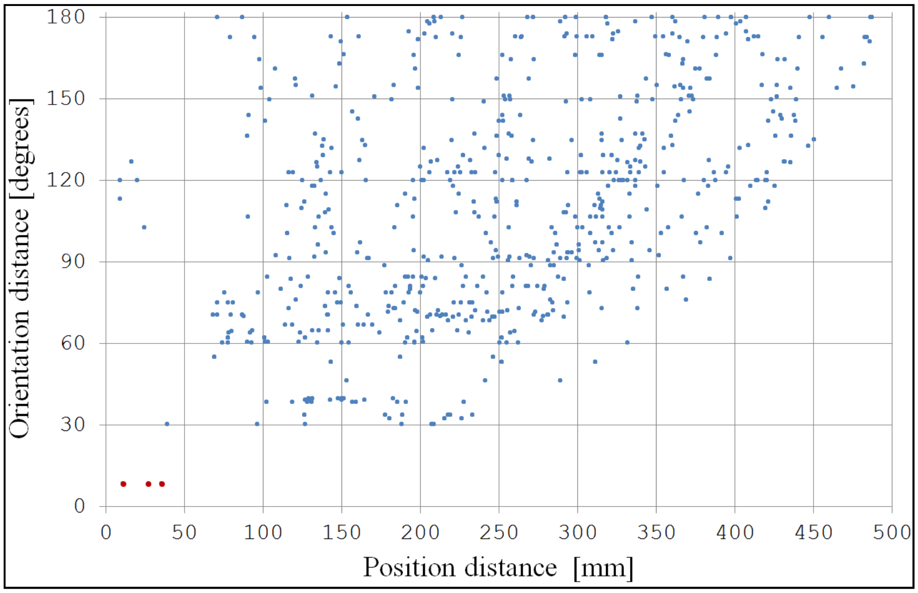

Figure 3.7 Position and orientation distances between the tool reference frames of each pairing of the 72 measurable poses shown in Figure 3.6

3.3 Direct Kinematics of our Hexapod Design

As mentioned above, the DKP of the $1^{12}2^{123}3^{1}$ hexapod design has eight solutions obtainable by solving three quadratic equations in cascade. Although there are 35 additional designs obtainable from the $1^{12}2^{123}3^{1}$ design by permutation, the DPK solution is presented only for the $1^{12}2^{123}3^{1}$ design shown in Figure 3.8. The solution for this design is nearly identical to that of the 35 other designs.

B_1, B_2, and B_3 represent the base attachment points, while T_1, T_2 and T_3 represent the tool fixture attachment points. The base reference frame xyz is set arbitrarily as shown in Figure 3.8. The distances between B_i and B_j, T_i and T_j, and B_i and T_j are respectively b_{ij}, t_{ij} (i, $j = 1, 2, 3$; $i \neq j$) and ρ_{ij} ($i,j = 1, 2, 3$). The algebraic vectors that define the positions of the base attachment points are:

$$\mathbf{b}_1 = \begin{bmatrix} 0 & 0 & 0 \end{bmatrix}^T \tag{3.1}$$

$$\mathbf{b}_2 = \begin{bmatrix} b_{12} & 0 & 0 \end{bmatrix}^T \tag{3.2}$$

$$\mathbf{b}_3 = \begin{bmatrix} \dfrac{b_{12}{}^2 - b_{23}{}^2 + b_{31}{}^2}{2b_{12}} & \dfrac{\sqrt{(b_{23}-b_{12}+b_{31})(b_{12}-b_{23}+b_{31})(b_{12}+b_{23}-b_{31})(b_{12}+b_{23}+b_{31})}}{2b_{12}} & 0 \end{bmatrix}^T \tag{3.3}$$

To find the pose of the tool, the DKP of a tripod (*e.g.* $B_1B_2B_3T_1$) must be solved. This can be achieved using the following function (Nair, 1992):

$$\mathbf{Tri}(\mathbf{v}_1, \mathbf{v}_2, \mathbf{v}_3, l_1, l_2, l_3) = \mathbf{p} + s\,\mathbf{k} \tag{3.4}$$

where $\mathbf{v}_1$, $\mathbf{v}_2$, and $\mathbf{v}_3$ are vectors containing the coordinates of the three base points of the tripod and l_1, l_2, and l_3 are the lengths of the three legs, and

$$\mathbf{p} = \left(\frac{\xi_1}{\mathbf{u}^T\mathbf{u}}\right)\mathbf{u} + \left(\frac{\xi_2\left(\mathbf{u}^T\mathbf{u}\right) - \xi_1\left(\mathbf{u}^T\mathbf{w}\right)}{\left(\mathbf{u}^T\mathbf{u}\right)\left(\left(\mathbf{u}\times\mathbf{w}\right)^T\left(\mathbf{u}\times\mathbf{w}\right)\right)}\right)\left(\mathbf{u}\times\mathbf{w}\right)\times\mathbf{u} \tag{3.5}$$

$$\xi_1 = \frac{1}{2}\left(l_1^2 - l_2^2 + \mathbf{v}_2^T\mathbf{v}_2 - \mathbf{v}_1^T\mathbf{v}_1\right) \tag{3.6}$$

$$\xi_2 = \frac{1}{2}\left(l_1^2 - l_3^2 + \mathbf{v}_3^T\mathbf{v}_3 - \mathbf{v}_1^T\mathbf{v}_1\right) \tag{3.7}$$

$$\mathbf{u} = \mathbf{v}_2 - \mathbf{v}_1 \tag{3.8}$$

$$\mathbf{w} = \mathbf{v}_3 - \mathbf{v}_1 \tag{3.9}$$

$$\mathbf{k} = \frac{\mathbf{u}\times\mathbf{w}}{\sqrt{\left(\mathbf{u}\times\mathbf{w}\right)^T\left(\mathbf{u}\times\mathbf{w}\right)}} \tag{3.10}$$

$$s = \left(\mathbf{v}_1^T\mathbf{k}\right) \pm \sqrt{\left(\mathbf{v}_1^T\mathbf{k}\right)^2 - \left(\mathbf{p}-\mathbf{v}_1\right)^T\left(\mathbf{p}-\mathbf{v}_1\right) + l_1^2} \tag{3.11}$$

To determine the pose of the tool, the positions of the tool fixture attachments points are determined in the following order:

$$\mathbf{t}_1 = \mathbf{Tri}\left(\mathbf{b}_1, \mathbf{b}_2, \mathbf{b}_3, \rho_{11}, \rho_{21}, \rho_{31}\right) \tag{3.12}$$

$$\mathbf{t}_2 = \mathbf{Tri}\left(\mathbf{b}_1, \mathbf{b}_2, \mathbf{t}_1, \rho_{12}, \rho_{22}, t_{12}\right) \tag{3.13}$$

$$\mathbf{t}_3 = \mathbf{Tri}\left(\mathbf{t}_2, \mathbf{b}_2, \mathbf{t}_1, t_{23}, \rho_{23}, t_{31}\right) \tag{3.14}$$

One of the two solutions for $\mathbf{t}_1$ is discarded because of its negative z coordinate, leaving a total of four solutions, already illustrated in Figure 3.5.

Therefore, the DKP of the $1^{12}2^{123}3^{1}$ hexapod design retained for our 6D measurement device can be solved in closed form, and there is virtually no numerical error for the chosen nominal lengths.

Given the above explanation of the $1^{12}2^{123}3^{1}$ design DKP, the choice of 150 mm for the nominal distance between the tool attachment points is justified. Indeed, if 300 mm is chosen, there will be a single feasible solution, since a tool attachment point will be extremely close to a base attachment point in all other solutions. The 100 mm option simply makes the tool fixture too small.

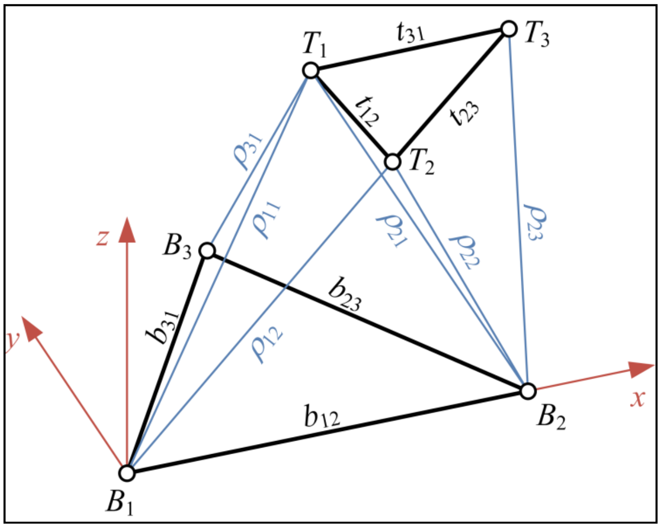

Figure 3.8 A schematic representation of the $1^{12}2^{123}3^{1}$ hexapod design

3.4 Calculating the Accuracy of the 6D Measurement Device

The accuracy of the 6D measurement device in its $1^{12}2^{123}3^{1}$ implementation (*i.e.* the four configurations shown in Figure 3.5) is calculated below for the nominal lengths only (*i.e.* $b_{12} = b_{23} = b_{31} = \rho_{11} = \rho_{12} = \rho_{22} = \rho_{23} = \rho_{21} = \rho_{31} = 300$ mm and $t_{12} = t_{23} = t_{31} = 150$ mm). It is clearly the same for the 72 configurations shown in Figure 3.6 and varies negligibly with ±1 mm variations of these 12 distances (*i.e.* the measurement range of the telescoping ballbar).

Using the following expression of uncertainty in measurement ("Uncertainty of measurement - Part 3: Guide to the expression of uncertainty in measurement," 2008), the uncertainty associated with the measurement of the coordinates of the three tool attachment points can be expressed in terms of the uncertainty of a single point-to-point distance measurement:

$$\mathbf{u}_{\mathbf{t},i} = \left[\sqrt{\sum_j \left(\frac{\partial \mathbf{t}_{i,x}}{\partial q_j} \right)^2 \sigma_s^{\,2}}, \sqrt{\sum_j \left(\frac{\partial \mathbf{t}_{i,y}}{\partial q_j} \right)^2 \sigma_s^{\,2}}, \sqrt{\sum_j \left(\frac{\partial \mathbf{t}_{i,z}}{\partial q_j} \right)^2 \sigma_s^{\,2}} \right]^T, \tag{3.15}$$

where $\mathbf{u}_{\mathbf{t},i}$ is the uncertainty associated with the measurement of the coordinates $\mathbf{t}_i$ of tool fixture attachment point i ($i = 1, 2, 3$), σ_s is the uncertainty associated with the measurement of the twelve distances (*i.e.* the uncertainty associated with the telescoping bar) and q_j ($j = 1, 2, \ldots, 12$) are the measurements that contribute to determining $\mathbf{t}_i$ (*i.e.* the twelve distances):

$$\mathbf{q} = [b_{12}, b_{23}, b_{31}, \rho_{11}, \rho_{21}, \rho_{31}, \rho_{12}, \rho_{22}, \rho_{23}, t_{12}, t_{23}, t_{31}] \tag{3.16}$$

The partial derivatives of $\mathbf{t}_i$ with respect to q_j are called the sensitivity coefficients, since $\mathbf{t}_i$ can be seen as a function that depends on $\mathbf{q}$. Since the uncertainty is calculated for each axis of the Cartesian space, the total measurement uncertainty associated with the coordinates $\mathbf{t}_i$ will be the Euclidean norm of $\mathbf{u}_{\mathbf{t},i}$.

By applying Eq. (3.15) to each of the four DKP solutions shown in Figure 3.5, the measurement uncertainties given in Table 3.1 are obtained. It should be noted that the uncertainty specified by the manufacturer of the QC20-W telescoping ballbar is 2 μm at the

95 % confidence level (i.e. $\sigma_s = 0.510$ µm). Therefore, the standard deviation with which our device measures the position of the three tool fixture attachment points is better than ±1.622 µm, and the accuracy is ±3.18 µm at the 95 % confidence level.

Finally, the position measurement accuracy of our device at the tool reference frame shown in Figure 3.5 depends on the uncertainty of the measurement of this frame with respect to the three tool fixture attachment points and on the repeatability associated with the tool changer. This will not be calculated here.

Table 3.1 Measurement uncertainties for each of the three tool attachment points in the four DKP solutions shown in Figure 3.5

$\mathbf{t}_i$	DKP solution number	Uncertainty $\mathbf{u}_{\mathbf{t},i}$	$\lVert\mathbf{u}_{\mathbf{t},i}\rVert$
$\mathbf{t}_1$	1, 2, 3, 4	[1.5, 1.6, 0.7] σ_s	2.309 σ_s
$\mathbf{t}_2$	1, 2	[1.5, 1.9, 1.1] σ_s	2.646 σ_s
$\mathbf{t}_2$	3, 4	[1.5, 1.2, 1.6] σ_s	2.480 σ_s
$\mathbf{t}_3$	1	[1.6, 2.6, 1.0] σ_s	3.179 σ_s
$\mathbf{t}_3$	2	[1.1, 2.5, 1.5] σ_s	3.054 σ_s
$\mathbf{t}_3$	3	[1.0, 2.1, 1.7] σ_s	2.853 σ_s
$\mathbf{t}_3$	4	[1.6, 2.2, 1.7] σ_s	3.180 σ_s

3.5 Experimental Validation

Experiments designed to test the effectiveness of our 6D measurement device are described below. The accuracy of the ballbar device was not validated, since no sub-micron CMM was available. The device was tested using an ABB IRB 120 industrial robot.

The rated payload of this robot is 3 kg and its unidirectional repeatability is about 20 µm. The robot was previously calibrated using a laser tracker (A Nubiola et al., 2013) and the same tool fixture (http://youtu.be/i0ztjX0jlSU). The tool and base fixtures of the 6D device are made of steel. For more flexibility, the base fixture of the device was attached to a pivoting platform (AP180 from Thorlabs) that can be locked into a large range of orientations.

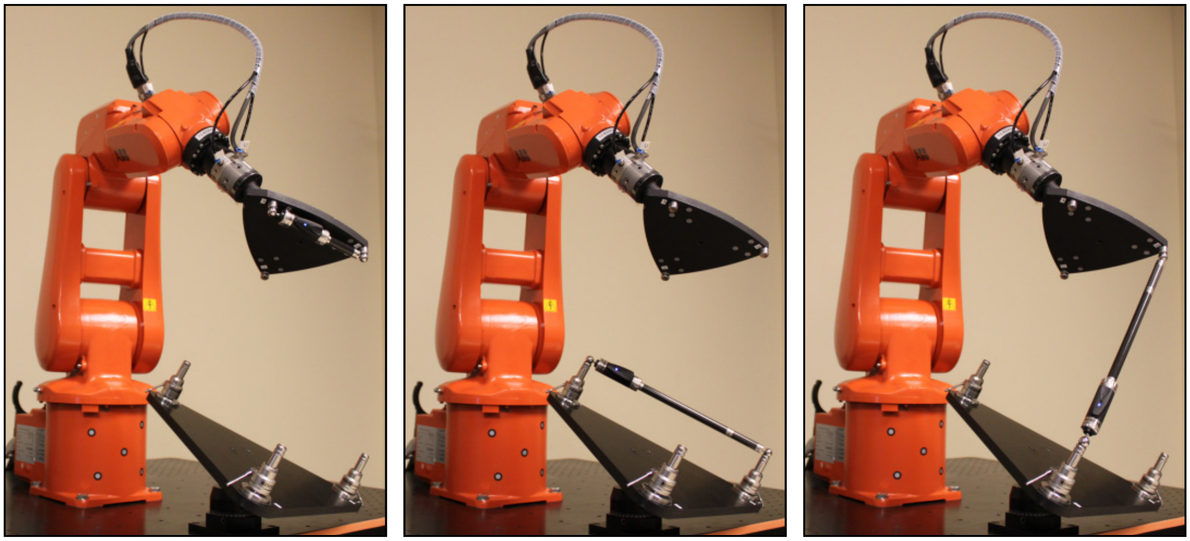

(a) measuring t_{12} (b) measuring b_{23} (c) measuring ρ_{12}

Figure 3.9 Measuring the base and tool distances as well as the leg distances in a given robot configuration

Figure 3.9 shows the ABB IRB 120 robot in one of the poses measurable using the 6D device. While the device can measure 72 distinct poses, of which only 54 are sufficiently distinct (see the end of Section 3.2), many of these poses are not attainable by a small industrial robot such as the IRB 120, regardless of the position of the base fixture. For the position shown in Figure 3.9, which was chosen almost arbitrarily, the robot can assume only 22 of the 72 measurable poses (Figure 3.10). Since the robot can assume 17 of these poses with both wrist configurations (known to some as flip and no-flip), the robot was tested in 39 of its configurations.

The procedure for measuring the accuracy of the robot using the device can be viewed at http://youtu.be/yMjUuv4J550, and is summarized as follows:

1. The ballbar is first assembled with the 50 mm extension bar, initialized on the Zerodur calibrator, and each of the three distances between the tool attachment points is measured (Figure 3.9a). Since the tool fixture is made of steel (rather than Invar or

Zerodur), these distances vary with fixture temperature and should be measured before each group of pose measurements.

2. The base fixture of the device is attached to the base of the robot. The position and orientation of the base fixture can be chosen using various criteria and robot simulation software (our RoKiSim program available at www.rokisim.com was used).
3. The clamping mechanisms of the three center pivot assemblies on the base fixture of the device are released. The setting ball is placed in one of the three magnetic cups of the triangular tool fixture, its center defined as the TCP (tool center point) of the robot, and the robot is moved with respect to each of the three base attachment points (by programming, not by manual jogging) such that the programmed distances between these three TCP positions are 300.000 mm. When the robot brings the setting ball to each center pivot assembly, the magnetic cup thereof snaps onto the ball (provided that the center of the setting ball is no more than about 2 mm from the center of the magnetic cup) and the clamping mechanism is then manually locked.
4. The ballbar is then assembled with the 150 mm and 50 mm extension bars, initialized on the Zerodur calibrator, and each of the three distances between the base attachment points is measured (Figure 3.9b). If the robot accuracy were perfect, these distances would be exactly 300.000 mm. In practice, there is an error of less than 1 mm (for an accurate robot), and the distances are measurable with the QC20-W.
5. The robot is finally programmed to move through each of its 39 configurations, and the six leg distances are measured one by one (Figure 3.9c). Initializing the ballbar on the Zerodur calibrator before each group of six measurements is strongly recommended, otherwise the repeated magnetic snaps and the manipulation of the ballbar produce an accumulated error of as much as 0.003 mm in the ballbar readings.

Since the above procedure may be very time consuming, it was automated using the application programming interface for the QC20-W telescoping ballbar, implemented in our robotics simulation software RoKiSim. Once the tool fixture is attached to the robot tool flange and the pose of the base fixture is selected manually, RoKiSim automatically calculates the feasible robotic configurations, which are displayed one by one with prompts (*e.g.* "Attach the ballbar between B_1 and T_1") using the Enter key. The entire procedure for measuring the pose of the end-effector of the robot in its 39 configurations (including attaching the base fixture to the robot's table) requires less than one hour. Initializing the ballbar with the calibrator and then measuring the six leg distances for a given pose of the tool is completed in one minute.

Table 3.2 shows the statistics of the position and orientation errors at the robot tool flange frame for the 39 robotic configurations measured, as well as of the position errors at the three tool fixture attachment points and the leg distance errors. Orientation errors are once again calculated as the rotation angle in the axis-angle orientation representation. Attachment point T_1 lies on axis 6 of the robot, while T_2 is the tool attachment point connected to the ballbar in Figure 3.9c. Attachment point T_3 is farthest from robot axis 6, which is why the position errors measured at this point are greatest.

Table 3.2 Errors for the 39 robotic configurations tested

	Pose errors at the robot tool flange frame		Position errors at T_1, T_2 and T_3			Leg distance errors
	position	orientation	T_1	T_2	T_3	
min.	0.115 mm	0.263°	0.127 mm	0.298 mm	0.602 mm	−0.452 mm
max.	0.916 mm	0.512°	0.785 mm	0.958 mm	1.107 mm	1.025 mm
mean	0.319 mm	0.333°	0.283 mm	0.643 mm	0.834 mm	0.220 mm

The pose errors measured at the robot tool flange frame are considerable, even though the robot was already calibrated. This is due in part to the relatively poor repeatability associated with the tool changer (*e.g.* point T_3 deviates as much as 0.100 mm between two successive attachments of the tool changer, even if the robot does not move), and to the delay (several months) between calibrating the robot and making the measurements shown in Table 3.2. Ideally, the validation procedure using our method should be performed immediately after robot calibration. However, as shown in the last column of Table 3.2, even though the robot was not very accurate, all leg measurements were within the ballbar measurement range of 2 mm (from −0.975 mm to +1.025 mm) except for only one measurement that reached the limit of 1.025 mm.

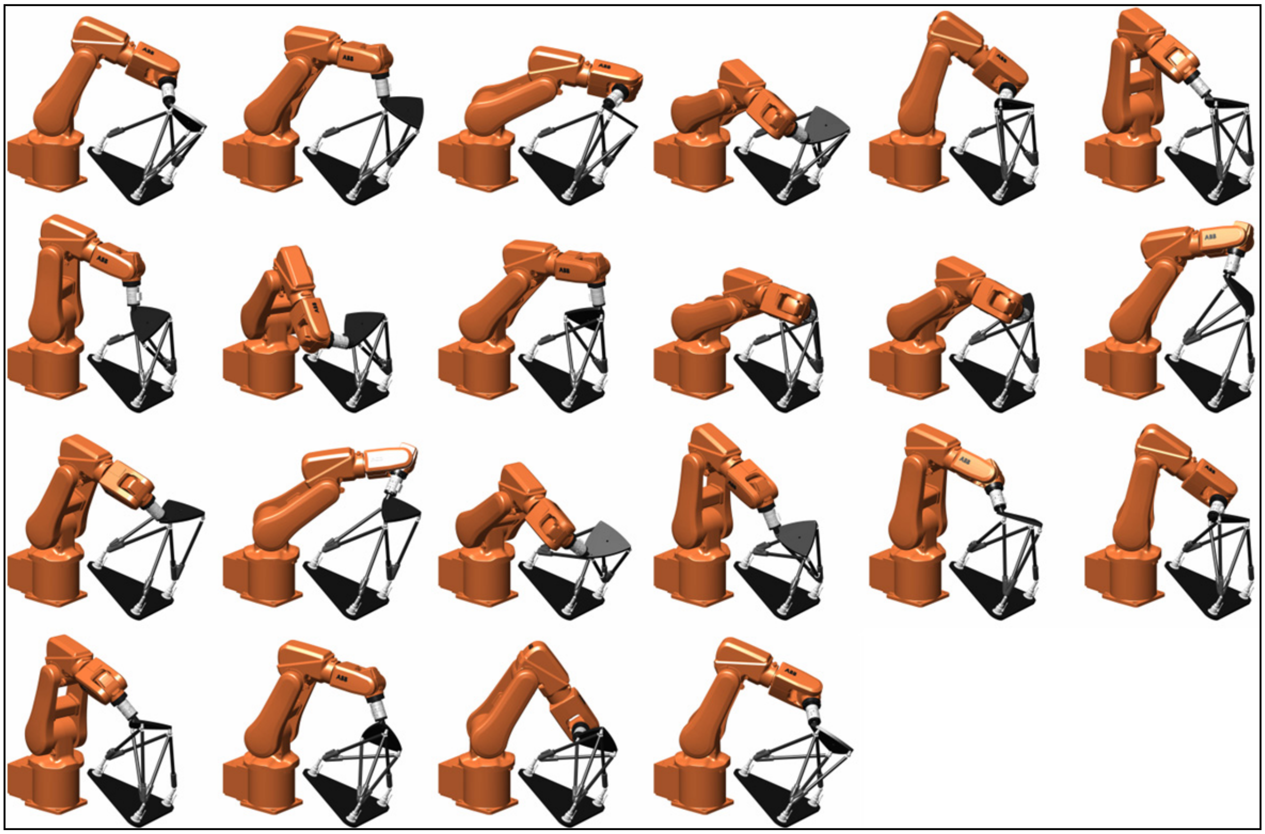

Figure 3.10 The 22 tool poses measurable using our device for a single setup of the base fixture. In 17 of these poses (not identified here), the robot can be positioned with two wrist configurations.

Although the measured robot configurations are sufficient in number and well distributed (as seen in Figure 3.10), there is no guarantee that the accuracy of the robot will not worsen in some other configuration in which the tool is in the vicinity of the base fixture. The positions of the three tool fixture attachment points were therefore measured using a four-foot FaroArm Platinum measurement arm equipped with a 0.5 inch steel ball probe in fifteen completely random robot configurations in which the tool fixture faced upwards rather than downwards. The results in Table 3.3 show that there is no major discrepancy between the robotic accuracy in these 15 random configurations and that observed with the 6D measurement device in the 39 configurations.

Table 3.3 Errors for 15 additional tool poses measured using the FaroArm

Statistical parameters	Pose errors at the robot tool flange frame		Position errors at T_1, T_2 and T_3		
	position	orientation	T_1	T_2	T_3
minimum	0.128 mm	0.261°	0.152 mm	0.373 mm	0.526 mm
maximum	0.454 mm	0.369°	0.444 mm	1.105 mm	1.160 mm
mean	0.246 mm	0.331°	0.256 mm	0.720 mm	0.980 mm

Finally, the multidirectional repeatability of the robot was measured using our device in four of the robot configurations shown in Figure 3.10, with five repetitions per configuration. The maximum multidirectional position repeatability measured at points T_1, T_2, and T_3 were 0.036 mm, 0.041 mm, and 0.043 mm, respectively. The maximum multidirectional position repeatability at the origin of the tool flange frame was 0.021 mm. ABB specifies that the unidirectional position repeatability at that point is 0.010 mm.

3.6 Conclusion

We propose a novel low-cost but high-accuracy device and method for measuring a set of more than fifty distinct poses of an industrial robot. The device consists of Renishaw's QC20-W telescoping ballbar standard kit plus certain accessories, a pivoting platform from Thorlabs, and two custom-machined steel triangular fixtures, for a total cost of about $13,000. The position accuracy of this novel 6D measurement device is approximately ±0.003 mm.

Our device can be used to measure the pose accuracy and multi-directional pose repeatability of any six-axis positioning mechanism, in particular six-axis industrial robots. Although the measurement procedure using our device does not comply with the ISO 9283 robot performance standard ("Manipulating industrial robots - Performance criteria and related test methods," 1998), we argue that it is in fact superior in some ways to the procedure proposed in that standard. In addition, our device can be used to calibrate any six-axis positioning mechanism (e.g., a hexapod (von Daake et al., 2013)). We intend to use it for calibrating industrial robots and believe that the improvement in robotic accuracy will be greater than that obtained using a laser tracker.

While our 6D device can measure more than fifty sufficiently distinct poses, the position distance between these is relatively small (no more than 500 mm) and might not be enough for large industrial robots. A bigger device could be constructed, but the corresponding calibrator required might not be available off-the-shelf. Such a calibrator (*e.g.* for 600 mm) could be obtained on a custom order basis from American companies such as Brunson Instrument or Micro Surface Engineering.

3.7 Acknowledgements

We thank the Canada Research Chair program, the Canada Foundation for Innovation and the Natural Sciences and Engineering Research Council of Canada for financing this work. We are also grateful to Renishaw for providing us with their application programming interface for communicating with the QC20-W telescoping ballbar.

CHAPTER 4

ABSOLUTE ROBOT CALIBRATION WITH A SINGLE TELESCOPING BALLBAR

Albert Nubiola and Ilian A. Bonev,
1100 Notre-Dame Ouest, Montréal, Québec, Canada H3C 1K3

This chapter has been published as an article in
Precision Engineering: vol. 38, n° 3 (2014), pp 472-480

Abstract

A novel 6D measurement system was recently proposed, comprising a single commercially available telescoping ballbar and two custom-made fixtures. One fixture is attached to the robot base and the other to the robot end-effector, and each having three magnetic cups. In each of 72 poses of the tool fixture, with respect to the base fixture, it is possible to measure six distances with the ballbar between the magnetic cups on the tool fixture and the magnetic cups on the base fixture, and thus calculate the pose with high accuracy. This paper is the first to present the successful use of this measurement system for absolute robot calibration. The robot calibrated is a Fanuc LR Mate 200iC six-axis industrial robot and the telescoping bar used is the QC20-W by Renishaw. The absolute position accuracy of the robot after calibration is validated with a Faro laser tracker in almost 10,000 robot configurations. Considering the validation data in only the front/up configurations, the mean absolute positioning error is improved from 0.873 mm to 0.479 mm. To allow a comparison, the robot is also calibrated using the laser tracker and the robot accuracy validated in the same 10,000 robot configurations.

4.1 Introduction

It is well-known that industrial robots are highly repeatable, but their nominal accuracy is relatively poor due to various sources of differences (errors) between the nominal robot model (used in the robot controller) and the real robot. These errors can be classified in five categories (Andrew Liou et al., 1993; Karan and Vukobratovic, 1994): environmental (such as those caused by temperature drifts), parametric (for example, manufacturing and assembly errors), measurement (caused by the limited resolution of the motor encoders), computational (computer round-off and steady-state control errors) and application (such as installation errors).

Fortunately, the accuracy of an industrial robot can be improved through calibration (Roth et al., 1987). The first step is to choose the mathematical model that will improve the representation of the position and orientation (pose) of the robot end-effector. This mathematical model is a function of the robot joint angles and takes into account the error parameters that need to be modelled. Models can be based on the Denavit-Hartenberg convention (Denavit and Hartenberg, 1955; Stone and Sanderson, 1987; Whitney et al., 1986), Denavit-Hartenberg Modified convention (Craig, 1986) or other conventions that improve error parameter identification, such as the complete and parametrically continuous model (CPC) (H Zhuang and Roth, 1992; Hanqi Zhuang et al., 1992) or other models based on the product of exponentials (POE) (He et al., 2010; Okamura and Park, 1996).

Depending on the type of errors modelled, the calibration can be classified as level-1, where only joint errors are modelled; level-2 calibration, also known as kinematic calibration (Ginani and Motta, 2011; Newman et al., 2000; Ye et al., 2006); and level-3 calibration, also called a non-kinematic calibration, which models errors other than geometric defaults such as stiffness (Jang et al., 2001; Lightcap et al., 2008; A Nubiola et al., 2013; Albert Nubiola and Bonev, 2013) and temperature (Gong et al., 2000).

The error parameters can be identified by measuring the *complete pose* or *partial pose* of the robot end-effector in a set of calibration robot configurations. Many measurement devices have been used for robot calibration or validation, such as: a touch probe and a reference artifact (Hayati and Mirmirani, 1985; Khalil and Besnard, 2002), a telescoping ballbar (M.R. Driels, 1993; Juneja and Goldenberg, 1997; Ota et al., 2002; Schiele et al., 1986; Vira and Lau, 1987), a small-range 3D (position) measurement device (such as a camera-based system), (Beyer and Wulfsberg, 2004) acoustic sensors(Stone and Sanderson, 1987), a large-range 3D measurement device (such as a laser tracker (Dumas et al., 2010; Meng and Zhuang, 2001; A Nubiola et al., 2013; Albert Nubiola and Bonev, 2013; Puskorius and Feldkamp, 1987) or CMM (M.R. Driels, 1993; Lightcap et al., 2008; B. W. Mooring and Padavala, 1989)) and a 6D (complete pose) measurement device (such as a camera-based system (Gatla et al., 2007; Meng and Zhuang, 2001; Puskorius and Feldkamp, 1987) or a laser tracker with a 6D probe (Boochs et al., 2010)).

In practice, the most critical issue is the choice of the measurement system, as the latter determines the efficiency and cost of the robot calibration process. For example, the so-called closed-loop method needs to be used if the robot tool is constrained to lie on a reference object of precisely known geometry (Besnard et al., 2000; Hayati and Mirmirani, 1985). Although the calibration algorithm might be more complex, this method is cheaper because it only needs a switch, such as a touch probe, to detect the contact with an obstacle and save the joint readings. On the other hand, open-loop calibration methods can be applied if a 3D or 6D measurement device is used. In general, these devices are either very expensive (such as laser trackers and CMMs), or not highly accurate (which is the case of some stereo cameras, also called optical CMMs).

In contrast, a new 6D measurement system based on a telescoping ballbar was recently proposed (Albert Nubiola et al., 2013). This new 6D measurement device has the advantage of being more accurate than laser trackers and yet cheaper than even the cheapest optical CMM. The principal disadvantage of this system is that it can only measure a limited number of poses (maximum 72), which is a relatively small working volume.

The goal of this work is to evaluate the use of this novel 6D measurement system for the absolute calibration of a small six-axis serial robot, a Fanuc LR Mate 200iC. The absolute calibration is validated with a laser tracker in nearly 10,000 arbitrary robot configurations.

The remainder of this paper is organized as follows: Section 4.2 presents the experimental setup, briefly outlines the 6D measurement system, and describes a new algorithm for setting up the world reference frame. Section 4.3 then describes the robot calibration model and the parameter identification procedure used. Section 4.4 presents the measurement procedure and the experimental results. Finally, conclusions are presented in Section 4.5.

4.2 Experimental Setup and Description of Measurement System

The experimental setup is shown in Figure 4.1. It consists of a Fanuc LR Mate 200iC six-axis industrial robot, a QC20-W telescoping ballbar from Renishaw, and custom-made base, and tool fixtures made of steel. A QC-5 tool changer from ATI is used for attaching the tool fixture to the robot flange.

The tool and base fixtures each consist of three equidistant magnetic cups for 0.5 inch precision steel balls. The tool fixture, including the tool changer and the adaptors, weighs approximately 2.7 kg, which is within the 5 kg rated payload of the robot. The base fixture is attached to a ball-in-socket pivoting platform (AP180 from Thorlabs) that can be locked into a large range of orientations.

The telescoping ballbar chosen for testing, the QC20-W, is the latest telescoping ballbar from Renishaw since it is compact and wireless. Renishaw's ballbars are also by far the most popular, many thousands of units having been sold. The nominal length of the QC20-W is 100 mm. The extension bars and calibrator allow highly accurate measurement of lengths near 100 mm, 150 mm, and 300 mm.

As described in (Albert Nubiola et al., 2013), several authors have proposed the use of six custom-made telescoping ballbars arranged as the legs of a hexapod for continuous 6D motion measurement. However, it is obviously preferable (and much cheaper) to use off-the-shelf telescoping ballbars such as the QC20-W. The problem with such ballbars is that their measurement range is very limited (only ±1 mm in the case of the QC20-W). To overcome this problem, and be able to measure a large number of discrete poses, the use of the so-called 3-3 hexapod design was proposed in (Albert Nubiola et al., 2013) (Figure 4.2). The main advantage of the 3-3 hexapod design is that no 3D measurement device is necessary in order to measure the relative positions of the three base and three tool attachment points. The telescoping ballbar itself can be used to measure the distances between the attachment points, with high accuracy. The nominal lengths provided with the standard QC20-W kit were chosen, 300 mm (the longest) for the distance between the base attachment points and 150 mm for the distance between the tool fixture attachment points. Legs of equal nominal length were chosen, and since the longer the legs the larger the measurement range of the device, this length was 300 mm.

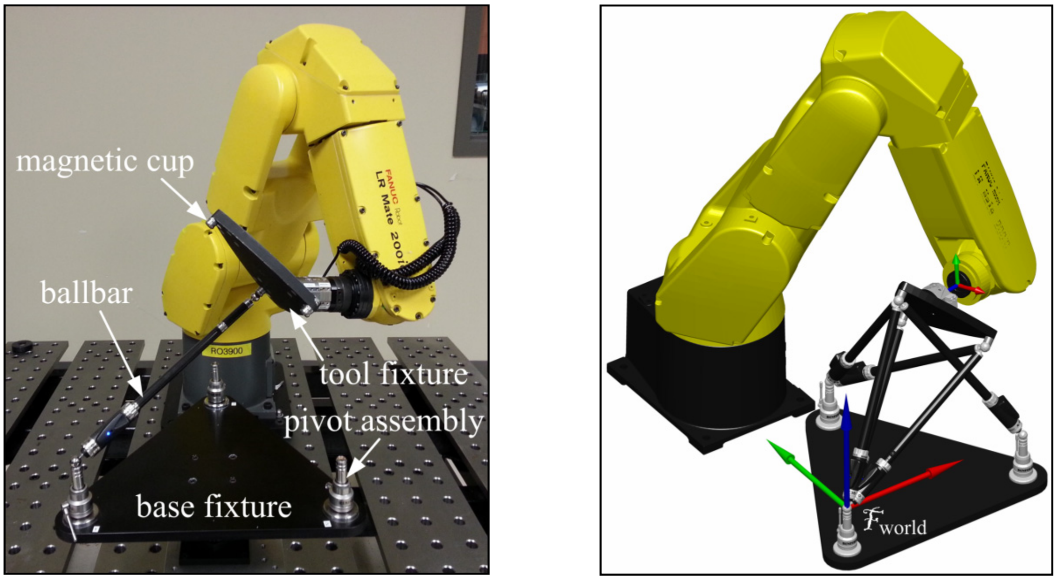

(a) experimental setup

(b) composite image of the six “leg” measurements

Figure 4.1 Experimental setup for measuring the pose of the robot end-effector

The main idea behind this novel 6D measurement device and method is that the 3-3 hexapod can be assembled in various configurations, thus allowing the measurement of several poses. To allow simpler and more robust computations of these poses (i.e. to simplify the direct kinematics of the hexapod), the triple-double-single attachment points arrangement was used (Zhang and Song, 1992), meaning that legs are attached to the base and tool fixtures in groups of three, two, and one (Figure 4.2). The four feasible assembly configurations for one such arrangement of the base attachment points (referred to as the “231” arrangement) are shown in Figure 4.3.

The ability to measure four poses is obviously insufficient. Fortunately, for each of these four poses, two additional measurable poses can be obtained simply by rotating the tool ±120° about the axis normal to, and passing through the center of the tool fixture triangle. Finally, all six permutations can be used, namely 123, 132, 213, 231, 312, and 321 for the base attachment points. The device can thus actually measure a total of 72 poses (4×3×6). Reference (Albert Nubiola et al., 2013) shows the complete set of poses and gives the equations for computing the coordinates of the tool attachment points from the six “leg” measurements with the ballbar.

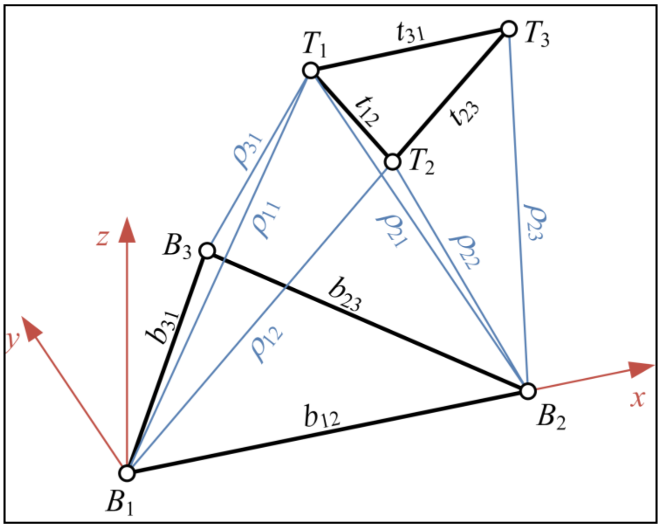

Figure 4.2 Illustration of one of the 3-3 hexapod designs used

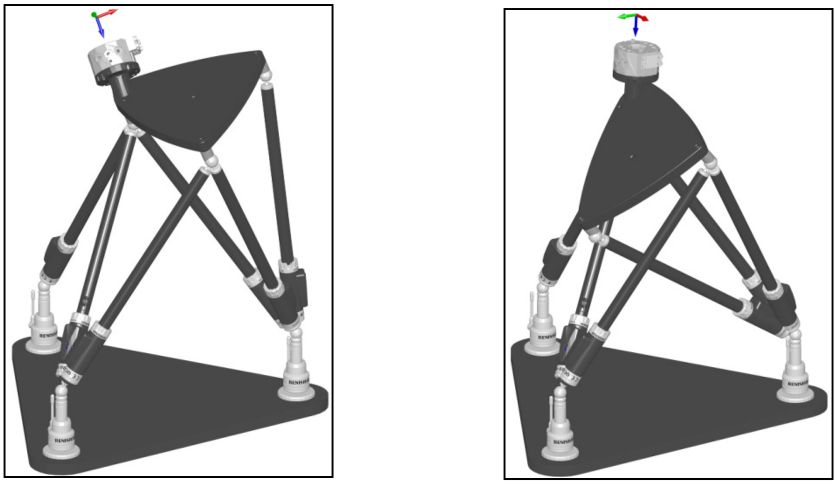

(a) assembly configuration 1 (b) assembly configuration 2

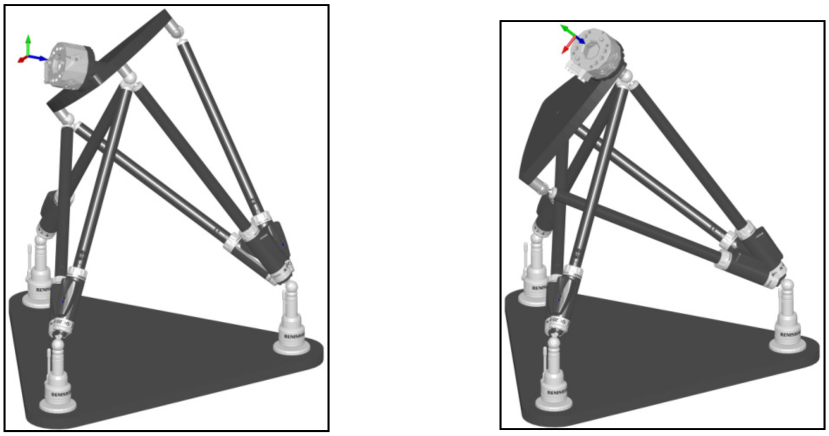

(c) assembly configuration 3 (d) assembly configuration 4

Figure 4.3 The four feasible assembly configurations for the 231 3-3 hexapod

The accuracy of this 6D measurement device, in the worst case, is found to be 3.18 times the accuracy of the 1D measurement system (telescoping ballbar) (Albert Nubiola et al., 2013). The telescoping ballbar used has an uncertainty of 2 µm at the 95% confidence level (i.e. σ_s = 0.510 µm). Therefore, the standard deviation, with which the 6D device measures the position of the three tool attachment points, is better than ±1.622 µm, and the accuracy is better than ±3.18 µm at the 95% confidence level.

A world reference frame (Φ_{world}) must be defined by the three base attachment points. In the original method (Albert Nubiola et al., 2013), the frame origin is placed at B_1, the x axis points to B_2, and the z axis is normal to the plane containing the three points (Figure 4.1b and Figure 4.2). However, in this definition, the error in measuring base attachment point 1 has a major influence on the position accuracy of the robot, while the errors in measuring the other two base measurement points have minor effect on the position accuracy according to the robot (the robot can be seen as an inaccurate measurement system in this case). The distance measured with the ballbar is redundant but more accurate than the distance seen by the robot, so it is better to combine both measurement systems to maximize accuracy. Since the distance between the three base attachment points is measured with very high accuracy using the ballbar, it is possible to take this information into account and define a new world reference frame. The goal of the algorithm explained next is to combine the 3D coordinates of the three base points given by the robot with the distances measured with the ballbar to find another three 3D points that improve the accuracy of the first three. Recall that the first three points are only measured with the robot.

Figure 4.4 shows the three base attachment points as measured by the robot or by the laser tracker, the coordinates of which are given by vectors $\mathbf{p}_i$ (i = 1, 2, 3). The initial world reference frame is denoted by Φ_A. The new world reference frame that is to be found is denoted by Φ_C, and the corrected coordinates of the base attachment points are given by vectors $\mathbf{q}_i$ (i = 1, 2, 3). The distances between these corrected base attachment points, d_{12}, d_{23} and d_{31}, are the ones measured with the ballbar, while d'_{12}, d'_{23} and d'_{31} are the distances as measured by the robot or laser tracker. For simplicity, the xy planes of both world frames coincide, and $\mathbf{p}_i$ and $\mathbf{q}_i$ (i = 1, 2, 3) are homogeneous vectors. The idea is to find the homogeneous transformation between Φ_A and Φ_C so that the sum $\|\mathbf{p}_1-\mathbf{q}_1\|^2+\|\mathbf{p}_2-\mathbf{q}_2\|^2+\|\mathbf{p}_3-\mathbf{q}_3\|^2$ is minimized.

Vectors $\mathbf{p}_i$ (i = 1, 2, 3) are defined as

$$\mathbf{p}_1 = \begin{bmatrix} 0 \\ 0 \\ 1 \end{bmatrix}, \tag{4.1}$$

$$\mathbf{p}_2 = \begin{bmatrix} d'_{12} \\ 0 \\ 1 \end{bmatrix}, \tag{4.2}$$

$$\mathbf{p}_3 = \begin{bmatrix} \dfrac{{d'_{12}}^2 - {d'_{23}}^2 + {d'_{31}}^2}{2d'_{12}} \\ \dfrac{\sqrt{\left(d'_{23} - d'_{12} + d'_{31}\right)\left(d'_{12} - d'_{23} + d'_{31}\right)\left(d'_{12} + d'_{23} - d'_{31}\right)\left(d'_{12} + d'_{23} + d'_{31}\right)}}{2d'_{12}} \\ 1 \end{bmatrix}, \tag{4.3}$$

while vectors $\mathbf{q}_i$ ($i = 1, 2, 3$) are given by

$$\mathbf{q}_1 = \mathbf{T}\begin{bmatrix} q_{1,a} \\ q_{1,b} \\ 1 \end{bmatrix} = \mathbf{T}\begin{bmatrix} 0 \\ 0 \\ 1 \end{bmatrix}, \tag{4.4}$$

$$\mathbf{q}_2 = \mathbf{T}\begin{bmatrix} q_{2,a} \\ q_{2,b} \\ 1 \end{bmatrix} = \mathbf{T}\begin{bmatrix} d_{1,2} \\ 0 \\ 1 \end{bmatrix}, \tag{4.5}$$

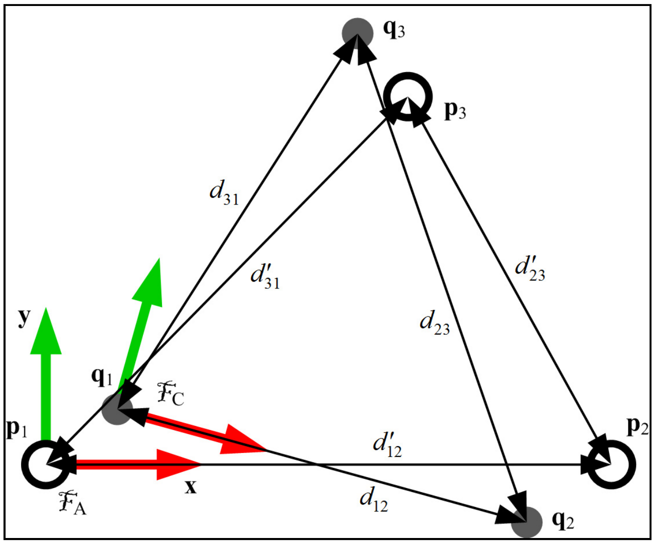

Figure 4.4 Relationship between the initial and corrected world reference frames

$$\mathbf{q}_3 = \mathbf{T}\begin{bmatrix} q_{3,a} \\ q_{3,b} \\ 1 \end{bmatrix} = \mathbf{T}\begin{bmatrix} \dfrac{{d_{12}}^2 - d_{23}^2 + d_{31}^2}{2d_{12}} \\ \dfrac{\sqrt{(d_{23}-d_{12}+d_{31})(d_{12}-d_{23}+d_{31})(d_{12}+d_{23}-d_{31})(d_{12}+d_{23}+d_{31})}}{2d_{12}} \\ 1 \end{bmatrix}, \tag{4.6}$$

where **T** is the 2D homogeneous matrix to be found

$$\mathbf{T} = \begin{bmatrix} \cos(\phi) & -\sin(\phi) & x \\ \sin(\phi) & \cos(\phi) & y \\ 0 & 0 & 1 \end{bmatrix}. \tag{4.7}$$

Thus, if vectors $\mathbf{q}_i$ (i = 1, 2, 3) are expressed as

$$\mathbf{q}_i = \begin{bmatrix} q_{i,\mathrm{x}} \\ q_{i,\mathrm{y}} \\ 1 \end{bmatrix} = \begin{bmatrix} x + q_{i,\mathrm{a}}\cos(\phi) - q_{i,\mathrm{b}}\sin(\phi) \\ y + q_{i,\mathrm{a}}\sin(\phi) + q_{i,\mathrm{b}}\cos(\phi) \\ 1 \end{bmatrix}, \tag{4.8}$$

their first-order partial derivatives is

$$\mathbf{D}_i = \begin{bmatrix} 1 & 0 & -q_{i,\mathrm{a}} \sin(\phi) - q_{i,\mathrm{b}} \cos(\phi) \\ 0 & 1 & +q_{i,\mathrm{a}} \cos(\phi) - q_{i,\mathrm{b}} \sin(\phi) \end{bmatrix}. \tag{4.9}$$

Then, the following system of six equations in three unknowns can be obtained:

$$\Delta\mathbf{p} = \mathbf{D}\Delta\mathbf{x} \tag{4.10}$$

$$\Delta\mathbf{p} = \begin{bmatrix} q_{1,\mathrm{x}} - p_{1,\mathrm{x}} \\ q_{1,\mathrm{y}} - p_{1,\mathrm{y}} \\ q_{2,\mathrm{x}} - p_{2,\mathrm{x}} \\ q_{2,\mathrm{y}} - p_{2,\mathrm{y}} \\ q_{3,\mathrm{x}} - p_{3,\mathrm{x}} \\ q_{3,\mathrm{y}} - p_{3,\mathrm{y}} \end{bmatrix} = \begin{bmatrix} 1 & 0 & 0 \\ 0 & 1 & 0 \\ 1 & 0 & -d_{12} \sin(\phi) \\ 0 & 1 & +d_{12} \cos(\phi) \\ 1 & 0 & -q_{3,\mathrm{a}} \sin(\phi) - q_{3,\mathrm{b}} \cos(\phi) \\ 0 & 1 & +q_{3,\mathrm{a}} \cos(\phi) - q_{3,\mathrm{b}} \sin(\phi) \end{bmatrix} \begin{bmatrix} \Delta x \\ \Delta y \\ \Delta\phi \end{bmatrix}. \tag{4.11}$$

This system of equations can be solved by using the least squares method. A solution can be obtained iteratively through the pseudo inverse, imposing zeros as first guess for the first iteration so that $\mathbf{T} = \mathbf{I}_3$:

$$\Delta\mathbf{x} = \left(\mathbf{D}^{\mathrm{T}}\mathbf{D}\right)^{-1} \mathbf{D}^{\mathrm{T}} \Delta\mathbf{p}\,. \tag{4.12}$$

Using this least squares approximation (instead of using the original method (Albert Nubiola et al., 2013)) improves about 15% the accuracy of the robot after calibration.

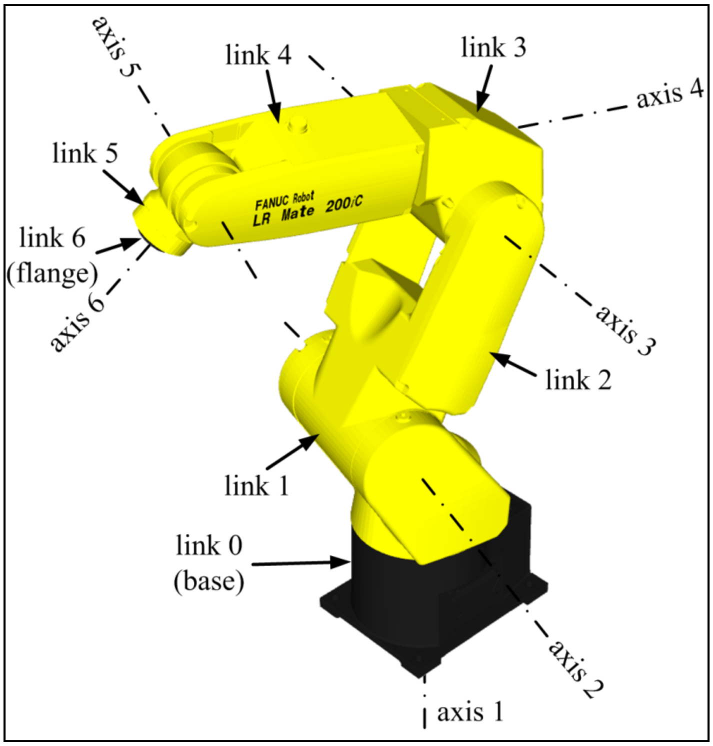

Figure 4.5 Robot axes and links

4.3 Robot Calibration Model and Parameter Identification Procedure

Figure 4.5 shows a CAD model of the robot studied with its seven links and the axes of the six joints. The level-3 robot model used in this paper corresponds to a complete kinematic calibration of the robot, including the end-effector, and five parameters related to the stiffness of the gearboxes of joints 2, 3, 4, 5, and 6. Table 4.1 summarizes the 25 error parameters. This model is very similar to the one used in (A Nubiola et al., 2013; Albert Nubiola and Bonev, 2013), the main difference being that it does not take into account the error parameters that locate the base frame. The D-H M (Denavit-Hartenberg Modified) model convention used is the one described in (Craig, 1986), which can be represented as

$$\mathbf{T}_{\mathrm{A6}} = \mathbf{A}_{1}^{0}\mathbf{A}_{\mathrm{A,2}}^{1}\mathbf{A}_{\mathrm{A,3}}^{2}\mathbf{A}_{\mathrm{A,4}}^{3}\mathbf{A}_{\mathrm{A,5}}^{4}\mathbf{A}_{\mathrm{A,6}}^{5}, \qquad (4.13)$$

where

$$\mathbf{A}_{\mathrm{A},i}^{i-1} = \mathrm{Rot}\left(\mathbf{x}, \alpha_i\right)\mathrm{Trans}\left(a_i, 0, 0\right)\mathrm{Rot}\left(\mathbf{z}, \theta_i\right)\mathrm{Trans}\left(0, 0, d_i\right), \tag{4.14}$$

for $i \geq 2$, constitute the homogeneous transformation matrix representing the pose of reference frame $\mathbf{\Phi}_i$ with respect to reference frame $\mathbf{\Phi}_{i-1}$.

It is important to note that although the robot base is not identified, an absolute calibration is performed. This is achieved with the relative model (Table 4.1) and the joint readings obtained when setting up the three 0.5 inch base attachment points (to be explained later). Using the relative calibrated model and computing the accurate forward kinematics for the joint readings just mentioned, the *world frame* $\mathbf{\Phi}_{\mathrm{world}}$ can be found with respect to the *base frame* $\mathbf{\Phi}_0$.

Table 4.1 Robot calibration model used (25 error parameters)

i	α_i (°)	a_i (mm)	θ_i (°)	d_i (mm)
1	0	0	θ_1	330
2	$-90+\delta\alpha_2$	$75+\delta a_2$	$\theta_2-90+\delta\theta_2+c_2\tau_2$	δd_2
3	$\delta\alpha_3$	$300+\delta a_3$	$\theta_3+\delta\theta_3+c_3\tau_3$	δd_3
4	$-90+\delta\alpha_4$	$75+\delta a_4$	$\theta_4+\delta\theta_4+c_4\tau_4$	$320+\delta d_4$
5	$90+\delta\alpha_5$	δa_5	$\theta_5+\delta\theta_5+c_5\tau_5$	δd_5
6	$-90+\delta\alpha_6$	δa_6	$\theta_6+\delta\theta_6+c_6\tau_6$	$80+\delta d_6$

Table 4.2 Estimated masses and centers of gravity of each robot link for Fanuc LR Mate 200iC robot

i	m_i [kg]	$c_{x,i}^{\;i}$ [mm]	$c_{y,i}^{\;i}$ [mm]	$c_{z,i}^{\;i}$ [mm]
1	0	0	0	0
2	10	150	0	0
3	0	0	0	0
4	10	0	0	−160
5	0	0	0	0
6 (with triangular artifact)	2.6	50	25	100

The five-parameter stiffness model is used to represent the elastic behavior of the robot (Albert Nubiola and Bonev, 2013). This model takes into account the elasticity of the gearboxes of joints 2, 3, 4, 5, and 6 (one parameter per joint). The elasticity in each gearbox is modeled as a linear torsional spring, so this parameter represents the effective constant compliance c_i of each joint i. Traction and compression effects are neglected. Torsional effects are also neglected.

The gravity forces due to the masses of links 2, 3, 4, and the tool, are taken into account but the weights of links 5 and 6 are neglected as they are relatively small, and so is the weight of link 0 (the base). The weight of link 1 is not needed because there is no compliance parameter that models the flexibility of joint 1, since the axis of that joint is parallel to the gravity vector.

Note that links 3 and 4 are considered as one, and the effect of link 3 is transferred to link 4. The center of gravity of these two links lies on axis 4, and therefore the compliance parameter for that axis is not affected by the weight of links 3 and 4.

In summary, the complete model consists of 25 error parameters: 20 geometric parameters (4 D-H M parameters for links 2 to 6), and 5 compliance parameters (for joints 2 to 6). However, since axes 2 and 3 are considered perfectly parallel, and because parameters are identified by linearization of the system, one of the 20 geometric parameters (δd_2 or δd_3) becomes redundant and is therefore excluded from the model.

All the kinematic error parameters are very small. The robot calibration model can be expressed as

$$\mathbf{f} = \mathbf{f}\left(\mathbf{r}, \boldsymbol{\theta}\right) \tag{4.15}$$

where $\mathbf{f} = [x, y, z]^T$ is the position of the end-effector (note that only the position data are taken into account), $\mathbf{r}$ is the vector containing all 25 error parameters, and $\boldsymbol{\theta} = [\theta_1, \theta_2, \ldots, \theta_6]^T$ is the vector of the joint variables. The expression of equation (4.15) is very complex. The Jacobian matrix of this robot model is even more complex. Fortunately, this expression can be obtained using the MATLAB Symbolic Toolbox, so the linearized equations can be expressed at iteration *i* as

$$\Delta\mathbf{f}^{i} = \mathbf{J}^{i}\Delta\mathbf{r}^{i} \tag{4.16}$$

where $\Delta\mathbf{f}^{i}$ is the difference between the measured position and the position predicted by the model for a given robot configuration, $\mathbf{J}^{i}$ is the Jacobian matrix, and $\Delta\mathbf{r}^{i}$ are the values to add to the error parameters. Using sufficiently many end-effector position measurements for different robot configurations, it is possible to obtain the least squares solution of the error parameters using the pseudo inverse of the Jacobian:

$$\Delta\mathbf{r} = \left(\mathbf{J}^{\mathrm{T}}\mathbf{J}\right)^{-1}\mathbf{J}^{\mathrm{T}}\Delta\mathbf{f}\,. \tag{4.17}$$

The first time that the Jacobian is calculated, it is verified whether the columns of **J** are linearly independent. If they are not, the redundant error parameters are discarded. Once the model parameters are chosen during the first iteration, the linear dependency is rechecked at each iteration. Through this verification, the error parameters δd_2 and δd_3 are found to be linearly dependent (because axes 2 and 3 are considered perfectly parallel), and so δd_3 is not considered in the model. The solution is stable after four iterations.

No observability analysis is performed since the choice of configurations is limited. Therefore, all possible measurements are used to calibrate the robot.

4.4 Experimental Results

For the base fixture disposition shown in Figure 4.1, it is possible to measure 46 different poses, and 124 configurations (the same pose may be measured twice or even three times using different robot joint configurations, i.e. front/up/flip, back/down/noflip, etc.). This is so, even though the ranges of axes 4 and 6 were limited to ±180º. Furthermore, front/down and back/up configurations were discarded because of mechanical interferences between the robot arm and the measurement device. In addition, to speed up the calibration process, instead of using both flip and noflip configurations (e.g. front/up/flip and front/up/noflip), when possible, only one of the configurations was randomly chosen. This leaves a total of 61 configurations that are used for calibration (46 are front/up/flip and front/up/noflip configurations and 15 are back/down/flip and back/down/noflip configurations).

The validation was performed using a Faro ION laser tracker by placing three 0.5 inch spherically mounted retro reflectors (SMRs) in the magnetic cups of the tool fixture. The position of an SMR was then measured in 9,905 robot configurations randomly generated in the robot joint space avoiding collisions with the table and the robot itself and reorienting the SMR to face the laser tracker. The position of each SMR was measured in approximately one third of the robot configurations.

The calibration procedure was automated with the RoKiSim simulation software (www.rokisim.com) and the Renishaw SDK to initialise, trigger, and retrieve the measurements of the telescopic ballbar. The procedure is summarized as follows (http://youtu.be/SDmH-FAxrtM):

1. The ballbar is first assembled with the 50 mm extension bar, initialized on the calibrator, and each of the three distances between the tool attachment points is measured.
2. The base fixture is attached to the base of the robot. A first guess of the three base fixture attachment points must be manually taught (approximately) with the center pivot assemblies released.
3. The setting ball is placed in one of the three magnetic cups of the tool fixture, its center defined as the *TCP* (*tool center point*) of the robot, and the robot is moved with respect to each of the three base attachment points (by programming, not by manual jogging) such that the programmed distances between these three TCP positions are 300.000 mm according to the robot kinematics. When the robot brings the setting ball to each center pivot assembly, the magnetic cup thereof snaps onto the ball and the clamping mechanism is then manually locked.

4. The ballbar is then assembled with the 150 mm and 50 mm extension bars, initialized on the Zerodur calibrator, and each of the three distances between the base attachment points is measured (Figure 4.1a). If the robot accuracy is perfect, these distances would be exactly 300.000 mm. In general, the error is usually less than 1 mm, and the distances are measurable with the QC20-W.
5. The robot is finally programmed to move through each of its 61 configurations, and the six leg distances are measured one by one. Verifying the ballbar bars on the calibrator is recommended from time to time, otherwise the repeated magnetic snaps and the manipulation of the ballbar produce an accumulated error of as much as 0.003 mm in the ballbar readings.

Once the tool fixture is attached to the robot tool flange and the pose of the base fixture is defined teaching the three base targets, RoKiSim automatically calculates the feasible robot configurations, which are displayed one by one with prompts using the Enter key (e.g. “Attach the ballbar between B_1 and T_1”).

Figure 4.6 shows the 61 configurations, where the tags F and B stand for front/up and back/down configuration, respectively, and the number identifies the pose of the end-effector (there are 46 different poses).

For each of the 61 configurations, it takes 6 measurements with the telescopic ballbar, of distances that are supposed to be equal to 300.000 mm (according to the robot kinematics). However the robot has not been calibrated and some errors may be more than ±1 mm. If this is the case, the non-measurable pose is skipped. After the calibration procedure was completed it was found that 15 configurations were not reachable. Not surprisingly, these 15 configurations are all the back/down configurations. Therefore, a preliminary calibration is performed using the first measurable 46 front/up configurations. After this preliminary calibration, it was possible to measure the end-effector pose in the remaining 15 back/down configurations. Once the end-effector pose is measured in all 61 configurations, the robot is recalibrated.

The entire procedure for measuring the pose of the end-effector of the robot in its 61 configurations requires less than one hour (including attaching the base fixture to the robot's table).

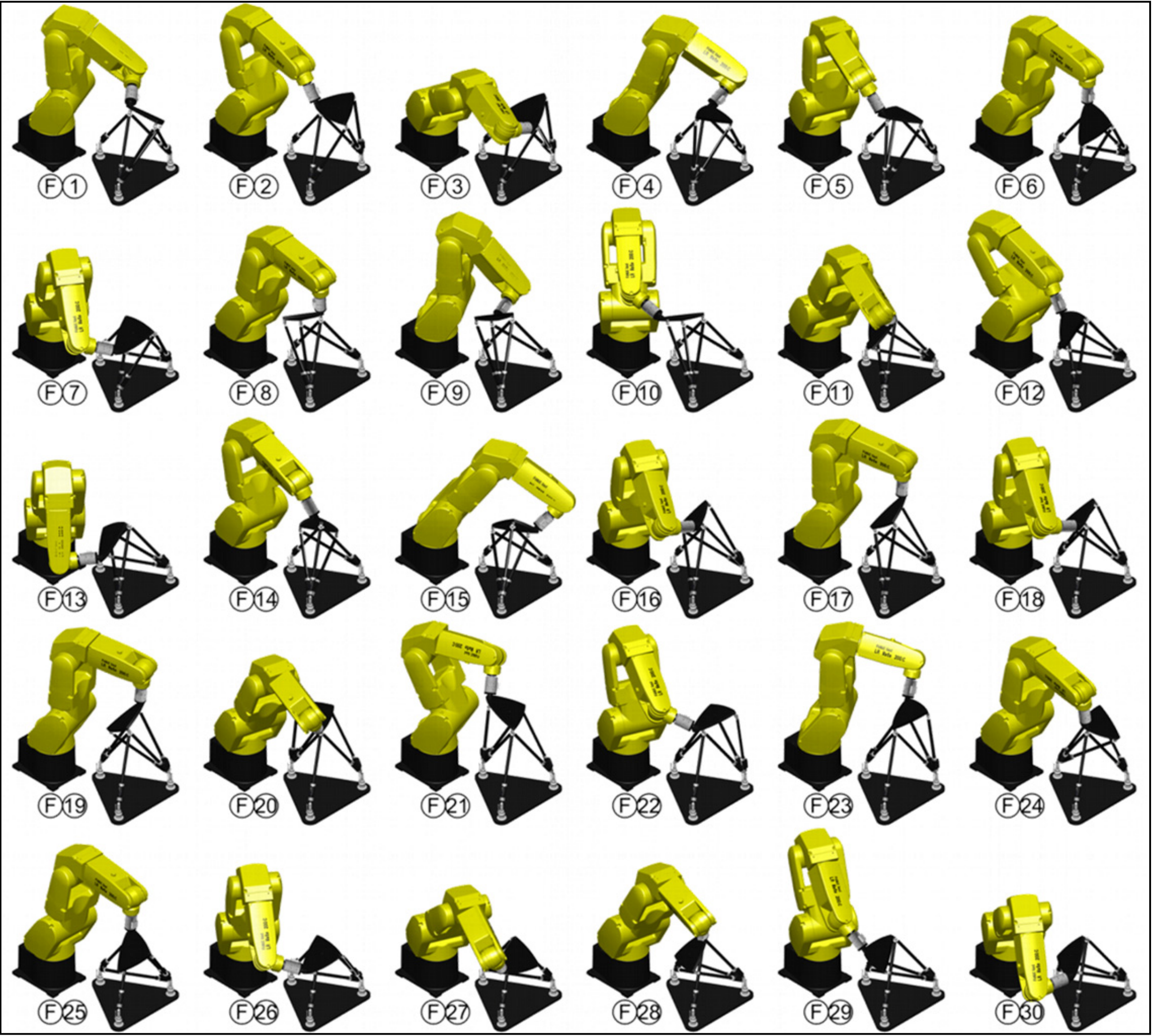

Figure 4.6 Robot configurations used for calibration (continues)

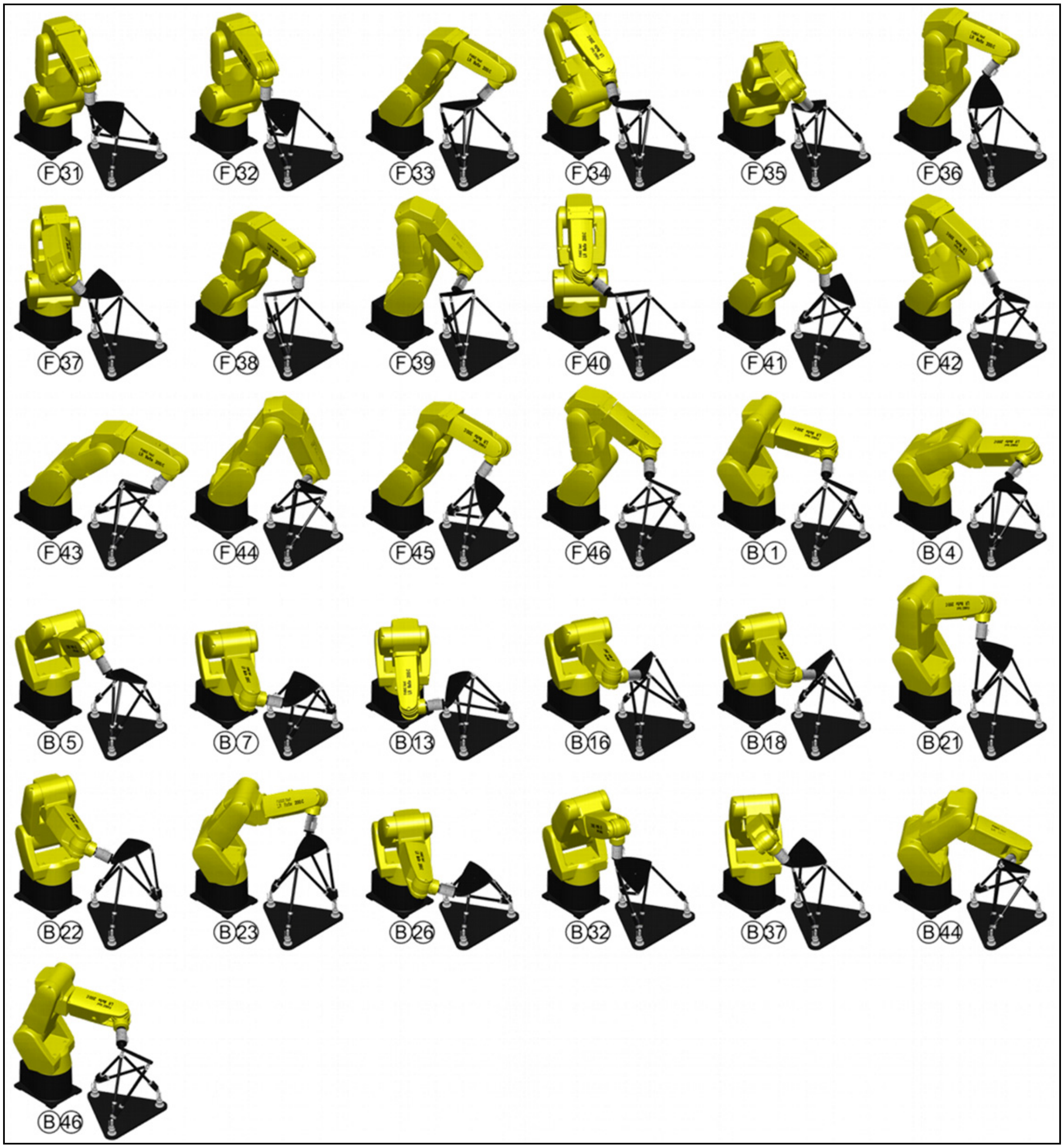

Figure 4.6 Robot configurations used for calibration (continued)

The position of each of the three SMRs mounted to the tool magnetic cups is measured with a laser tracker, before calibration, after the preliminary calibration (only front/up configurations measured) and after the final calibration (in 9,905 robot configurations, of which 3,672 are front/up configurations). Tables 4.3 and 4.4 show the statistics for the absolute position errors with respect to the world frame defined in Section 4.2.

Note that the base of the robot needs to be identified for the validation of the nominal model (i.e. the robot before calibration) using the laser tracker. It was placed relative to robot axes 1 and 2, which were identified by rotating only joint 1 and then only joint 2 and measuring the position of one of the SMRs.

Table 4.3 Absolute position errors (in mm) in 9,905 robot configurations

Robot model	Mean error	Standard deviation	Mean + 3*std	Maximum error
Nominal model	1.355	1.029	4.444	5.197
Pre-calibrated model	0.517	0.219	1.174	1.223
Final calibrated model	0.796	0.275	1.622	1.630

Table 4.4 Absolute position errors (in mm) in 3,672 front/up robot configurations

Robot model	Mean error	Standard deviation	Mean + 3*std	Maximum error
Nominal model	0.873	0.416	2.122	2.717
Pre-calibrated model	0.479	0.214	1.121	1.039
Final calibrated model	0.697	0.253	1.454	1.406

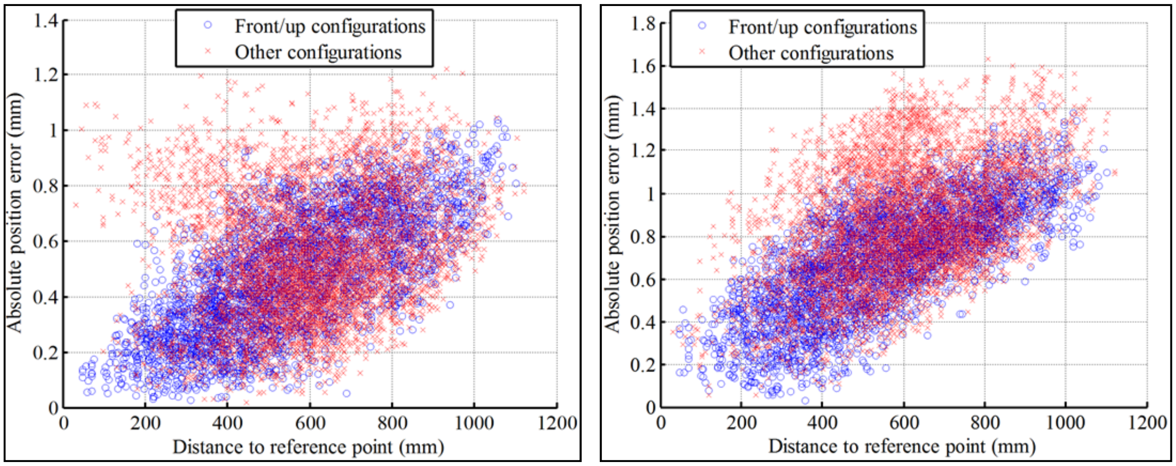

(a) Preliminary calibration (b) Final calibration

Figure 4.7 Absolute position error for the two steps of the calibration process

Results show clearly that the robot accuracy is improved significantly for both calibrated models. However, results also show that the accuracy of the robot is better when only front/up configurations are considered into the identification process (i.e. the preliminary calibration is not only sufficient, it is better).

Figure 4.7 shows the correlation between the position accuracy and the distance to a reference point that is 300 mm away from the three base points and above the base fixture. It can be clearly seen that there is a strong correlation between the position error after calibration and the distance to the calibration area (i.e. to the reference point). Naturally, the farther the end-effector position from the reference point, the less accurate the robot is. It can also be seen that not using the 15 back/down configurations leads to an even better improvement of the robot accuracy if only front/up configurations are used for the validation. For example, the position accuracy will be better than 0.4 mm if the end-effector position is no farther than 200 mm from the reference point and the robot is in a front/up configuration. However, if all 61 configurations are used for calibration (Figure 4.7b), the robot position accuracy is more homogeneous with regards to the different types of configurations.

Table 4.5 Distance errors (in mm) for all pairs of the 9,905 robot configurations

Robot model	Mean error	Standard deviation	Mean + 3*std	Maximum error
Nominal model	1.062	0.960	3.941	7.873
Pre-calibrated model	0.318	0.219	0.976	1.706
Final calibrated model	0.400	0.244	1.132	1.666

Table 4.6 Distance errors (in mm) for all pairs of the 3,672 front/up robot configurations

Robot model	Mean error	Standard deviation	Mean + 3*std	Maximum error
Nominal model	0.595	0.511	2.127	4.963
Pre-calibrated model	0.384	0.237	1.093	1.231
Final calibrated model	0.456	0.243	1.185	1.394

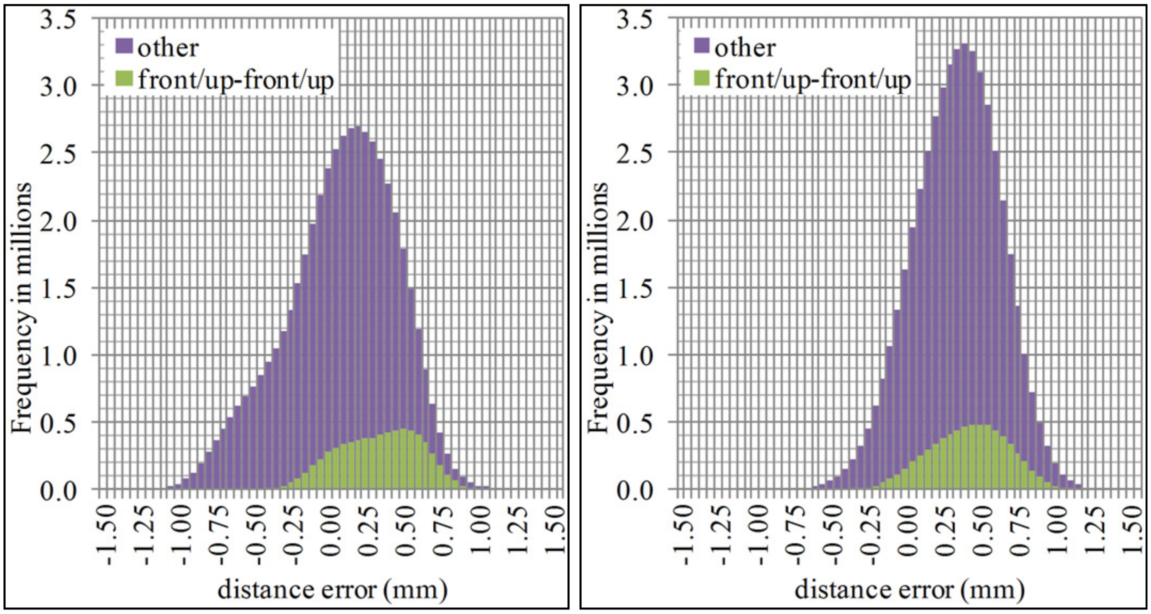

(a) Preliminary calibration (b) Final calibration

Figure 4.8 Distance errors between the two types of measured configurations

In addition, the distance accuracy was validated by calculating the distance error between each possible pair out of the 9,905 measured positions, which makes more than 49 million pairs. Tables 4.5 and 4.6 show the statistics of this distance error, while Figures.4.8(a) and 4.8(b) each shows two histograms for this error, one (the smaller) for pairs in which both configurations are front/up, and another for all other pairs. It is interesting to note that about 60% of the distance errors are positive for the preliminary calibration model, and this ratio is 86% for the final model. This time, the difference between the preliminary calibration (Figure 4.8a) and the final one (Figure 4.8b) is very small. Furthermore, even if only front/up configurations are considered in the validation process, the distance accuracy is not significantly better.

Finally, in order to allow a more objective evaluation of the calibration method proposed, a "standard" calibration was performed with 50 laser tracker position measurements (the same calibration method used in (A Nubiola et al., 2013)), where the 50 robot configurations were selected using observability analysis (only some of these configurations are front/up). After this new calibration, and validating in the same 9,905 robot configurations with respect to the same world frame, the mean position error was 0.156 mm, the standard deviation was 0.067 mm, and the maximum position error was 0.490 mm. Similarly, considering each possible pair of position measurements (the same 49 million pairs), the mean distance error was 0.110 mm, the standard deviation was 0.083 mm, and the maximum distance error was 0.803 mm. It is interesting to note that even if only front/up robot configurations (50 again) are considered for the identification process, and if the validation is then performed only in the 3,672 front/up robot configurations, the mean absolute position error, the standard deviation of the absolute position error and even the maximum position error are nearly the same.

4.5 Conclusions

This paper demonstrated through rigorous experimentations that the 6D measurement device proposed in (Albert Nubiola et al., 2013) is highly suitable for absolute calibration of small industrial robots, particularly if a relatively small workspace area is of interest (e.g. a sphere of radius 0.2 mm). The calibration process is manual and labour intensive, but takes less than an hour to perform. Most importantly, the cost of the 6D measurement device is less than $13,000.

Naturally, the use of a laser tracker for calibrating the same industrial robot produces significantly better results. The mean values and the standard deviation for the absolute position and the distance errors are about three times as small. However, if time is not an issue, there are various possible improvements to the method proposed. For example, the calibration can be repeated for different poses of the base fixture. Different calibration models can also be used for different workspace zones. Furthermore, it is possible to install a fourth magnetic cup on the base fixture, 300 mm away from the three other magnetic cups, and thus extend the range of measurable robot configurations by as much as four times.

It is therefore believed that the proposed calibration procedure has a great potential for becoming a popular lower-cost alternative for absolute calibration of (small) industrial robots. Contrary to other lower-cost robot calibration procedures (e.g. the ones offered by Wiest AG, Teconsult GmbH and Isios GmbH), the method proposed can also be used to validate the absolute pose accuracy of the robot.

4.6 Acknowledgements

The authors thank the Canada Research Chair program, the Canada Foundation for Innovation, the Natural Sciences and Engineering Research Council of Canada and Pratt & Whitney Canada for financing this work and GE Aviation Canada for lending the industrial robot. The first author also thanks La Caixa d’Estalvis i Pensions de Barcelona, “la Caixa”.

GENERAL CONCLUSION

The goal of this thesis was to develop new robot calibration methods that improve the absolute accuracy of six-revolute serial robots. The calibration methods used provide successful accuracy results after calibration and work using low cost measurement equipment. The major contribution of this thesis remains in the novel 6D-measurement system based on a single telescopic ballbar. This measurement system is accurate and inexpensive and can measure 144 different poses by groups of six one-dimensional measurements.

Two robots from two different brands have been used to test the methods presented in this work. The accuracy of an ABB IRB 120 robot was improved using a Faro laser tracker and a Creaform's C-Track stereo camera separately. A validation through spherical movements with a ballbar showed that the accuracy is improved equally for both systems and there is no advantage in using one measurement system or the other for robot calibration.

The Fanuc LR Mate 200 iC was successfully calibrated using a single Renishaw QC20-W by implementing the novel 6D-measurement system. Among the 144 measurable poses, 62 were used to perform an absolute calibration. The validation is done in 10,000 measurements throughout the complete robot workspace, improving the mean position error from 1.355 mm to 0.795 mm. The accuracy results of this method were compared to a calibration performed using a laser tracker. Although the robot calibration using a ballbar requires user interaction, it is inexpensive, accurate, and can be completed in less than one hour.

The Renishaw QC20-W telescopic ballbar is designed and used for validating the accuracy of CMM's and CNC's. These machines operate in the order of microns, therefore, the measurement range of the device is very limited (±1.0 mm) but very accurate (1 μm). If the robot that needs to be calibrated is not very accurate, some robot configurations might not be measurable; therefore, some calibration iterations may be needed to perform a complete robot calibration (50 configurations or more). The accuracy of the 6D-measurement system is

3.2 times the accuracy of the ballbar (0.003 µm); however, if we had to redesign a new ballbar from scratch, it would be preferable to cease some accuracy for an increased measurement range. For example, there exist some optical scales or linear gages that operate in the range of ±5 mm while maintaining the accuracy under 0.005 µm (such as the Mitutoyo LGK 542-157 linear gage). A ballbar with such specifications would be more suitable for robot calibration.

Calibrating a robot using a 3D measurement system is the most straightforward way to calibrate a robot if we do not take into account the price of the equipment. However, regarding the price of the measurement equipment, a 3D measurement system usually costs as much as a small-sized robot. Furthermore, this price can be twice or even three times the price of the robot if we use a laser tracker or a CMM for example. In this work, we proved that the robot accuracy after calibration is not proportional to the money spent on the measurement equipment.

FUTURE WORK

The main goal of this thesis was to find cheaper calibration methods for robot calibration. Although the last calibration method explained in this thesis is quite inexpensive, it is still not as accurate as if we performed a conventional robot calibration using a laser tracker.

Future work about robot calibration should be focused on improving the robot accuracy results while maintaining cheap and simple measurement systems, such as a double ballbar. An interesting example would be calibrating a robot using one or multiple linear gages. Linear gages are very accurate and offer sufficient measurement range for robots. For example, the Mitutoyo LGB 542-222H has 1 µm accuracy and 10 mm of measurement range. Linear gages are usually cheaper than touch probes. A robot calibration using a single linear gage would work the same way as if we used a touch probe. However, with a linear gage we can provide some feedback to the robot to quickly touch at a predefined distance from the tool flange.

Additionally, we could set up a fixture with three linear gages placed in a perpendicular pattern, which would measure an offset in the 3D space (X,Y,Z). This would allow calibrating the robot by reaching the same point with many different orientations.

ANNEX I

CALIBRATED ROBOT MODEL

The robot model chosen to fit the accurate kinematics of the robot is based on the model defined by (Craig 1986), also known as the D-H M notation (Denavit-Hartenberg Modified). The robot's forward kinematic model can be represented as

$$\mathbf{H}(\mathbf{q}) = \mathbf{A}_0^{\text{world}} \mathbf{A}_1^0 \mathbf{A}_2^1 \mathbf{A}_3^2 \mathbf{A}_4^3 \mathbf{A}_5^4 \mathbf{A}_6^5 \mathbf{A}_{\text{tool}}^6, \tag{I.1}$$

where

$$\mathbf{A}_0^{\text{world}} \mathbf{A}_1^0 = \text{Trans}\left(x_{\text{b}}, y_{\text{b}}, d_1 + z_{\text{b}}\right) \text{Rot}\left(\mathbf{x}, \alpha_{\text{b}}\right) \text{Rot}\left(\mathbf{y}, \beta_{\text{b}}\right) \text{Rot}\left(\mathbf{z}, \gamma_{\text{b}} + \theta_1\right) \tag{I.2}$$

and

$$\mathbf{A}_i^{i-1} = \text{Rot}\left(\mathbf{x}, \alpha_i\right) \text{Trans}\left(a_i, 0, 0\right) \text{Rot}\left(\mathbf{z}, \theta_i\right) \text{Trans}\left(0, 0, d_i\right) \tag{I.3}$$

for $i \geq 2$ is the homogeneous transformation matrix representing the pose of the reference frame $\mathbf{\Phi}_i$ with respect to reference frame $\mathbf{\Phi}_{i\text{-}1}$, $\mathbf{A}_0^{\text{world}}$ is the transformation matrix representing the pose of the *base frame* $\mathbf{\Phi}_0$ with respect to the *world frame* $\mathbf{\Phi}_{\text{world}}$, $\mathbf{A}_{\text{tool}}^6$ is the transformation matrix representing the pose of the *tool frame* $\mathbf{\Phi}_{\text{tool}}$ with respect to *the mechanical interface* (*tool flange*) *frame* $\mathbf{\Phi}_6$ (also referred to as *tool0* by ABB), and **q** is the vector of the joint coordinates (θ_1, θ_2, …, θ_6).

Five error parameters are used to represent the robot elasticity. This model takes into account the elasticity of joints 2, 3, 4, 5 and 6 (one parameter per joint). The elasticity of joint 1 is ignored, because the axis of that joint coincides with the direction of gravity. Joint traction and compression effects are not taken into account. Torsional effects are also ignored. The elasticity is modeled as linear torsional springs, so this parameter represents the effective constant compliance c_i of each joint i:

$$\delta\theta_i = c_i \tau_i \,. \tag{I.4}$$

Torques due to gravity are calculated based on the mass of the links and end-effector (recall that only static errors are modeled without any other external force being applied). The deformations are supposed to be small enough so that we can apply the superposition theory and neglect beam foreshortening. The center of gravity of the end-effector can be estimated from its CAD model. The next figure represents an arbitrary configuration of the robot arm for joints 2 and 3. This configuration can be considered as two generic links.

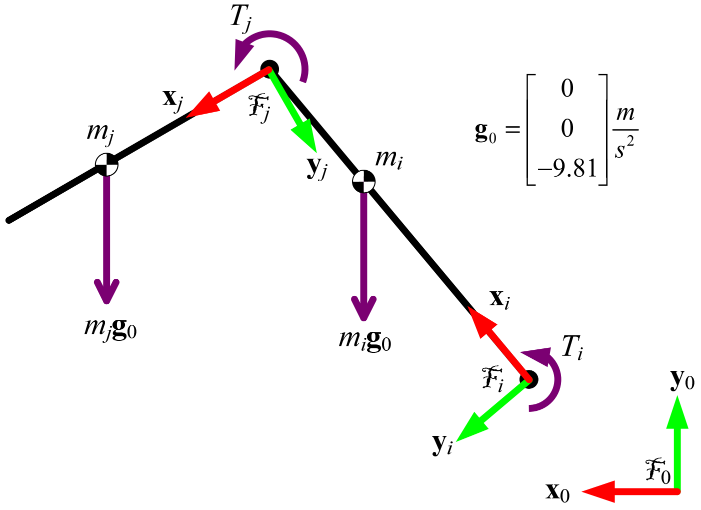

Figure A I-1 Schematics of two consecutive links under the effect of gravity

Torques are calculated recursively from joint 6 down to joint 1, so for example joint 5 is affected by link 5, link 6 and the end-effector, joint 4 is affected by links 4, 5, 6 and the end-effector, etc. In fact, the end-effector weight and its center of gravity can be combined with link 6 as they do not move with respect to each other, so this recursive method already includes the end-effector.

The gravity vector seen by joint *i* corresponds to

$$\mathbf{g}_i = \left(\mathbf{H}_i^0\right)^{-1} \mathbf{g}_0 \,, \tag{I.5}$$

where

$$\mathbf{H}_b^a = \mathbf{A}_{a+1}^a \mathbf{A}_{a+2}^{a+1} \cdots \mathbf{A}_b^{b-1}, \tag{I.6}$$

if $b > a$. Then, the gravity force on link *j* seen by link *i* can be found as

$$\mathbf{f}_j^i = m_j \mathbf{g}_i = m_j \left(\mathbf{H}_i^0\right)^{-1} \mathbf{g}_0 = \left[fx_j^i, fy_j^i, fz_j^i, 1\right]^{\mathrm{T}}. \tag{I.7}$$

On the other hand, we can also find the center of gravity of link *j* with respect to the coordinates of frame $i, \mathbf{u}_j^i$ if we know the center of gravity of link *j* with respect to the local coordinates, $\mathbf{u}_j$.

$$\mathbf{u}_j^i = \mathbf{H}_j^i \mathbf{u}_j = \left[cx_j^i, cy_j^i, cz_j^i, 1\right]^{\mathrm{T}} \tag{I.8}$$

where $\mathbf{H}_j^i$ is the identity if *i*=*j*.

Once we have calculated all the combinations where $i \le j$, we can calculate the torque applied at each joint:

$$\tau_i = \tau_{i,\text{link}\, i} + \tau_{i,\text{link}\, i+1} + \cdots + \tau_{i,\text{link}\, 6}, \tag{I.9}$$

where $\tau_{i,\text{link}\, j}$ is the contribution of the torque applied at joint *i* because of link *j*:

$$\tau_{i,\text{link}\, j} = fy_j^i cx_j^i - fx_j^i cy_j^i. \tag{I.10}$$

In our case, we took into account the gravity forces due to the masses of links 2, 3, 4 and the end-effector. We neglected the mass of link 5 and 6 as it is very small compared to the other links. The mass of link 1 is not necessary because we do not consider the compliance of joint 1, as the robot base is horizontally mounted.

The level-3 robot model that we use corresponds to a complete kinematic calibration of the robot, including the base frame, and the five parameters related to the stiffness (Albert Nubiola and Bonev, 2013) of joints 2, 3, 4, 5, and 6. The next two tables show a summary of all 31 parameters using the ABB IRB 120 robot as an example.

Table A I-1 Pose of the base frame with respect to the world frame with six error parameters

Parameter	x	y	z	α	β	γ
Value	$x_w + \delta x_w$	$y_w + \delta y_w$	$z_w + \delta z_w$	$\alpha_w + \alpha x_w$	$\beta_w + \delta\beta_w$	$\gamma_w + \delta\gamma_w$

* The parameters α, β, and γ are the Euler angles, according to the XYZ convention.

Table A I-2 Complete D-H M (Craig, 1986) robot model with 25 error parameters

i	α_i [º]	a_i [mm]	θ_i [º]	d_i [mm]
1	0	0	θ_1	290
2	$-90 + \delta\alpha_2$	δa_2	$\theta_2 - 90 + \delta\theta_2 + c_2\tau_2$	δd_2
3	$\delta\alpha_3$	$270 + \delta a_3$	$\theta_3 + \delta\theta_3 + c_3\tau_3$	δd_3
4	$-90 + \delta\alpha_4$	$70 + \delta a_4$	$\theta_4 + \delta\theta_4 + c_4\tau_4$	$302 + \delta d_4$
5	$90 + \delta\alpha_5$	δa_5	$\theta_5 + \delta\theta_5 + c_5\tau_5$	δd_5
6	$-90 + \delta\alpha_6$	δa_6	$\theta_6 + 180 + \delta\theta_6 + c_6\tau_6$	$72 + \delta d_6$

REFERENCES

«*Manipulating industrial robots - Performance criteria and related test methods*». 1998. ISO 9283.

«*Test code for machine tools - Part 4: Circular tests for numerically controlled machine tools*». 2005. ISO 230-4.

«*Uncertainty of measurement - Part 3: Guide to the expression of uncertainty in measurement*». 2008. ISO/IEC Guide 98-3.

Abderrahim, M., Khamis, A., Garrido, S., and Moreno, L. 2007. «*Accuracy and calibration issues of industrial manipulators*». *Industrial Robotics: Programming, Simulation and Applications*, p. 131.

Andrew Liou, Y. H., Lin, P. P., Lindeke, R. R., and Chiang, H. D. 1993. «*Tolerance specification of robot kinematic parameters using an experimental design technique--the Taguchi method*». *Robotics and Computer-Integrated Manufacturing*, vol. 10, n° 3, p. 199–207.

Angeles, J. 1985. «*On the numerical solution of the inverse kinematic problem*». *The International Journal of Robotics Research*, vol. 4, n° 2, p. 21–37.

Angeles, J. 2007. *Fundamentals of robotic mechanical systems: theory, methods, and algorithms*. Springer-Verlag New York Inc.

Aoyagi, S., Kohama, A., Nakata, Y., Hayano, Y., and Suzuki, M. 2010. «*Improvement of Robot Accuracy by Calibrating Kinematic Model Using a Laser Tracking System - Compensation of Non-Geometric Errors Using Neural Networks and Selection of Optimal Measuring Points Using Genetic Algorithm*». In *IEEE/RSJ International Conference on Intelligent Robots and Systems* (pp. 5660–5665).

Bai, Y., Zhuang, H., and Roth, Z. S. 2003. «*Experiment study of PUMA robot calibration using a laser tracking system*». In *Soft Computing in Industrial Applications, 2003. SMCia/03. Proceedings of the 2003 IEEE International Workshop on* (pp. 139–144).

Barker, L. K. 1983. «*Vector-algebra approach to extract Denavit-Hartenberg parameters of assembled robot arms*». *NASA Tech. Paper 2191.*

Besnard, S., Khalil, W., and Garcia, G. 2000. «*Geometric calibration of robots using multiple plane constraints*». In *Advances in robot kinematics* (pp. 61–70). Springer.

Beyer, L., and Wulfsberg, J. 2004. «*Practical robot calibration with ROSY*». *Robotica*, vol. 22, n° 05, p. 505–512.

Bonev, I. A. 2003. «*The true origins of parallel Robots*». *ParalleMIC*, vol. online art,.

Bonnans, J. F., and Lemaréchal, C. 2006. *Numerical optimization: theoretical and practical aspects* (p. 493). Springer-Verlag New York Inc.

Boochs, F., Schutze, R., Simon, C., Marzani, F., Wirth, H., and Meier, J. 2010. «*Increasing the accuracy of untaught robot positions by means of a multi-camera system*». In *International Conference on Indoor Positioning and Indoor Navigation* (pp. 1–9).

Borm, J. H., and Meng, C. H. 1991. «*Determination of optimal measurement configurations for robot calibration based on observability measure*». *The International Journal of Robotics Research*, vol. 10, n° 1, p. 51.

Bricard, R. 1897. «*Mémoire sur la théorie de l'octaèdre articulé*». *Journal de Mathématiques Pures et Appliquées*, vol. 3,, p. 113–148.

Bricard, R. 1906. «*Mémoire sur les déplacements à trajectoire sphériques*». *Journal de l'École Polytechnique*, vol. 11, n° 2, p. 1–96.

Brockett, R. 1984. «*Robotic manipulators and the product of exponentials formula*». *Mathematical Theory of Networks and Systems*.

Bryan, J. B. 1982. «*A simple method for testing measuring machines and machine tools Part 1: Principles and applications*». *Precision Engineering*, vol. 4, n° 2, p. 61–69.

Bryan, J. B. 1984. «*Telescoping magnetic ball bar test gage*». US Patent No. 4,435,905.

Caenen, J. L., and Angue, J. C. 1990. «*Identification of geometric and nongeometric parameters of robots*». In *Robotics and Automation, 1990. Proceedings., 1990 IEEE International Conference on* (Vol. 2, pp. 1032–1037).

Chen, I.-M., Yang, G., and others. 1997. «*Kinematic calibration of modular reconfigurable robots using product-of-exponentials formula*». *Journal of Robotic Systems*, vol. 14, n° 11, p. 807–821.

Chen, N., and Parker, G. A. 1994. «*Inverse kinematic solution to a calibrated puma 560 industrial robot*». *Control Engineering Practice*, vol. 2, n° 2, p. 239–245.

Craig, J. J. 1986. *Introduction to robotics: mechanics and control* (p. 400). Addison-Wesley.

De Smet, P. 2001. «*Method for calibration of a robot inspection system*». Google Patents.

Denavit, J., and Hartenberg, R. S. 1955. «*A kinematic notation for lower-pair mechanisms based on matrices*». *Trans. ASME J. Appl. Mech*, vol. 22, n° 1, p. 215–221.

Dietmaier, P. 1998. «*The Stewart-Gough platform of general geometry can have 40 real postures*». In *Advances in Robot Kinematics: Analysis and Control* (pp. 7–16). Springer.

Diolez, G. 2006. «Maîtrise de la position géométrique des solides: vers de nouveaux outils plus efficaces». ENSAM, CER de Lilles, France.

Driels, M. R. 1993. «*Using passive end-point motion constraints to calibrate robot manipulators*». *Journal of Dynamic Systems, Measurement, and Control*, vol. 115, n° 3, p. 560–566.

Driels, M. R., and Pathre, U. S. 1990. «*Significance of observation strategy on the design of robot calibration experiments*». *Journal of Robotic Systems*, vol. 7, n° 2, p. 197–223.

Driels, M. R., Swayze, W., and Potter, S. 1993. «*Full-pose calibration of a robot manipulator using a coordinate-measuring machine*». *The International Journal of Advanced Manufacturing Technology*, vol. 8, n° 1, p. 34–41.

Dumas, C., Caro, S., Che rif, M., Garnier, S., and Furet, B. 2010. «*A methodology for joint stiffness identification of serial robots*». In *IEEE/RSJ International Conference on Intelligent Robots and Systems* (pp. 464–469).

Dumas, C., Caro, S., Garnier, S., and Furet, B. 2011. «*Joint stiffness identification of six-revolute industrial serial robots*». *Robotics and Computer-Integrated Manufacturing*, vol. 27, n° 4, p. 881–888.

Faugère, J.-C., and Lazard, D. 1995. «*Combinatorial classes of parallel manipulators*». *Mechanism and Machine Theory*, vol. 30, n° 6, p. 765–776.

Gatla, C. S., Lumia, R., Wood, J., and Starr, G. 2007. «*An automated method to calibrate industrial robots using a virtual closed kinematic chain*». *IEEE Transactions on Robotics*, vol. 23, n° 6, p. 1105–1116.

Ginani, L. S., and Motta, J. M. S. T. 2011. «*Theoretical and practical aspects of robot calibration with experimental verification*». *Journal of the Brazilian Society of Mechanical Sciences and Engineering*, vol. 33, n° 1, p. 15–21.

Goldenberg, A. A., Apkarian, J. A., and Smith, H. W. 1987. «*A new approach to kinematic control of robot manipulators*». *Journal of Dynamic Systems, Measurement, and Control*, vol. 109,, p. 97.

Gong, C., Yuan, J., and Ni, J. 2000. «*Nongeometric error identification and compensation for robotic system by inverse calibration*». *International Journal of Machine Tools and Manufacture*, vol. 40, n° 14, p. 2119–2137.

Goswami, A., Quaid, A., and Peshkin, M. 1993. «*Complete parameter identification of a robot from partial pose information*». In *Proceedings of the 1993 IEEE International Conference on Robotics and Automation* (pp. 168–173). IEEE.

Greenway, B. 2000. «*Robot accuracy*». *Industrial Robot: An International Journal*, vol. 27, n° 4, p. 257–265.

Gupta, K., and Kazerounian, K. 1985. «*Improved numerical solutions of inverse kinematics of robots*». *Robotics and Automation.*, p. 743–748.

Hayati, S., and Mirmirani, M. 1985. «*Improving the absolute positioning accuracy of robot manipulators*». *Journal of Robotic Systems*, vol. 2, n° 4, p. 397–413.

He, R., Zhao, Y., Yang, S., and Yang, S. 2010. «*Kinematic-parameter identification for serial-robot calibration based on POE formula*». *EEE Transactions on Robotics*, vol. 26, n° 3, p. 411–423.

Hoppe, W. C. 2011. «*Method and system to provide improved accuracies in multi-jointed robots through kinematic robot model parameters determination*». *US Patent*.

Houde, G. 2006. «*A closed-loop method for the geometric calibration of serial robots*». *Department of Mechanical Engineering*. Montréal: McGill University.

Husty, M. L. 1996. «*An algorithm for solving the direct kinematics of general Stewart-Gough platforms*». *Mechanism and Machine Theory*, vol. 31, n° 4, p. 365–379.

Ikits, M., and Hollerbach, J. M. 1997. «*Kinematic calibration using a plane constraint*». In *Robotics and Automation, 1997. Proceedings., 1997 IEEE International Conference on* (Vol. 4, pp. 3191–3196).

Innocenti, C., and Parenti-Castelli, V. 1990. «*Direct position analysis of the Stewart platform mechanism*». *Mechanism and Machine Theory*, vol. 25, n° 6, p. 611–621.

Jang, J. H., Kim, S. H., and Kwak, Y. K. 2001. «*Calibration of geometric and non-geometric errors of an industrial robot*». *Robotica*, vol. 19, n° 03, p. 311–321.

Judd, R. P., and Knasinski, A. B. 2002. «*A technique to calibrate industrial robots with experimental verification*». *Robotics and Automation, IEEE Transactions on*, vol. 6, n° 1, p. 20–30.

Juneja, N., and Goldenberg, A. A. 1997. «*Kinematic calibration of a re-configurable robot (RoboTwin)*». In *IEEE International Conference on Robotics and Automation* (Vol. 4, pp. 3178–3183).

Karan, B., and Vukobratovic, M. 1994. «*Calibration and accuracy of manipulation robot models--An overview*». *Mechanism and Machine Theory*, vol. 29, n° 3, p. 479–500.

Khalil, W., and Besnard, S. 2002. «*Geometric calibration of robots with flexible joints and links*». *Journal of Intelligent and Robotic Systems*, vol. 34, n° 4, p. 357–379.

Knoll, A., and Kovacs, P. 2001. «*Method and device for the improvement of the pose accuracy of effectors on mechanisms and for the measurement of objects in a workspace*». Google Patents.

Lightcap, C., Hamner, S., Schmitz, T., and Banks, S. 2008. «*Improved positioning accuracy of the PA10-6CE robot with geometric and flexibility calibration*». *IEEE Transactions on Robotics*, vol. 24, n° 2, p. 452–456.

Marie, S., Courteille, E., and Maurine, P. 2013. «*Elasto-geometrical modeling and calibration of robot manipulators: Application to machining and forming applications*». *Mechanism and Machine Theory*, vol. 69,, p. 13–43.

McMurtry, D. R. 2007. «*Performing measurement or calibration on positioning machines*». *US Patent*.

Meggiolaro, M. A., Dubowsky, S., and Mavroidis, C. 2005. «*Geometric and elastic error calibration of a high accuracy patient positioning system*». *Mechanism and Machine Theory*, vol. 40, n° 4, p. 415–427.

Meggiolaro, M. A., Scriffignano, G., and Dubowsky, S. 2000. «*Manipulator calibration using a single endpoint contact constraint*». In *Proceedings of DETC2000: 2000 ASME Design Engineering Technical Conference* (pp. 1–8). Baltimore.

Meng, Y., and Zhuang, H. 2001. «*Self-calibration of camera-equipped robot manipulators*». *The International Journal of Robotics Research*, vol. 20, n° 11, p. 909–921.

Mooring, B., Driels, M., and Roth, Z. 1991. *Fundamentals of manipulator calibration* (p. 329). John Wiley & Sons, Inc. New York, NY, USA.

Mooring, B. W., and Padavala, S. S. 1989. «*The effect of kinematic model complexity on manipulator accuracy*». In *IEEE International Conference on Robotics and Automation* (Vol. 1, pp. 593–598).

Nahvi, A., and Hollerbach, J. M. 1996. «*The noise amplification index for optimal pose selection in robot calibration*» (Vol. 1, pp. 647–654 vol. 1). IEEE.

Nahvi, A., Hollerbach, J. M., and Hayward, V. 1994. «*Calibration of a parallel robot using multiple kinematic closed loops*». In *Proceedings of the 1994 IEEE International Conference on Robotics and Automation* (pp. 407–412). IEEE Comput. Soc. Press.

Nair, R. 1992. «On the Kinematic Geometry of Parallel Robotic Manipulators». University of Maryland, College Park, MD, USA.

Nelder, J. A., and Mead, R. 1965. «*A simplex method for function minimization*». *The Computer Journal*, vol. 7, n° 4, p. 308.

Newman, W. S., Birkhimer, C. E., Horning, R. J., and Wilkey, A. T. 2000. «*Calibration of a Motoman P8 robot based on laser tracking*». In *IEEE International Conference on Robotics and Automation* (Vol. 4, pp. 3597–3602).

Nubiola, A., and Bonev, I. A. 2013. «*Absolute calibration of an ABB IRB 1600 robot using a laser tracker*». *Robotics and Computer-Integrated Manufacturing*, vol. 29, n° 1, p. 236–245.

Nubiola, A., and Bonev, I. A. 2014. «*Absolute robot calibration with a single telescoping ballbar*». *Precision Engineering*, vol. 38, n° 3, p. 472–480.

Nubiola, A., and Bonev, I. A. 2014. «*Geometric approach to solving the inverse displacement problem of calibrated decoupled 6R serial robots*». *Transactions of the Canadian Society for Mechanical Engineering*, vol. 38, n° 1, p. 31–44.

Nubiola, A., Slamani, M., and Bonev, I. A. 2013. «*A new method for measuring a large set of poses with a single telescoping ballbar*». *Precision Engineering*, vol. 37, n° 2, p. 451–460.

Nubiola, A., Slamani, M., Joubair, A., and Bonev, I. A. 2013. «*Comparison of two calibration methods for a small industrial robot based on an optical CMM and a laser tracker*». *Robotica*, vol. 32, n° 03, p. 447–466.

Okamura, K., and Park, F. C. 1996. «*Kinematic calibration using the product of exponentials formula*». *Robotica*, vol. 14, n° 4, p. 415–422.

Ota, H., Shibukawa, T., Tooyama, T., and Uchiyama, M. 2002. «*Forward kinematic calibration and gravity compensation for parallel-mechanism-based machine tools*». *Proceedings of the Institution of Mechanical Engineers, Part K: Journal of Multi-Body Dynamics*, vol. 216, n° 1, p. 39–49.

Park, F. C. 1994. «*Computational aspects of the product-of-exponentials formula for robot kinematics*». *IEEE Transactions on Automatic Control*, vol. 39, n° 3, p. 643–647.

Paul, R. P. 1981. *Robot manipulators: mathematics, programming, and control: the computer control of robot manipulators* (p. 279). The MIT Press.

Puskorius, G., and Feldkamp, L. 1987. «*Global calibration of a robot/vision system*». In *IEEE International Conference on Robotics and Automation* (Vol. 4, pp. 190–195).

Roth, Z., Mooring, B., and Ravani, B. 1987. «*An overview of robot calibration*». *IEEE Journal of Robotics and Automation*, vol. 3, n° 5, p. 377–385.

Saund, B., and DeVlieg, R. 2013. «*High accuracy articulated robots with CNC control systems*». *SAE International Journal of Aerospace*, vol. 6, n° 2.

Schiele, G., Hofmann, R., Diep, T. van, Kunzmann, H., Wäldele, F., and Busch, K. 1986. «*Transportable measuring instrument for testing the positional accuracy of a program-controlled appliance arm (in German)*». *German Patent*.

Schröer, K. 1999. «*Precision and calibration*».

Sheldon, P. C. 1999. «*Six-axis metrology sensor device*». US Patent No. 5,870,834.

Shirinzadeh, B. 1998. «*Laser-interferometry-based tracking for dynamic measurements*». *Industrial Robot: An International Journal*, vol. 25, n° 1, p. 35–41.

Siciliano, B. 2009. «*A closed-loop inverse kinematic scheme for on-line joint-based robot control*». *Robotica*, vol. 8, n° 03, p. 231.

Slotine, J. J. E., and Asada, H. 1992. *Robot analysis and control* (p. 266). Wiley-Interscience.

Snell, J. E. 1997. «*Method and device for calibration of movement axes of an industrial robot*». Google Patents.

Sornmo, O., Olofsson, B., Schneider, U., Robertsson, A., and Johansson, R. 2012. «*Increasing the milling accuracy for industrial robots using a piezo-actuated high-dynamic micro manipulator*». *2012 IEEE/ASME International Conference on Advanced Intelligent Mechatronics (AIM)*, p. 104–110.

Stone, H., and Sanderson, A. 1987. «*A prototype arm signature identification system*». In *IEEE International Conference on Robotics and Automation* (Vol. 4, pp. 175–182).

Summers, M. 2005. «*Robot capability test and development of industrial robot positioning system for the aerospace industry*». *SAE Transactions*, vol. 114, n° 1, p. 1108–1118.

Sun, Y., and Hollerbach, J. M. 2008. «*Observability index selection for robot calibration*» (pp. 831–836). IEEE.

Tsai, Y. T., and Orin, D. E. 1987. «*A strictly convergent real time solution for inverse kinematics of robot manipulators*». *Journal of Robotic Systems*, vol. 4, n° 4, p. 477–501.

Veitschegger, W. K., and Wu, C.-H. 1987. «*A method for calibrating and compensating robot kinematic errors*». In *Proceedings 1987 IEEE International Conference on Robotics and Automation* (pp. 39–44).

Vincze, M., Prenninger, J. P., and Gander, H. 1994. «*A laser tracking system to measure position and orientation of robot end effectors under motion*». *The International Journal of Robotics Research*, vol. 13, n° 4, p. 305.

Vira, N., and Lau, K. 1987. «*An extensible ball bar for evaluation of robots' positioning performance*». *Journal of Robotic Systems*, vol. 4, n° 6, p. 799–814.

Von Daake, A., Vetter, C., Böhm, E., and Zirn, O. 2013. «*Contribution to calibration of hexapod positioning units in industrial environment*». *Precision Engineering*, vol. 37, n° 1, p. 73–80.

Vuskovic, M. I. 1989. «*Compensation of kinematic errors using kinematic sensitivities*». In *Robotics and Automation, 1989. Proceedings., 1989 IEEE International Conference on* (Vol. 2, pp. 745–750).

Wang, K. 2009. «*Application of genetic algorithms to robot kinematics calibration*». *International Journal of Systems Science*, vol. 40, n° 2, p. 147–153.

Wang, L. C. T., and Chen, C. C. 1991. «*A combined optimization method for solving the inverse kinematics problems of mechanical manipulators*». *Robotics and Automation, IEEE Transactions on*, vol. 7, n° 4, p. 489–499.

Wei, G., and De Ma, S. 1993. «*A complete two-plane camera calibration method and experimental comparisons*». *Computer Vision, 1993. Proceedings., Fourth*, p. 439–446.

Whitney, D. E., Lozinski, C. A., and Rourke, J. M. 1986. «*Industrial robot forward calibration method and results*». *Journal of Dynamic Systems, Measurement, and Control*, vol. 108, n° 1, p. 1–8.

Wiest, U. 2003. «*(EN) 3D Coordinate measure system*».

Ye, S. H., Wang, Y., Ren, Y. J., and Li, D. K. 2006. «*Robot Calibration Using Iteration and Differential Kinematics*». In *International Symposium on Instrumentation Science and Technology* (Vol. 48, p. 1). IOP Publishing.

Zhang, C.-D., and Song, S.-M. 1992. «*Forward kinematics of a class of parallel (Stewart) platforms with closed-form solutions*». *Journal of Robotic Systems*, vol. 9, n° 1, p. 93–112.

Zhuang, H., and Roth, Z. 1993. «*Optimal design of robot accuracy compensators*». *Robotics and Automation,*, vol. 9, n° 6, p. 9–12.

Zhuang, H., and Roth, Z. S. 1992. «*Robot calibration using the CPC error model*». *Robotics and Computer-Integrated Manufacturing*, vol. 9, n° 3, p. 227–237.

Zhuang, H., and Roth, Z. S. 2002. «*A linear solution to the kinematic parameter identification of robot manipulators*». *Robotics and Automation, IEEE Transactions on*, vol. 9, n° 2, p. 174–185.

Zhuang, H., Roth, Z. S., and Hamano, F. 1992. «*A complete and parametrically continuous kinematic model for robot manipulators*». *IEEE Transactions on Robotics and Automation*, vol. 8, n° 4, p. 451–463.

Zhuang, H., Wang, L. K., and Roth, Z. S. 1993. «*Error-model-based robot calibration using a modified CPC model*». *Robotics and Computer-Integrated Manufacturing*, vol. 10, n° 4, p. 287–299.